The biomechanics and evolution of impact resistance in human walking and running

Share Your Story

The biomechanics and evolution of impact resistance in human walking and running

A dissertation presented

by

Brian James Addison

to

The Department of Human Evolutionary Biology

in partial fulfillment of the requirements

for the degree of

Doctor of Philosophy

in the subject of

Human Evolutionary Biology

Harvard University

Cambridge, Massachusetts

November 2015

Dissertation Adviser: Professor Daniel E. Lieberman   Brian James Addison

The biomechanics and evolution of impact resistance in human walking and running

Abstract

How do humans generate and resist repetitive impact forces beneath the heel during walking and heel strike running? Due to the evolution of long day ranges and larger body sizes in the hominin lineage modern human hunter-gatherers must resist millions of high magnitude impact forces per foot per year. As such, impact forces may have been a selective pressure on many aspects of human morphology, including skeletal structure. This thesis therefore examines how humans generate impact forces under a variety of conditions and how variation in skeletal structure influences impact resistance.

This thesis includes four studies that can be separated into two parts. In the first part, I test two models of how variation in the stiffness and height of footwear affect the generation of impact peaks during walking and heel strike running. The first model predicts that variation in the stiffness of footwear introduces tradeoffs between three crucial impact force related variables: impact loading rate, vertical impulse and effective mass. The prediction of the second model is that higher heels have the same effects on impact forces as do footwear of lower stiffness. These hypotheses were tested using 3D motion data and force data in human walkers and runners wearing a variety of footwear. Experimental results show that soft footwear introduces tradeoffs between impact loading rate, vertical impulse and effective mass, and that high heeled shoes influence impact duration, loading rate and vertical impulse in predictable ways.

In the second part of this thesis, I document variation in hominoid skeletal structure and experimentally test how this variation affects function during impact forces. In particular, I examine trabecular bone volume fraction in the calcaneus of gorillas, chimpanzees and several *H. sapiens*

populations that vary widely in geologic age and subsistence strategy. I then develop and test a model of how variation in trabecular bone volume fraction affects several mechanical properties of trabecular bone tissue, including the stiffness, strength and energy dissipation. The comparative data indicates that trabecular bone volume fraction in the human calcaneus has declined after the Pleistocene. The experimental data shows that larger trabecular bone volume fraction results in increased stiffness and strength but reduced energy dissipation of trabecular bone tissue. A final examination of the comparative data relative to the experimental data suggests that the human calcaneus resists impacts by being stiff strong rather than by dissipating mechanical energy.

The results of this thesis suggest that way in which impacts are both generated and resisted has changed in recent human history, as modern footwear alters impact loading rate and vertical impulse and decline in trabecular bone volume fraction negatively influence trabecular bone strength. These results also have implications for how bones evolve to resist impacts, suggesting that bone structures than favor stiffness and strength are favored to cope with impacts. Finally, the results of this thesis are important for understanding the etiology of osteoarthritis, and musculoskeletal disease that has been linked to both repetitive impact forces during human locomotion and to variation in trabecular bone volume fraction.

Table of Contents

List of Figures

List of Tables

Acknowledgements

I often tell folks that doing a Ph.D. has a lot of similarities to starting your own business. You have to come up with the idea. You have to figure out a way to implement that idea. You have to raise money. You have to build awareness. You have to sell your idea and your work. And yet, the business of my dissertation could not have been done without the kindness, generosity and support of others. I owe many people many thanks.

My first and most heartfelt thanks go out to my wife Tory Wobber. A fellow graduate student in HEB, she knew all the ins and outs, all the ups and downs, and had experienced all of the trials and all of the rewards of graduate school, and was therefore the person best able to help and support me. She filled innumerable roles, including editor, mentor, confidant, sounding board and guidance counselor. And outside of graduate school she's filled my life with encouragement, happiness, fun, laughter, innumerable inside jokes, and countless stories and adventures. Love you!

To my adviser Daniel Lieberman – Dan's biggest strength (among many) as an adviser is his unyielding support and advocacy for his students. Not once during my six years as a graduate student did I feel unsupported or left out in the cold. We may have butted-heads or disagreed on writing documents or ways to conduct experiments, but I knew that he always had my back. Many, many thanks!

To the other members of my thesis committee: David Pilbeam, Andrew Biewener and Lorna Gibson. Thanks to you all for the helpful and insightful comments and edits on my thesis; this document and future publications are immeasurably better because of your feedback. An additional thanks to Lorna for letting me use all sorts of different equipment from her lab. And many additional thanks to David – you believed in me, and I can't tell you how much I appreciate it!

To current and former members of the skeletal biology lab: Heather Dingwall, Eric Castillo, Anna Warrener, Carolyn Eng, Neil Roach, Katie Zink, Brenda Fraser, Meir Barak, Andrew Yegian, Eamon Collison, Kristi Lewton, Adam Daoud and Sara Wright. Your friendship and support on our shared adventures through graduate school and the HEB department are innumerable and not forgotten. Whether it be lab meetings, Tuesday lunches, help with lab equipment or analyzing or presenting data, you all helped me to produce the best possible work I could. Thank you! Ps – you learned that I was the messiest lab-mate ever and you tolerated it. Thanks!

To my HEB graduate student cohort: Daniel Green, Bridget Alex and Sam Urlacher. We had a great run in the beginning until everyone but me got an NSF DDIG! But I finished my thesis first, so I think I win. Just playing – I couldn't have asked to share my graduate school experience with a better group. Thank you and best of luck!

To the HEB department staff: Meg Lynch, Meg Jarvi, Laura Christoffels and Lenia Constantinou. Thank you thank you thank you! Whether it be managing my grants (because we know I couldn't do it), quickly responding to silly questions, or keeping me informed about important deadlines – you guys were on top of it and made my graduate student life so much easier. Thank you!

To some other notable HEBers: Michele Morgan and Olivia Herschenshon. You were such a great help with making Peabody Museum material available to scan and cooperating with my last minute requests to view and scan material. To Larry Flynn – thank you for all your help around the department, including helping me getting access to equipment like dollies or finding space to store my stuff. To Carole Hooven – you became such a large part of my support network during my last few years of graduate school; I just wish you would've eaten lunch with us more often! Thank you all!

To others that helped me gain access to materials or equipment: Judy Chapsko – thanks for all the help with the mammal collections and for the lively conversation! Fettah Kosar – thank you for all

the help with the microCT scanner. Managing all the users and all the data must've been incredibly difficult, but I know all the users appreciate your knowledge and effort. Dan Brooks – many thanks for your time and effort in getting me up to speed with everything concerning my materials testing experiment. My final study would not have been possible without your help!

To my BSC crew: Frank McNamara, Emily McWilliams, Tyler Neill, Sheila Reindl and Adam Stack. I don't think I can concisely say how much 'group' meant to me over the last 12 to 15 months of my thesis. You all provided a welcoming, comfortable place where I could be myself without any strings attached. A thousand thanks!

To the folks at Adams House, in particular Emmy Smith, Tanmoy Laskar, Kris Trujillo and Joe Lee. Emmy – thanks for being my chaperone and point person for everything Adams! Tanmoy – I loved problem set nights with you and I appreciated your sense of humor regarding my obsession with fantasy sports. And Kris and Joe – first, thank you for officiating Tory and I's wedding (it was unforgettable). And second, thank you for being great friends (and introducing us to Bitmoji and Gourmet Dumpling House).

To many undergraduate students: Haley Adams, Mackenzie Hild, Kathryn Kelley, Allie Pace, India Peek-Jensen, Sara Providence, Michael Senter-Zapata, Lauren Tomkinson and Megan Walcek. I believe I told you all at some point in some way, but of all the things I had to do in graduate school, working you guys and getting to know you was easily the most enjoyable. I wish you all the best and I hope we can stay in touch!

To Zarin Machanda, Terry Capellini and Darren Rand: thank you for taking care of me after Tory left for California! So many things are memorable about our friendship: chimp Snuggies, Hockey Night in Cambridge, 'Parlez-vous-ing,' etc, etc... I miss you guys all the time!

To the Bukowski's Mug Club crew – Eric Castillo, Erik Otarola-Castillo, Heather Dingwall and Collin McCabe. We spent thousands of dollars joining a mug club at a bar that is now just. plain. awful.

But hey, we got to keep the mugs. And have gallons and gallons of Blanche. And we got to have so much 'serious time' (\/). "Bobby Sands" would be proud of us. Good times!

And finally, thank you to my family. Mom, Dad and Steve - you guys had barely any idea what I was doing for 6 years at Harvard, but it didn't matter. You were there to support me the whole way. Thank you for all your love and support during graduate school, prior to graduate school and into the future.

Chapter 1 – An Introduction

Why impacts?

How do humans generate and resist repetitive impact forces beneath the ground during walking and heel strike running? Ever since the evolution of obligate bipedalism in the hominin lineage, the human skeleton has been exposed to millions of impact forces beneath the heel per year. Our closest living relatives, chimpanzees, also heel strike but do so irregularly and often without visible peaks in vertical ground reaction force, suggesting that highly repetitive impact peaks beneath the heel bone (calcaneus) evolved in the hominin line. Impact forces to the heel are likely to have been a selective pressure on human skeletal morphology, particularly the calcaneus, and trabecular bone tissue is often hypothesized to act as a 'shock absorber' of impact forces (Radin et al. 1972; Latimer and Lovejoy 1989; Currey 2002; Latimer 2005). Despite the potential role that impact forces may have played in shaping the trabecular architecture of the calcaneus, many questions remain about the generation and variation in impact forces as well as how patterns of variation in trabecular tissue reflect impact resistance. This thesis investigates how humans generate impacts under a variety of conditions relevant to ancient and modern times, and studies how variations in calcaneal trabecular bone structure resist repetitive impact forces.

Thesis summary

This thesis includes four studies that can be separated into two parts. The first part (chapters 2 and 3) investigates the generation and variation in impact forces beneath the heel during walking and heel strike running. Chapter 2 considers how walking and heel strike running impacts vary in response to variation in interface stiffness. Chapter 3 tests a model of how heel strike running impacts vary with changes in both heel height and heel-ground interface elastic modulus (the size-independent measure of stiffness). The second part of this thesis (chapters 4 and 5) investigates the patterns of variation in trabecular bone volume fraction (BVF) of the calcaneus and how this variation affects the mechanical

properties of trabecular tissue. Chapter 4 investigates patterns of variation in calcaneal trabecular BVF

of gorillas, chimpanzees and several human populations as well as BVF variation in the C2 vertebrae of

H. sapiens. Chapter 5 studies how energy dissipation varies with trabecular BVF, tests a model that

predicts that BVF mediates a trade-off between energy dissipation and the mechanical properties elastic

modulus, yield strength and work-to-failure, and finally compares the patterns of variation found in

Chapter 4 to the experimental data to understand how human calcaneal trabecular tissue resists

impacts.

Part I

 In Chapter 2, I investigate the effects of variation in heel-ground interface elastic modulus on

walking and heel strike running impact peaks. During walking and heel strike running, an exchange of

momentum occurs between the foot and the ground, generating high magnitude forces over a very brief

period of time (the impact peak). Previous studies have shown that decreased elastic modulus interfaces

lead to a longer duration of the impact peak and slower rates of loading (Light et al. 1980; Wakeling et

al. 2003). However, these studies have not investigated how the exchange of momentum between the

foot and the ground on interfaces of varying modulus influence aspects of the impact peak frequently

implicated in musculo-skeletal injuries. Chapter 2 accordingly tests an impulse-momentum model of

walking and heel strike running impact peaks that predicts that lower elastic modulus interfaces slow

the exchange of momentum between the foot and the ground, resulting in reduced impact loading rates

(F') but greater effective mass (m_{eff}) and larger vertical impulses on lower modulus interfaces. The

model also predicts a trade-off between F' and m_{eff}, as well as a trade-off relationship between F' and

vertical impulse. My findings show that vertical impulse and m_{eff} increase in walkers and heel strike

runners as interface modulus decreases. My results also indicate trade-off relationships between F' and

m_{eff}, and between F' and vertical impulse. Given that both F' and vertical impulse have been

hypothesized to be related to various musculo-skeletal injuries, the trade-off between these two

variables suggests that impact peaks present a formidable challenge to the human skeleton regardless of the stiffness of the interface between the foot and the ground.

In Chapter 3, I examine the effects of both heel height and heel elastic modulus variation on heel strike running impact peaks. I develop a model that predicts that increasing heel height and decreasing heel elastic modulus should have similar effects on heel strike running impacts peaks, such as increasing the time duration of impact and reducing F'. The model also predicts that the effects of increasing heel height while simultaneously decreasing heel elastic modulus will be multiplied. My results confirm that increasing heel height results in increased impact duration and decreased F'. However, I find that the effects of heel height and heel elastic modulus variation on impact peaks are not multiplied; instead, the effect of heel elastic modulus on impact peaks depends on the height of the heel. In addition, I find that impact force magnitude is unaffected by the elastic modulus of the interface but decreases as heel height increases. I also find that the amount of knee flexion during the impact peak is a strong predictor of impact force magnitude, impact time duration, F', vertical impulse and m_{eff}. These results suggest that variations in heel height influence the generation of the impact peak in predictable ways and that impact peak generation is affected by a complicated interaction between the elastic modulus of the interface and heel height. The results also imply that lower extremity kinematic play an important role in the generation of impact and that the human body can regulate impact force magnitudes when interface elastic modulus varies but not when heel height varies.

Part II

In Chapter 4, I test the hypothesis that variations in mechanical loading due to physical activity are the primary cause of variation in BVF between populations. Mechanical loading stimulates trabecular bone growth, and thus bones that experience higher magnitudes or frequencies of mechanical loading are expected to have larger trabecular BVF (Simkin et al. 1987; Davee et al. 1990; Joo et al. 2003; Pontzer et al. 2006; Barak et al. 2011; Chirchir et al. 2015; Ryan and Shaw 2015). Thus,

individuals from populations that have more physically active lifestyles, such as hunter-gatherers, are expected to have larger trabecular BVF in any given bone than individuals from populations that live more sedentary lifestyles, such as industrialized Westerners. I test this hypothesis in the calcaneus, a bone in which the loads applied during locomotion are relatively well known, and in C2 vertebrae, a bone that may be relatively unaffected by variation in mechanical forces applied to the appendicular skeleton (Giddings et al. 2000; Gefen and Seliktar 2004). I examine calcanei from gorillas, chimpanzees, a Pleistocene *H. sapiens* population (Natufians – hunter-gatherers from the Levant) and three Holocene *H. sapiens* populations that vary widely in subsistence strategy: hunter-gatherers from Point Hope, Alaska (Point Hope), nomadic pastoralists from medieval Europe (Mistihalj) and modern industrialized Americans. I also examine C2 vertebrae from the Natufians, Point Hope and Mistihalj populations. I test three specific hypotheses relevant to the general hypothesis that variations in mechanical loading are the primary cause of variation in trabecular BVF. First, I predict that modern sedentary Americans should have lower calcaneal trabecular BVF than more active, non-industrial *H. sapiens* populations. Second, I predict that *H. sapiens,* particularly those from active, non-industrial populations, have greater calcaneal trabecular BVF than the comparatively sedentary African apes. Finally, I predict that trabecular BVF in C2 vertebrae should remain unchanged across human populations because this region of the skeleton experiences relatively low magnitudes of mechanical loading from normal physical activities. These hypotheses were not supported by the data. Instead, my results indicate that the Natufians have larger calcaneal BVF than any of the Holocene *H. sapiens* populations, and that modern Americans have calcaneal BVF values equivalent to non-industrial Holocene populations. In addition, I found that Natufian calcaneal BVF was equivalent to chimpanzees and gorillas, while calcaneal BVF in Holocene populations was lower than chimpanzees. Finally, I found that trabecular BVF in Natufian C2 vertebrae was greater than either of the Holocene populations tested. These results suggest that trabecular BVF in the *H. sapiens* calcaneus and C2 vertebra has declined since the Pleistocene, and suggests a systemic

4

decline in trabecular BVF from Pleistocene to Holocene *H. sapiens* for reasons other than or in addition to variation in mechanical loading.

In Chapter 5, I test how variations in trabecular BVF affect the mechanical properties of trabecular tissue and use population-level data from Chapter 4 to test competing models of how the human calcaneus resist impacts during walking and heel strike running. Trabecular bone is often thought to act as a 'shock-absorber' during impact loads, but researchers have differing opinions on how trabecular bone is adapted structurally to resist impacts. Some researchers argue that trabecular bone is adapted to avoid fracture during impacts and thus would evolve increased trabecular BVF in order to increase stiffness, strength and toughness (Currey 2002). Other scholars argue that trabecular tissue is adapted to 'cushion' impact loads and as such would evolve lower trabecular BVF in order to increase energy absorption and dissipation under a given force (Latimer and Lovejoy 1989; Currey 2002; Goodwin and Horner 2004; Latimer 2005). In this chapter, I first develop a model that predicts that energy dissipation (W_d) varies with the inverse of trabecular BVF squared under stress-controlled conditions. Second, I predict that tradeoffs, mediated by BVF, exist between W_d and each of the following mechanical properties: elastic modulus (E), yield strength (σ_y) and work-to-failure (W_f). I also predict that the tradeoffs in these variables will identify a BVF that optimizes W_d and each of E, σ_y, and W_f. Finally, I use the experimental data to develop tradeoff models and compare the population-level data from Chapter 4 to understand how the human calcaneus resists impacts. I test these predictions in stress-controlled cyclic mechanical testing of human calcaneal trabecular tissue. The experimental data indicate that W_d varies with the inverse of BVF squared. The data also support the hypothesis that tradeoffs mediated by BVF exist between W_d and E, σ_y, and W_f , and that a BVF of 0.15 optimizes W_d and each of E, σ_y, and W_f. Finally, I find that the optimum BVF is greater than 2 standard deviations below the average calcaneal tuberosity BVF of Pleistocene *H. sapiens* (0.26), and falls within 1 standard deviation of the average Holocene calcaneal tuberosity BVF (0.18). These findings suggest that

trabecular tissue of low BVF dissipates more energy under a given load. The findings also imply that

Pleistocene *H. sapiens* calcaneal trabecular bone resisted impacts by being stiff, strong and tough rather

than by dissipating impact energy.

Finally, Chapter 6 summarizes the results and major conclusions from Chapters 2 through 5. I

then discuss some of the broader implications of the data. First, I discuss competing models of how

bone tissue resists impacts and how the results from Chapter 5 test these models. Second, I discuss how

data from Chapters 2 through 5 suggest that the generation and resistance of impact forces during

walking and heel strike running are different in industrialized modern *H. sapiens* compared to those

from hunter-gatherer and subsistence farming economies. Finally, I discuss the relevance of Chapters 2

through 5 to the etiology of osteoarthritis, a disease of articular cartilage degeneration that is thought to

be caused in part by high bone density and repetitive impact forces (Radin et al. 1991; Hardcastle et al.

2015).

References

Barak, M. M., D. E. Lieberman, et al. (2011). "A Wolff in sheep's clothing: Trabecular bone adaptation in response to changes in joint loading orientation." Bone **49**(6): 1141-1151.

Chirchir, H., T. L. Kivell, et al. (2015). "Recent origin of low trabecular bone density in modern humans." Proceedings of the National Academy of Sciences of the United States of America **112**(2): 366-371.

Currey, J. D. (2002). Bones: Structure and Mecanics. Princeton, Princeton University Press.

Davee, A. M., C. J. Rosen, et al. (1990). "Exercise patterns and trabecular bone-density in college-women." Journal of Bone and Mineral Research **5**(3): 245-250.

Gefen, A. and R. Seliktar (2004). "Comparison of the trabecular architecture and the isostatic stress flow in the human calcaneus." Medical Engineering & Physics **26**(2): 119-129.

Giddings, V. L., G. S. Beaupre, et al. (2000). "Calcaneal loading during walking and running." Medicine and Science in Sports and Exercise **32**(3): 627-634.

Goodwin, M. B. and J. R. Horner (2004). "Cranial histology of pachycephalosaurs (Ornithischia : Marginocephalia) reveals transitory structures inconsistent with head-butting behavior." Paleobiology **30**(2): 253-267.

Hardcastle, S. A., P. Dieppe, et al. (2015). "Osteoarthritis and bone mineral density: are strong bones bad for joints?" BoneKEy reports **4**: 624.

Joo, Y. I., T. Sone, et al. (2003). "Efects of endurance on three-dimensional trabecular bone microarchitecture in young growing rats." Bone **33**(4): 485-493.

Latimer, B. (2005). "The perils of being bipedal." Annals of Biomedical Engineering **33**(1): 3-6.

Latimer, B. and C. O. Lovejoy (1989). "The calcaneus of australopithecus-afarensis and its implications for the evolution of bipedality." American Journal of Physical Anthropology **78**(3): 369-386.

Light, L. H., G. E. McLellan, et al. (1980). "Skeletal transients on heel strike in normal walking with different footwear." Journal of Biomechanics **13**(6): 477-480.

Pontzer, H., D. E. Lieberman, et al. (2006). "Trabecular bone in the bird knee responds with high sensitivity to changes in load orientation." Journal of Experimental Biology **209**(1): 57-65.

Radin, E. L., D. B. Burr, et al. (1991). "Mechanical determinants of osteoarthrosis." Seminars in Arthritis and Rheumatism **21**(3): 12-21.

Radin, E. L., R. M. Rose, et al. (1972). "Role of mechanical factors in pathogenesis of primary osteoarthritis." Lancet **1**(7749): 519-&.

Ryan, T. M. and C. N. Shaw (2015). "Gracility of the modern Homo sapiens skeleton is the result of decreased biomechanical loading." <u>Proceedings of the National Academy of Sciences of the United States of America</u> **112**(2): 372-377.

Simkin, A., J. Ayalon, et al. (1987). "Increased trabecular bone-density due to bone-loading exercises in postmenopausal osteoporotic women." <u>Calcified Tissue International</u> **40**(2): 59-63.

Wakeling, J. M., A. M. Liphardt, et al. (2003). "Muscle activity reduces soft-tissue resonance at heel-strike during walking." <u>Journal of Biomechanics</u> **36**(12): 1761-1769.

Chapter 2 – Tradeoffs between impact loading rate, vertical impulse and effective mass for walkers and heel strike runners wearing footwear of varying stiffness

Introduction

The human foot is subjected to repeated impact forces during walking and heel strike running, evident as visible impact peaks in vertical ground reaction forces. Impact peaks are caused by the inertial change in some portion of the body over a brief period of time, usually during the first 10 to 50 ms of stance. The generation and attenuation of impact forces have been the focus of much research because their potential role in the etiology of various repetitive stress injuries is unclear and intensely debated (Folman et al. 1986; Collins and Whittle 1989; Nigg 2001; Gill and O'Connor 2003; Gill and O'Connor 2003; Milner et al. 2006; Wen 2007; Pohl et al. 2009; Nigg 2010; Daoud et al. 2012). In addition, how footwear affects the generation of impact forces has been heavily investigated because of the perceived role of footwear in mitigating discomfort and preventing injuries that may result from impact peaks (Hume et al. 2008; Nigg 2010).

During the impact phase of stance, defined as the time period from the onset to the zenith of the impact peak, the impulse of the net external force changes the momentum of some portion of the body:

Equation 1: $\int_{t_i}^{t_f}(F_z - m_{eff}g)dt = m_{eff}(v_f - v_i)$

where t_i and t_f are the beginning and end times of the impact phase, F_z is the vertical ground reaction force, m_{eff} is the effective mass, g is acceleration due to gravity, and v_i and v_f are the vertical velocities of m_{eff} at t_i and t_f, respectively. We define m_{eff} as the portion of the body's mass that decelerates to zero during the period of the impact peak; m_{eff} therefore may contain mass from the foot, shank, thigh or other body segments (Dempster and Gaughran 1967; Bobbert et al. 1991; Chi and Schmitt 2005; Lieberman et al. 2010; Shorten and Mientjes 2011). We define the impact peak as the first

peak in vertical ground reaction force, and it thus contains the summation of both high and low frequency ground reaction forces. (Shorten and Mientjes 2011).

While the frequency components of the vertical ground reaction force are important for understanding how the body generates impact peaks, the purpose of this study is to understand how impact peak magnitude (F_{max}), impact loading rate (F'), and vertical impulse, variables that have been implicated in the etiology of various musculo-skeletal injuries, are influenced by footwear heel stiffness. Extensive experimental and modeling studies of the effects of footwear heel stiffness on F_{max} and F' have shown that softer footwear heels decrease F' largely due to increases in the time duration of impact (Δt) rather than changes in F_{max} (Light et al. 1980; Lafortune et al. 1996; Wakeling et al. 2003). Experimental results concerning F_{max} are largely inconclusive, with studies finding that less stiff footwear heels can increase, decrease or have no influence on F_{max} (Clarke et al. 1983; Nigg et al. 1987; Lafortune and Hennig 1992; Hennig et al. 1993; Wakeling et al. 2003). Modeling studies predict that footwear heel stiffness should decrease F_{max} and that muscle activity in the lower limb can modulate F_{max} (Nigg and Liu 1999; Zadpoor et al. 2007; Zadpoor and Nikooyan 2010). Vertical impulse and m_{eff} have been studied in the context of kinematic variation (Chi and Schmitt 2005; Lieberman et al. 2010), but have yet to be studied in the context of variations in footwear heel stiffness.

We can use the impulse-momentum model (equation 1) to investigate how footwear heel stiffness influences F_{max}, F', m_{eff} and vertical impulse by solving equation 1 for m_{eff}:

Equation 2: $m_{eff} = \dfrac{\int_{t_i}^{t_f} F_z dt}{\Delta v + g \Delta t}$

Previous experiments using this impulse-momentum model on barefoot individuals have found that m_{eff} varies with gait pattern, kinematics and joint stiffness, and that m_{eff} averages 6.3% of body mass during walking heel strikes and ranges between 2 and 10% of body mass during heel strike running (Chi

and Schmitt 2005; Lieberman et al. 2010). m_{eff} is also expected to change with footwear heel stiffness because a less stiff interface between the foot and ground slows the exchange of momentum between the body and the ground. Decreasing the stiffness of footwear heels while holding all other variables constant increases Δt (Figure 2.1) (Light et al. 1980; Nigg et al. 1987; Lafortune et al. 1996; Whittle 1999; Shorten and Mientjes 2011), which will result in a greater portion of the body coming to a stop during the period of the impact peak. Thus, less stiff footwear heels will result in larger m_{eff} within a given gait pattern. In turn, a larger vertical impulse will result from the increase in m_{eff} in less stiff footwear (Figure 2.1).
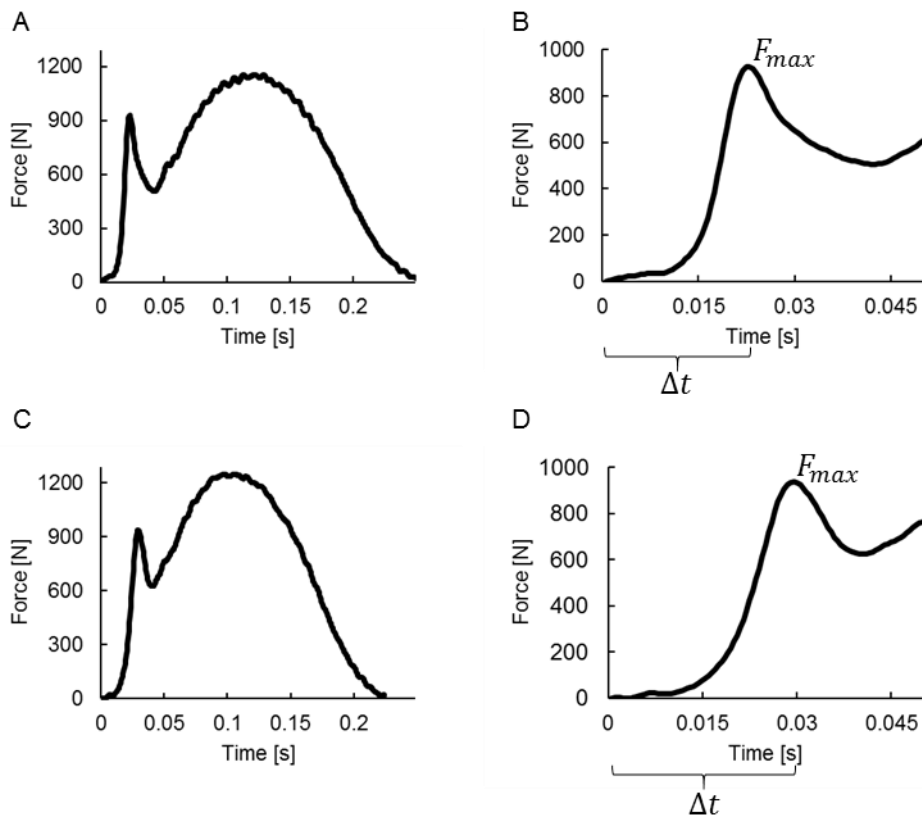
Figure 2.1: Vertical ground reaction force of a barefoot heel strike runner on a hard surface (A) and corresponding vertical impact peak emphasized (B). Frames C and D are a vertical ground reaction force for a heel strike runner in soft footwear (C) with the corresponding vertical impact peak emphasized (D). The impact in the less stiff footwear increases Δt, leading to larger m_{eff}. A larger m_{eff} will in turn create a larger vertical impulse (the integral of force over Δt) in the less stiff footwear.

The impulse-momentum model makes additional predictions. If less stiff footwear heels decrease F' as reported elsewhere and increase m_{eff} as predicted by the model, then there should be a tradeoff between F' and m_{eff} in walkers and heel strike runners wearing footwear of varying stiffness. Similarly, if less stiff footwear decreases F' and increases vertical impulse as predicted by the model, then there should be also be a tradeoff between these variables in walkers and runners wearing footwear of varying stiffness. The objective of this study is to test these predictions in human walkers and runners wearing footwear of varying stiffness.

Material and Methods

Subjects

Twenty-two healthy adult subjects (13 female – average (SD) body mass (kg): 59.2 (6.63), height (cm): 165 (7.99); 9 male – body mass (kg) 78.9 (7.64), height (cm) 181 (6.93)) between the ages of 19 and 37 participated in this study, which was approved by the Institutional Review Board of Harvard University. Subjects gave their informed consent to participate and the experiments were conducted at the Skeletal Biology and Biomechanics Lab of the Department of Human Evolutionary Biology at Harvard University.

Criteria for subject inclusion in the data analysis were that the subject was able to wear minimal footwear comfortably and was able to heel strike in both walking and running for the full 30 second trial duration on all footpads (forefoot strikes were not included in the study because they generate no measureable impact peak (Lieberman et al. 2010)). Subjects were asked to heel strike in all walking and running trials, regardless of their natural strike pattern. Of the 22 subjects enrolled in the study, 19 were used for data analysis. In the running analysis, two subjects were removed because they were uncomfortable heel striking for the full trial duration. In walking, one subject was removed because of data collection problems and another was removed because heel strikes were not apparent in one of

the trials. An additional subject was removed from walking and running analyses because of discomfort in the minimal footwear.

Experimental design and measurements

Subjects walked and ran in minimal footwear (model: M116 Sprint, Vibram USA, Concord MA, USA) and on two different experimental footpads (Figure 2.2; 'hard pad': rubber, Product No. RB4000, On Deck Sports, Brockton, MA, USA. Thickness - 0.25 inches, elastic modulus – 5.64 MPa; 'soft pad': foam, Product No. 150553488-32, Future Foam, Council Bluffs, IA, USA. Thickness – 0.5 inches, elastic modulus 0.095 MPa) cut specifically for each subject and attached to the bottom of the minimal footwear using duct tape. Elastic modulus of the pads was measured between 25 N and 25% strain, and calculated as $\Delta stress/\Delta strain$. Footpads were chosen to decrease the interface stiffness between the foot and the ground – the 'hard' pad was less stiff than the control condition, and the 'soft' pad less stiff than the 'hard' pad. The order in which these conditions were performed was randomized across subjects. Subjects walked and ran at Froude numbers of 0.28 and 1.2, respectively (actual forward velocities: 1.48 m/s to 1.68 m/s for walking; 3.06 m/s to 3.48 m/s for running). Froude number was controlled to ensure dynamic similarity between subjects that varied in leg length (Alexander 2003). Before data collection, each subject practiced walking and running on the treadmill at the prescribed Froude number and their preferred step frequency in walking and running was recorded. Each subjects' preferred step frequency was played back via electronic metronome during each trial, and subjects were instructed to keep to this step frequency to the best of their ability to avoid complications with changes in support mechanics with changes in footpad stiffness (Kerdok et al. 2002).

We measured ground reaction forces and lower limb kinematics during the period of the impact peak. The impact peak was defined as the first peak in vertical force. A treadmill instrumented with a force-plate (BERTEC, Columbus, Ohio, USA) recorded ground reaction force data at 2 kHz. Kinetic data were low-pass filtered at 100 Hz prior to data analysis. The impact peak was considered to begin when

the vertical ground reaction force value exceeded 3 standard deviations above treadmill noise and ended at F_{max}. Lower limb kinematic data were collected at 1,000 HZ with an eight camera Oqus system (QUALYSIS, Gothenburg, Sweden). Markers (12.7 cm in diameter) were placed on the skin over the anterior superior iliac spine (ASIS), greater trochanter, medical and lateral femoral condyles, medial and lateral malleoli, the calcaneal tuberosity, and the distal joints of the 5th and 2nd metatarsals.
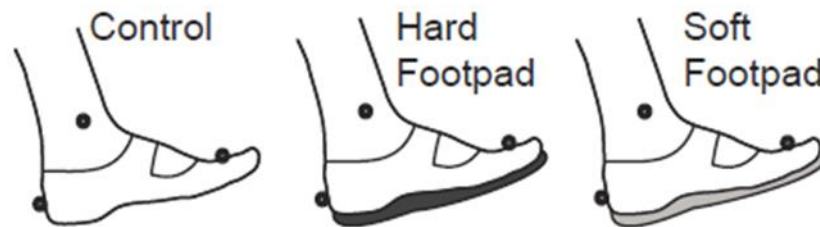
Figure 2.2: Schematic of the control, hard footpad and soft footpad conditions run in this experiment. Footpads were attached to the bottom of minimal footwear using duct tape.

We measured F_{max}, Δt, impact velocity (Δv) in the vertical direction, as well as knee and ankle angles in the sagittal plane. We considered only the vertical components of the kinetic and kinematic variables because over 90% of the total ground reaction force during the impact phase of gait is due to the vertical force (Cavanagh 1990). Δv was calculated as the change in lateral malleolus position divided by the change in time for the four frames immediately prior to the beginning of the impact peak. Knee and ankle angles were measured at the beginning of the impact peak and at F_{max}. Knee angle was measured between the greater trochanter, lateral femoral condyle and lateral malleolus markers, and ankle angle was measured between the lateral femoral condyle, lateral malleolus and 5th metatarsal markers. Heel strikes were verified by comparing the plantar foot angle (the angle made between the treadmill horizontal and a line formed between the posterior calcaneus and 5th metatarsal markers) during locomotion to the plantar foot angle made during a standing trial.

We calculated F', m_{eff} and vertical impulse during the period of the impact peak. F' was calculated as F_{max} divided by Δt. Vertical impulse was calculated as the integral of the impact peak over Δt. m_{eff} was calculated using equation 2 above. Only the vertical components of force and velocity were used to calculate m_{eff}. In running, we calculated lower extremity stiffness, which was defined as F_{max} divided by the vertical displacement of the greater trochanter.

Data analyses

Individual steps were removed from the analysis when F_{max} was 3 standard deviations from the average F_{max} for the given subject and condition. We then analyzed 25 steps from the right leg per subject per condition. Averages for all variables were taken from these 25 steps and used in all subsequent analyses.

Regression and ANOVA analyses were performed in MATLAB (v. 2011a, Mathworks, Inc.) and JMP Pro 10. We used one-way ANOVA to test how the experimental footpads affected kinematic and kinetic variables, and walking and running trials were considered separately. Bonferroni corrections were used to correct p-values for multiple comparison tests. In all cases that required multiple comparisons, a comparison between each of the three conditions (control, hard pad, soft pad) were made. We used mixed models to test relationships between F' and vertical impulse and F' and m_{eff} in order to control for the random effect that each subject contributed to the results. Briefly, a mixed model is a statistical model that uses both fixed (F', vertical impulse and m_{eff}) and random (subject) effects and controls for repeated sampling of subjects. Each subject that participated in this study had their own unique response to the three experimental conditions and the mixed model accounts for the repeated sampling within-subject. R^2 and p-values for F' versus vertical impulse and for F' vesrus m_{eff} represent R^2 and p-values for the mixed model. For all statistical analyses, significance was assigned to p-values < 0.05.

Results

Effect of footpad stiffness on measured and calculated variables

In both walking and running, F' was significantly different between conditions (Figure 2.3A, 2.3D; Table 2.1; walking: F(2,54)=18.12, p=9.5E-7; running F(2,54)=15.33, p=5.3E-6). F' was 19% and 29% greater in the control condition than on the hard pad for walking and running, respectively (walking: p=2.7E-7; running: 3.4E-6). F' was 20% and 24% greater on the hard pad than on the soft pad for walking and running respectively (walking: p=0.0001; running: p=0.0002).

Vertical impulse was 28% and 35% greater in the soft pad than in the hard pad for walking and running, respectively (Figure 2.3B, 2.3E; Table 2.1; walking: p=3.4E-8, running: p=6.7E-8). Vertical impulse was 20% and 21% greater on the hard pad then in the minimally shod condition during walking and running, respectively (Figure 2.3B, 2.3E; walking: p=2.6E-6, running: p=0.01). F_{max} was not significantly different between conditions (Table 2.1; walking: F(2,54)=0.67, p=0.52, running: F(2,54)=0.21, p=0.81). Δt was significantly different between conditions (Table 2.1; walking: F(2,54)=35.6, =1.4E-10; running F(2,54)=33.9, p=2.9E-10). Δt was 13% and 26% longer in the soft pad than in the hard pad for walking and running, respectively (Table 2.1; walking: p=2E-8; running: p=8.6E-8). Δt was 21% and 24% longer in the hard pad than in the control condition for walking and running, respectively (Table 2.1; walking: p=1E-6; running: p=0.0001).

During both walking and running, m_{eff} (measured in %BW) differed significantly between conditions (Figure 2.3C, 2.3F; Table 2.1; walking: F(2,54)=12.08, p=4.6E-5; running: F(2,54)=15.52, p=4.7E-6). During walking, m_{eff} averaged 6.0%, 7.0% and 8.1% of body weight in the control, hard footpad and soft footpad conditions, respectively. During running, m_{eff} averaged 6.8%, 8.2% and 10.3% of body weight in the control, hard footpad and soft footpad conditions, respectively. Δv was not significantly different between groups (Table 2.1; walking: F(2,54)=1.68, p=0.2, running F(2,54)=.77,

p=0.47). Lower extremity stiffness was significantly different between conditions during running (Table 2.1; $F_{(2,51)}=9.75$, p=0.0003). Lower extremity stiffness was 30% greater in the hard pad than in the soft pad, and 39% greater in the control condition than in the hard pad.

During walking, no difference was found between conditions for the ankle angle at the beginning of the impact peak (Table 2.2; $F_{(2,51)}=0.06$, p=0.93) or for the change in ankle angle during the impact peak (Table 2.2; $F_{(2,51)}=2.07$, p=0.14). Also in walking no difference was found between conditions for the knee angle at the beginning of the impact peak (Table 2.2; $F_{(2,48)}=0$, p=0.99) or for the change in knee angle during the duration of impact peak (Table 2.2; $F_{(2,48)}=2.16$, p=0.13).

In running, there was no difference between conditions for the ankle angle at the beginning of the impact peak (Table 2.2; $F_{(2,51)}=0.27$, p=.77) or the change in in ankle angle during the impact peak (Table 2.2; $F_{(2,51)}=2.07$, p=0.14). There was no difference between conditions in knee angle at the beginning of the impact peak (Table 2.2; $F_{(2,48)}=0.02$, p=0.98), but knee flexion angle during the duration of the impact peak was significantly different between conditions (Table 2.2; $F_{(2,48)}=13.42$, p=2.3 E-5). Subjects had 31% more knee angle flexion when wearing the soft footpad than the hard pad (p=1.5E-6), and 21% more knee angle flexion when wearing the hard pad than in the control condition (p=0.008).

F' vs vertical impulse and F' vs. m_{eff}

F' varied inversely with vertical impulse in both walking and running (Figure 2.4A, 2.4B; Table 2.3; walking: R^2 = 0.77, p < 0.0001; running: R^2 = 0.61, p < 0.0001). F' also varied inversely with m_{eff} in both walking and running (Figure 2.4C, 2.4D; Table 2.3; walking: R^2 = 0.77, p < 0.0001; running: R^2 = 0.67, p < 0.0001).
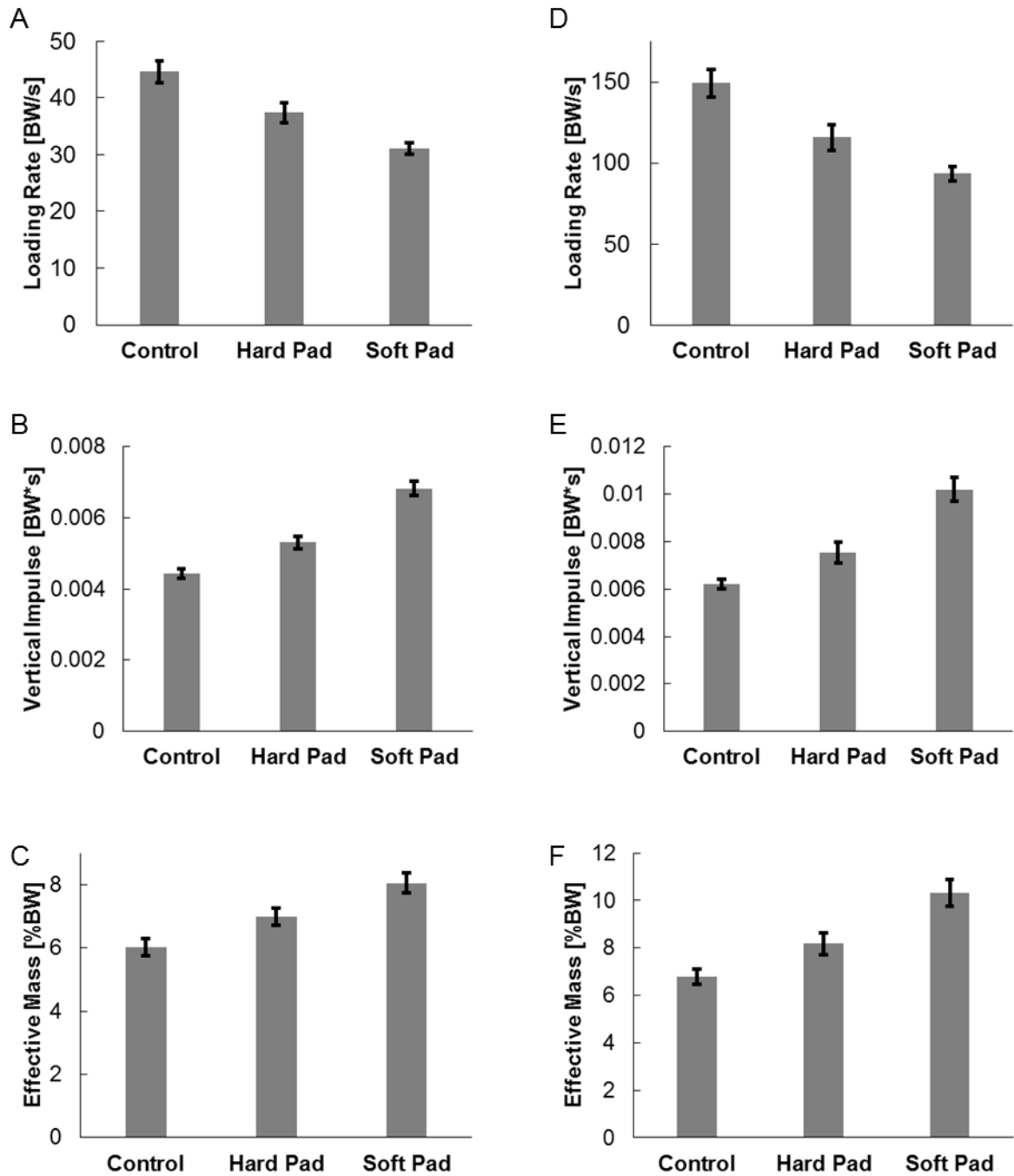
Figure 2.3: A through C: Impact loading rate, vertical impulse and effective foot mass for all three conditions in walking. D through F: Impact loading rate, vertical impulse and effective foot mass for all three conditions in running. Error bars represent standard error. In each case, control was significantly different the hard condition and the hard condition significantly different from the soft condition (see text and Table 2.1 for details).

Table 2.1: The mean and standard deviation of impact kinetic variables ($Fmax$, F', vertical impulse, m_{eff}, Δt, Δv, and lower extremity stiffness) for all conditions in both walking and running. P-values are recorded from ANOVA tests between conditions. See text for Bonferroni corrections for multiple comparisons.

	WALKING				RUNNING			
	Mean (SD)			p-value	Mean (SD)			p-value
	Control	Hard	Soft		Control	Hard	Soft	
F_{max}(BW)	0.80 (0.11)	0.76 (0.11)	0.77 (0.08)	0.52	1.66 (0.29)	1.60 (0.31)	1.65 (0.23)	0.81
F' (BW/s)	44.6 (8.21)	37.4 (7.63)	31.1 (4.27)	9.5E-7	149 (37.4)	116 (34.0)	93.4 (19.6)	5.3E-6
Vertical impulse (BW*ms)	4.4 (0.6)	5.3 (0.7)	6.8 (0.9)	2.6E-13	6.2 (0.9)	7.5 (1.9)	10.2 (2.2)	1.8E-8
m_{eff} (%BW)	6.0 (1.2)	7.0 (1.2)	8.1 (1.4)	4.6E-5	6.8 (1.4)	8.2 (2.0)	10.3 (2.4)	4.7E-6
Δt (ms)	17.9 (2.2)	20.4 (2.7)	24.6 (2.4)	1.4E-10	11.4 (1.5)	14.4 (2.9)	17.9 (2.5)	2.9E-10
Δv (m/s)	0.56 (0.09)	0.56 (0.07)	0.60 (0.08)	0.19	0.80 (0.11)	0.77 (0.09)	0.81 (0.10)	0.47
Lower extremity stiffness (BW/m)	N/A				255 (112)	183 (66.6)	141 (41.3)	3.0E-4

Table 2.2: The mean and standard deviation of kinematic variables during impact (ankle angle approach, ankle plantarflexion, knee angle approach, knee flexion) for all conditions in both walking and running. P-values are recorded from ANOVA statistical tests. See text for Bonferroni corrections for multiple comparisons.

	WALKING				RUNNING			
	Mean (SD)			p-value	Mean (SD)			p-value
	Control	Hard	Soft		Control	Hard	Soft	
Ankle Angle Approach (deg)	103 (3.6)	103 (3.9)	103 (3.7)	0.93	97.2 (3.8)	96.8 (4.4)	97.9 (4.8)	0.77
Ankle Plantarflexion (deg)	2.65 (1.0)	3.03 (1.1)	3.41 (1.3)	0.14	3.36 (1.1)	3.85 (1.8)	3.56 (2.6)	0.14
Knee Angle Approach (deg)	163 (5.1)	163 (5.1)	163 (5.2)	0.99	156 (3.7)	156 (3.9)	155 (3.5)	0.98
Knee Flexion (deg)	2.88 (0.7)	2.81 (0.9)	3.4 (1.0)	0.13	2.79 (0.8)	3.37 (1.0)	4.42 (1.1)	2.3E-5
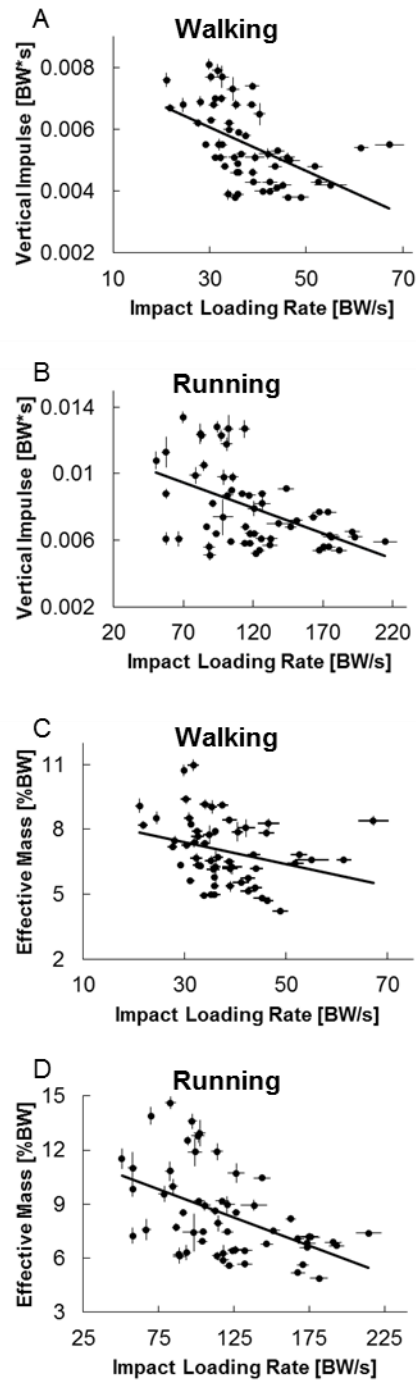
Figure 2.4: Repeated measures regression of impact loading rate versus vertical impulse in walking (A) and running (B). Repeated measures regression of impact loading rate versus effective foot mass in walking (C) and running (D). Error bars represent standard error. Strong correlations and significant relationships were found for each relationship (see text and Table 2.3 for details).

Table 2.3: Correlation coefficients and p-values for the relationships between F' and vertical impulse as well as for F' and m_{eff} for both walking and running.

	WALKING	RUNNING
F' vs. vertical impulse	R^2=-0.77; p<0.0001	R^2=-0.61; p<0.0001
F' vs. m_{eff}	R^2=-0.77; p<0.0001	R^2=-0.67; p<0.0001

Discussion

In this study, we investigated how variations in footwear heel stiffness influenced several aspects of walking and heel strike running impact peaks (including F_{max}, F' and vertical impulse) that have been implicated in the etiology of various repetitive stress injuries. Our study used impulse-momentum mechanics, which models impact events as the exchange of momentum that occurs between the ground and some portion of the body (m_{eff}) over a brief period of time (Δt). It is important to note that the impact peak (as defined above) does not occur instantaneously, and that several portions of the body including the foot, the shank, the thigh and other body segments may contribute to m_{eff}. This means that the impact peaks we examined in this study were composed of both low and high frequency forces (Shorten and Mientjes 2011). However, the focus of this study was not to examine how footwear influences high and low frequency components of the impact peak, nor was it to investigate contributions of different parts of the body to the total m_{eff}. Rather, our focus was on F', F_{max} and vertical impulse, variables that are often cited as risk factors for several musculo-skeletal injuries (Voloshin et al. 1981; Folman et al. 1986; Collins and Whittle 1989; Gill and O'Connor 2003; Davis et al. 2004; Milner et al. 2006; Wen 2007).

The prediction that both vertical impulse and m_{eff} would increase in walkers and heel strike runners wearing less stiff footwear was supported by experimental data. Our data also supported the predictions that tradeoff relationships exist between F' and vertical impulse as well as between F' and

m_{eff}. In sum, less stiff footwear heels decrease F' while increasing m_{eff} and the vertical impulse of the ground reaction force during the impact phase of walking and heel strike running.

m_{eff} was influenced solely by changes in Δt in the different conditions, and not by changes in F_{max}, Δv or sagittal plane knee and ankle kinematics at the beginning of the impact peak. Knee flexion during Δt for running significantly increased in the softer footpads, likely indicating reduced knee joint stiffness. However, the changes were minimal and unlikely to have had a profound effect on running m_{eff} values because walking m_{eff} changed with condition despite no change in knee or ankle angles during the period of the impact peak (Table 2.1; Table 2.2).

Our calculation of m_{eff} uses a measure of instantaneous velocity of the lower extremity at impact which we obtained by averaging the displacement of the lateral malleolus over 4 ms prior to impact. Measuring impact velocity at the foot may over- or under-estimate the velocity of the portion of the body that stops during impact. However, any discrepancies that this might cause in absolute values of m_{eff} would be consistent across conditions and would likely have no effect on the differences in m_{eff} we found between conditions. Moreover, our results from control conditions are consistent with previously published data. We found m_{eff} to average 6.0% BW (SD +/-1.2) in the walking control condition, which is in agreement with the value of 6.3% BW found by Chi and Schmidt (2005) for barefoot walkers. We found m_{eff} during running to average 6.8% BW (SD +/- 1.4) in the control condition, which is greater than the average of 5.3% BW found by Chi and Schmidt (2005) but identical to the value found by Lieberman et al. 2010 for barefoot heel strike runners. One potential reason for the discrepancy between our data and Chi and Schmidt 2005 in heel strike running m_{eff} is that our runners had a forward speed between 3.06 and 3.42 m/s, while runners in Chi and Schmidt 2005 averaged 2.65 (SD +/- 0.44) m/s. F_{max} tends to increase as forward speed increases (Nigg et al. 1987), which is likely indicative of larger m_{eff} at faster running speeds. Although the hypothesis that m_{eff}

increases with running speed has not been tested, this would explain why this study and Lieberman 2010 (running speeds between 4 and 6 m/s) found greater m_{eff} than Chi and Schmidt 2005.

This study has several limitations. Instrumented treadmills may influence walking and running kinematics, kinetics and muscle activation compared to embedded force plates (Nigg et al. 1995; Wank et al. 1998). In addition, our definition that the impact peak begins when the vertical force reaches 3 standard deviations above treadmill noise (this averaged 25 N across subjects) likely influences the values of Δt, Δv, F', m_{eff} and the vertical impulse. For example, increasing the threshold for the beginning of the impact peak would decrease both Δt and Δv. Despite these methodological limitations, our values for F_{max}, Δv, Δt and m_{eff} are comparable to other studies that have used embedded force plates or that have slightly different definitions for the beginning of impact (Gill and O'Connor 2003; Chi and Schmitt 2005; Lieberman et al. 2010), suggesting our methodology does not confound our results.

Further, F' in previous studies has been measured using smaller force intervals (e.g. from 200N to 90% of F_{max} (Williams et al. 2000; Lieberman et al. 2010)). The method of calculating F' in this study includes the toe and peak regions of the impact peak, where the rate of change of force is not constant. We measured F' using this method because F_{max} during walking often reached no greater than 400 N for some individuals. We would have had low temporal and spatial resolution for measuring F' and foot motion had we chosen a smaller force interval.

An additional limitation of this study is that the footpads necessarily added mass to the subjects' feet. While an ideal experiment would have used experimental footpads of equal mass, we think it is unlikely that the observed changes in m_{eff} were due to the actual mass added by the footpads or differences in mass between the footpads. The hard and soft footpads had an average mass of 0.12 kg and 0.024 kg across subjects, respectfully. The change in m_{eff} from the hard pad to the control

condition was 0.97% and 1.4% of body weight in walking and running, respectively. These percentages are equivalent to 0.63 kg and 0.91 in a 65 kg individual, respectively, which are much greater than the mass of the hard pad alone. Further, the soft pad condition resulted in greater m_{eff} than the hard pad despite having lower mass than the hard pad. Therefore, it is improbable that the mass of the footpads had more than a negligible effect on changes in m_{eff} observed in this study.

This study was designed to test predictions about how impact kinetics change as a result of variations in footwear heel stiffness. An important implication is that the tradeoff relationship between F' and vertical impulse in the experimental footwear used in this study likely also exists for walkers and runners using any kind of footwear. Because both F' and vertical impulse have been hypothesized to be risk factors for some repetitive stress injuries, walking or heel strike running in less stiff footwear heels may decrease injury risk from impact loading rates but increase injury risk from larger vertical impulses. This hypothetical trade-off has yet to be tested, but merits further investigation in order to better understand the effects of different types of footwear heels. Future work in this area should consider how common shoe materials influence F' and vertical impulse, as well as investigate the relationship between specific repetitive stress injuries and elevated values of F' and vertical impulse. A related question is whether larger vertical impulses due to extended impact time durations (as found in this study) have the same effect on skeletal tissues as large vertical impulses due to elevated F_{max}.

An important follow-up question deriving from these results is how muscles modulate the way impact forces are generated and dampened. Lower limb muscle activity changes around the time of impact when individuals walk and run in footwear of varying stiffness (Wakeling and Nigg 2001; Wakeling et al. 2002; Wakeling et al. 2003). These changes may occur in order to modulate F_{max} or to reduce vibrations of soft tissues (Wakeling et al. 2003; Zadpoor and Nikooyan 2010). It is unknown, however, how these changes in muscular activity influence the vertical impulse and m_{eff}. Also, models

that use muscle activity to explain experimental findings concerning impact kinetics would benefit from

incorporating changes in m_{eff} and lower extremity stiffness documented here (Zadpoor and Nikooyan

2010). Changes in muscle activity also function to increase damping when heel striking in less stiff

footwear (Wakeling et al. 2003), but it remains unclear how changes in muscle activation influence m_{eff}

or the vertical impulse.

Acknowledgements

Statement on Conflicts of Interest

The authors have no known conflicts of interest

References

Alexander, R. (2003). <u>Principles of Animal Locomotion</u>. Princeton, NJ., Princeton University Press.

Bobbert, M. F., H. C. Schamhardt, et al. (1991). "Calculation of vertical ground reaction force estimates during running from positional data." <u>Journal of Biomechanics</u> **24**(12): 1095-1105.

Cavanagh, P. R. (1990). <u>Biomechanics of distance running</u>. Champaign, Human Kinetics Publishers.

Chi, K. J. and D. Schmitt (2005). "Mechanical energy and effective foot mass during impact loading of walking and running." <u>Journal of Biomechanics</u> **38**(7): 1387-1395.

Clarke, T. E., E. C. Frederick, et al. (1983). "Effects of shoe cushioning upon ground reaction forces in running." <u>International Journal of Sports Medicine</u> **4**(4): 247-251.

Collins, J. J. and M. W. Whittle (1989). "Impulsive forces during walking and their clinical implications." <u>Clinical Biomechanics</u> **4**(3): 179-187.

Daoud, A. I., G. J. Geissler, et al. (2012). "Foot Strike and Injury Rates in Endurance Runners: A Retrospective Study." <u>Medicine and Science in Sports and Exercise</u> **44**(7): 1325-1334.

Davis, I., C. E. Milner, et al. (2004). "Does increased loading during running lead to tibial stress fractures? A prospective study." <u>Medicine and Science in Sports and Exercise</u> **36**(5): S58-S58.

Dempster, W. T. and G. R. Gaughran (1967). "Properties of body segments based on size and weight." <u>American Journal of Anatomy</u> **120**(1): 33-&.

Folman, Y., J. Wosk, et al. (1986). "Cyclic impacts on heel strike - a possible biomechanical factor in the etiology of degenerative disease of the human locomotor system." <u>Archives of Orthopaedic and Trauma Surgery</u> **104**(6): 363-365.

Gill, H. S. and J. J. O'Connor (2003). "Heelstrike and the pathomechanics of osteoarthrosis: a pilot gait study." <u>Journal of Biomechanics</u> **36**(11): 1625-1631.

Gill, H. S. and J. J. O'Connor (2003). "Heelstrike and the pathomechanics of osteoarthrosis: a simulation study." <u>Journal of Biomechanics</u> **36**(11): 1617-1624.

Hennig, E. M., T. L. Milani, et al. (1993). "Use of ground reaction force parameters in predicting peak tibial accelerations in running." <u>Journal of Applied Biomechanics</u> **9**(4): 306-314.

Hume, P., W. Hopkins, et al. (2008). "Effectiveness of foot orthoses for treatment and prevention of lower limb injuries - A review." <u>Sports Medicine</u> **38**(9): 759-779.

Kerdok, A. E., A. A. Biewener, et al. (2002). "Energetics and mechanics of human running on surfaces of different stiffnesses." <u>Journal of Applied Physiology</u> **92**(2): 469-478.

Lafortune, M. A. and E. M. Hennig (1992). "Cushioning properties of footwear during walking - accelerometer and force platform measurements." <u>Clinical Biomechanics</u> **7**(3): 181-184.

Lafortune, M. A., E. M. Hennig, et al. (1996). "Dominant role of interface over knee angle for cushioning impact loading and regulating initial leg stiffness." Journal of Biomechanics **29**(12): 1523-1529.

Lieberman, D. E., M. Venkadesan, et al. (2010). "Foot strike patterns and collision forces in habitually barefoot versus shod runners." Nature **463**(7280): 531-U149.

Light, L. H., G. E. McLellan, et al. (1980). "Skeletal transients on heel strike in normal walking with different footwear." Journal of Biomechanics **13**(6): 477-480.

Milner, C. E., R. Ferber, et al. (2006). "Biomechanical factors associated with tibial stress fracture in female runners." Medicine and Science in Sports and Exercise **38**(2): 323-328.

Nigg, B. M. (2001). "The role of impact forces and foot pronation: A new paradigm." Clinical Journal of Sport Medicine **11**(1): 2-9.

Nigg, B. M. (2010). "Biomechanics of Sport Shoes. Calgary, Alberta, Canada.".

Nigg, B. M., H. A. Bahlsen, et al. (1987). "The influence of running velocity and midsole hardness on external impact forces in heel toe running." Journal of Biomechanics **20**(10): 951-959.

Nigg, B. M., R. W. Deboer, et al. (1995). "A kinematic comparison of overground and treadmill running." Medicine and Science in Sports and Exercise **27**(1): 98-105.

Nigg, B. M. and W. Liu (1999). "The effect of muscle stiffness and damping on simulated impact force peaks during running." Journal of Biomechanics **32**(8): 849-856.

Pohl, M. B., J. Hamill, et al. (2009). "Biomechanical and Anatomic Factors Associated with a History of Plantar Fasciitis in Female Runners." Clinical Journal of Sport Medicine **19**(5): 372-376.

Shorten, M. and M. I. V. Mientjes (2011). "The 'heel impact' force peak during running is neither 'heel' nor 'impact' and does not quantify shoe cushioning effects." Footwear Science **3**(1): 41-58.

Voloshin, A., J. Wosk, et al. (1981). "Force wave transmission through the human locomotor system." Journal of Biomechanical Engineering-Transactions of the Asme **103**(1): 48-50.

Wakeling, J. M., A. M. Liphardt, et al. (2003). "Muscle activity reduces soft-tissue resonance at heel-strike during walking." Journal of Biomechanics **36**(12): 1761-1769.

Wakeling, J. M. and B. M. Nigg (2001). "Soft-tissue vibrations in the quadriceps measured with skin mounted transducers." Journal of Biomechanics **34**(4): 539-543.

Wakeling, J. M., S. A. Pascual, et al. (2002). "Altering muscle activity in the lower extremities by running with different shoes." Medicine and Science in Sports and Exercise **34**(9): 1529-1532.

Wank, V., U. Frick, et al. (1998). "Kinematics and electromyography of lower limb muscles in overground and treadmill running." International Journal of Sports Medicine **19**(7): 455-461.

Wen, D. (2007). "Risk factors for overuse injuries in runners." Current Sports Medicine Reports **6**(5): 307-313.

Whittle, M. W. (1999). "Generation and attenuation of transient impulsive forces beneath the foot: a review." Gait & Posture **10**(3): 264-275.

Williams, D. S., I. S. McClay, et al. (2000). "Lower extremity mechanics in runners with a converted forefoot strike pattern." Journal of Applied Biomechanics **16**(2): 210-218.

Zadpoor, A. A. and A. A. Nikooyan (2010). "Modeling muscle activity to study the effects of footwear on the impact forces and vibrations of the human body during running." Journal of Biomechanics **43**(2): 186-193.

Zadpoor, A. A., A. A. Nikooyan, et al. (2007). "A model-based parametric study of impact force during running." Journal of Biomechanics **40**(9): 2012-2021.

Chapter 3 – Effects of height and elastic modulus of footwear heels on heel strike running impact peaks

Introduction

Impact peaks in vertical ground reaction force during heel strike running are caused by an inertial change in some portion of the lower extremity over the first 10-50 ms of stance. Impact peaks have received considerable attention because of their potential but debated role in the onset and progression of some musculoskeletal injuries (Folman et al. 1986; Collins and Whittle 1989; Nigg 2001; Gill and O'Connor 2003; Davis et al. 2004; Milner et al. 2006; Wen 2007; Pohl et al. 2009; Nigg 2010; Daoud et al. 2012; Addison and Lieberman 2015). Consequently, the ways in which footwear influences impact peaks has been the focus of much research because of the roles that aspects of footwear, especially the heel, play in terms of enhancing comfort and possibly preventing or mitigating impact peak-related injuries (Wakeling et al. 2002; Hume et al. 2008; Nigg 2010). Many of these studies have focused on how the elasticity of the shoe's heel influences variables that have been implicated in musculoskeletal injuries, especially the magnitude of the impact peak (F_{max}) and its rate of loading (F') (McKenzie et al. 1985; Davis et al. 2004; Milner et al. 2006; Zadpoor and Nikooyan 2010; Zadpoor and Nikooyan 2011; van der Worp et al. 2015).When the impact peak is defined as the first peak in vertical ground reaction force containing all frequency components, studies find that interfaces with a lower elastic modulus (E – the size-corrected stiffness of a material) lead to impact peaks with decreased F' caused by greater impact duration (Δt), while the magnitude of the impact peak (F_{max}) remains mostly unaffected (Light et al. 1980; Clarke et al. 1983; Nigg et al. 1987; Nigg et al. 1988; Lafortune and Hennig 1992; Hennig et al. 1993; Addison and Lieberman 2015). These studies also find heel materials with lower *E* lead to larger effective mass and increased vertical impulse (Addison and Lieberman 2015). Mass-spring-damper models of heel strike running impacts confirm that reducing the interface between the foot and the ground increases Δt and decreases F', and suggest that variations in F_{max} are

29

regulated primarily by changes in lower limb muscular activity (Nigg and Liu 1999; Zadpoor et al. 2007; Zadpoor and Nikooyan 2010).

Although variations in E of the heel are an important source of variation in the generation of impact peaks, modern footwear also varies in the height of the heel, which is likely to have additional important effects on impact peaks during heel strikes. Studies that have investigated the influence of heel height on walking find that it alters plantar pressure distributions, lower extremity kinematics, impact force magnitudes, and accelerations of lower limb segments (Snow and Williams 1994; Voloshin and Loy 1994; Esenyel et al. 2003; Hong et al. 2005). The few studies that have examined the effects of heel height variation on running find that higher heels reduce peak ankle plantarflexion moment but have no effect on foot pronation across the stance phase (Clarke et al. 1983; Reinschmidt and Nigg 1995). Knowledge of how heel height specifically affects heel strike running impact peaks comes primarily from comparisons of the relatively extreme conditions of individuals who are barefoot, minimally shod, or in conventional running shoes with cushioned, elevated heels. These studies indicate that runners in conventional and minimal shoes tend to have a higher incidence of heel strike gaits than barefoot runners, and that barefoot and minimalist shoe runners tend to land with more plantarflexed ankles than conventionally shod runners (Squadrone and Gallozzi 2009; Lieberman et al. 2010; Bonacci et al. 2013; Larson 2014), However, because of the focus on extreme experimental conditions, we know little about the effects of variation in heel height on impact peak kinetics during heel strike running. Moreover, despite the fact that modern footwear varies widely in both the elastic modulus and height of the heel material, there are no data on how variations in both heel height and heel E interact to influence heel strike running impact peaks.

Here we explore how both E and heel height affect the stiffness of the heel-ground interface by using a simple model derived from solid mechanics. The stiffness (k) of any object under compression, including a footwear heel, is equal to E times the cross-sectional area (A) divided by the length. In the

context of footwear heels, the stiffness of the heel material between the foot and the ground (k_{heel}) is

equal to the elastic modulus of the material that comprises the interface (E_{heel}) times A divided by the

vertical length (or height) of the heel:

Equation 1: $k_{heel} = \frac{E_{heel}A}{Heel\ height}$

Equation 1 indicates that k_{heel} is directly influenced by E_{heel} and inversely affected by heel height. In

other words, decreasing E_{heel} and increasing heel height have the same effect: decreasing the value of

k_{heel}.

It is therefore possible to use findings from studies that experimentally alter foot-ground

interface stiffness by varying E to predict how heel strike running impact peaks will be influenced by

variations in heel height. As mentioned above, several studies have found that decreasing the elastic

modulus of the foot-ground interface results in increases to Δt, decreases in F', and increased vertical

impulse and effective mass (Light et al. 1980; Hennig et al. 1993; Wakeling et al. 2003; Addison and

Lieberman 2015). Equation 1 suggests that increasing heel height will also have the same effects

because higher heels, like materials with lower E, reduce the stiffness of the interface. In addition,

modeling studies of heel strike running have shown that lower limb muscle activity regulates impact

force magnitudes, rendering F_{max} independent of variations in foot-ground interface stiffness (Zadpoor

and Nikooyan 2010). We therefore hypothesize that reducing foot-ground stiffness by increasing heel

height will result in heel strike running impact peaks that have longer Δt, slower F', increased effective

mass, and increased vertical impulse for a given individual. We also hypothesize that F_{max} will be

unaffected by variations in heel height for a given individual.

Equation 1 further indicates that the effects of heel height and E on interface stiffness are

multiplied. Practically speaking, simultaneously increasing the height of a running shoe's heel while

decreasing E of the heel will both act to decrease foot-ground interface stiffness, amplifying their

effects on impact peaks. Specifically, we hypothesize that the highest footwear heels made of materials with the lowest E will result in the longest Δt, the slowest F', the largest vertical impulse and the greatest effective mass for a given individual. We hypothesize that F_{max} within an individual will remain unaffected by variation in heel height or elastic modulus.

This study therefore tests two main hypotheses about how variation in footwear heel construction affects heel strike running impact peaks within individuals. First, we hypothesize that increasing heel height will have similar effects on heel strike running impact peaks as reducing interface modulus. That is, a given individual heel strike running in high heeled footwear will generate impact peaks that have longer Δt, slower F', increased vertical impulse and greater effective mass. Second, the effects of heel height and E_{heel} will be multiplied such that individuals will generate impact peaks with the longest Δt, slowest F', largest vertical impulse and greatest effective mass when wearing footwear with the highest heels that are made of materials with the lowest E. Additionally, we hypothesize that F_{max} will remain unaffected by heel height or E within an individual.

Methods

Subjects

Fifteen healthy adult males between the ages of 19 and 26 (body mass (kg): 68.7 (+/- 4.9), height (cm) 176.3 (+/- 6.1)) participated in this study, which was approved by the Institutional Review Board of Harvard University. We used only males with a shoe size of 10M (American) in order to limit the number of experimental shoes constructed for this study (see below). Participants gave their informed consent and the experiments were conducted at the Skeletal Biology and Biomechanics Lab of the Department of Human Evolutionary Biology at Harvard University.

Mechanical testing of heel materials

We used 3 different materials that encompass the stiffness range of commercially available shoe materials. Each material was cut into squares with edge lengths of 25.4 mm and thickness of 6 mm and mechanically tested under compression to measure E. Compression testing was performed using an Instron model 4201 (Instron, Norwood, MA, USA) at a rate of 10 mm/min and data were collected at 1kHz. Stress (change in force divided by area) and strain (change in length divided by original length) were calculated from the raw data. E was measured between 0 and .5 strain (50% strain) and calculated as the slope of the best-fit least-squares regression line of the raw data (the slopes of stress vs. strain from 0 to 50% were approximately linear for each material; see Appendix 2). The measured E of the materials from smallest to largest was 1.6 MPa (soft), 32 MPa (medium) and 45 MPa (hard).

Footwear construction

In order to create footwear that varied in both heel height and elastic modulus, an experienced, professional cobbler (Felix Shoe Repair, Cambridge, MA, USA) was hired to add heels to the bottom of zero-drop minimal shoes with a 5.5 mm stack height that lacked any elevation or added cushioning (make: Merrell (Rockford, Michigan, USA), model: Vapor Glove, shoe size M10 (American)). We used the three materials described above that differed in E combined with three different heel heights to create 9 different sets of footwear. The lowest heel height condition (6mm) was made so that the varying elastic modulus material (6 mm height) was attached directly to the bottom of the heel region of the minimal shoes. The medium heel height condition (14 mm) was created by gluing a stiff heel riser 8 mm thick directly to the bottom of the heel region of the shoes, and then gluing the materials that varied in elastic modulus (6 mm height) to the bottom of the heel riser. The highest heel height condition (20 mm) was designed in the same manner as the medium height condition, but a 14 mm thick heel riser was used (Figure 3.1).
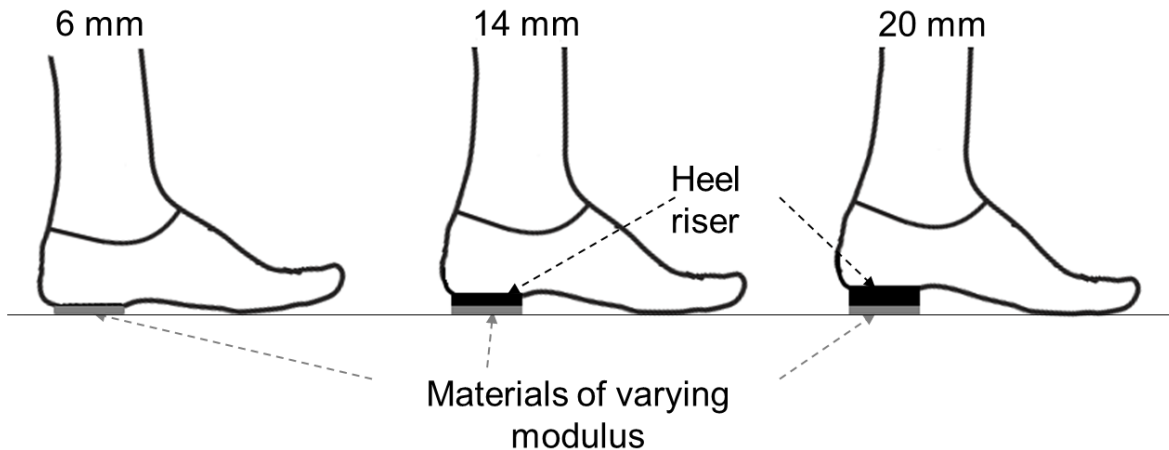
Figure 3.1: Construction of experimental footwear. In the 6 mm height condition, the materials of varying elastic modulus were glued directly to the bottom of the heel region of minimal footwear. In the 14 and 20 mm height conditions, stiff heel risers (8 and 14 mm in height, respectively) were glued in between the bottom of the minimal footwear and the materials of varying elastic modulus.

Experimental design and measurements

Participants ran in each of the 9 footwear conditions described above. The order of footwear condition was randomized across subjects. Participants ran at a Froude number of 1.25 (actual forward velocities ranged from 3.20 to 3.43 m/s) in order to ensure dynamic similarity between participants that varied in leg length (Alexander 2003). Prior to data collection, each subject practiced running on the treadmill in minimal footwear at the prescribed Froude number and their preferred step frequency was recorded. Each subjects' preferred step frequency was played back via an electronic metronome during each trial and subjects were instructed to keep to this step frequency to the best of their ability to avoid complications with changes in support mechanics when the foot-ground interface stiffness is altered (Kerdok et al. 2002).

Ground reaction forces and lower limb kinematics were measured during the period of the impact peak. The impact peak was defined as the first peak in vertical force containing all frequency components. A treadmill instrumented with a force-plate (BERTEC, Columbus, Ohio, USA) recorded

ground reaction force data at 2 kHz. Kinetic data were low-pass filtered at 100 Hz prior to data analysis.

The impact peak was considered to begin when the vertical ground reaction force value exceed 50 N and

ended at F_{max}. Lower limb kinematic data were collected at 1 kHz with an eight camera Oqus system

(QUALYSIS, Gothenburg, Sweden) with a spatial resolution of 0.5 mm. Markers (12.7 mm in diameter)

were placed on the skin of the right lower extremity over the anterior superior iliac spine (ASIS), greater

trochanter, medial and lateral femoral condyles, medial and lateral malleoli. Three additional markers

(also 12.7 mm diameter) were placed on the exterior of the footwear: two markers spanning the medial-

lateral distance of the toe box of the shoe and a single marker on the rear heel region of the shoe facing

posteriorly. Kinematic data was collected only from the right leg, and all subsequent analyses were

performed on data from only the right leg.

We measured several kinetic variables of the impact peak that have been hypothesized to be

related to the etiology of repetitive stress injuries, including F_{max}, F' and vertical impulse (Voloshin et

al. 1981; Collins and Whittle 1989; Davis et al. 2004; Milner et al. 2006; Zadpoor and Nikooyan 2011).

We also measured Δt, impact velocity (Δv) in the vertical direction and effective mass (m_{eff}). In

addition, we measured sagittal plane hip, knee and ankle angles because these kinematic variables

influence both F_{max} and F' (Lafortune et al. 1996; Derrick 2004). Only the vertical components of kinetic

and kinematic variables were considered because over 90% of the total ground reaction force during the

impact phase of running is due to the vertical force (Cavanagh 1990). We calculated F' between 200 N

and 90% of F_{max} following the methods of previous studies (Williams et al. 2000; Lieberman et al. 2010).

We measured instantaneous velocity of the foot (Δv) by dividing the change in lateral malleolus position

by the change in time for the four time frames (4 ms) prior to the beginning of the impact peak. We

measured m_{eff} and vertical impulse during the period of the impact peak using previously published

methods (Chi and Schmitt 2005; Lieberman et al. 2010). Briefly, vertical impulse was calculated as the

integral of the impact peak over Δt, and m_{eff} was calculated as the vertical impulse divided by ($\Delta v +$

$g\Delta t$), where v, g and t are velocity, the acceleration due to gravity and time, respectively. Knee and ankle angles were measured at the beginning of the impact peak and at F_{max}. Knee angle was measured between the greater trochanter, lateral femoral condyle and lateral malleolus markers, and ankle angle was measured between the lateral femoral condyle, lateral malleolus and the most lateral marker on the shoe toe-box. Ankle contact angle and knee contact angle were measured as the ankle and knee angle at the onset of impact, respectively. Ankle plantarflexion was measured as the ankle angle at F_{max} minus ankle contact angle, and knee flexion was measured as the knee angle at F_{max} minus knee contact angle.

Data analysis

Individual steps were removed from the analysis when F_{max} was three standard deviations from the average F_{max} for the given subject and condition. We then analyzed 25 steps from the right leg per subject per condition. Averages for all variables were taken from these 25 steps and used in all subsequent analyses.

Our study tested how footwear heel height and elastic modulus influenced heel strike running impact peaks within participants and required repeated sampling of participants. We therefore used general linear mixed models (GLMM) to test how heel height and elastic modulus affected kinetic aspects of the impact peak for a given participant. Briefly, GLMMs use both fixed effects (effects that are directly manipulated in the experiment) and random effects (effects that are randomly selected from a population) as predictors while accounting for the auto-correlation that results from repeated measures of participants (McCulloch and Searle 2001). The GLMM thus models the correlation of outcome measures within participants for the 9 experimental conditions used in this study. Heel height and E were considered fixed effects in the GLMMs because we directly altered these variables in the experiment. Participants were random effects because each individual was randomly selected from the population.

Our first hypothesis was that increasing heel height would have the same effects on heel strike running impacts as decreasing the elastic modulus of the heel material. We tested this hypothesis using two different GLMMs. The first GLMM considers the effects of heel height and elastic modulus on impact peak kinetic variables. A second GLMM was used to further assess the influence of lower extremity kinematics, and thus considers the effects of heel height, elastic modulus of the heel, and of lower extremity kinematics on the impact peak kinetic variables. The first GLMM equation used to test this hypothesis took the following form:

$$Kinetic\ variable = \beta_1 Heel\ Height + \beta_2 Heel\ Elastic\ Modulus + \beta_3\ Interaction + ZU + \in$$

The kinetic variables examined were F_{max}, Δt, F', vertical impulse and m_{eff}. β_i is the fixed-effect coefficient of the ith predictor, Z is the matrix for the random grouping variable, U is the vector of random effects (participants), and $\in$ is the residual model error. Interaction refers to the interaction between heel height and the elastic modulus of the heel.

The second GLMM equation used to test this hypothesis was:

$$
\begin{aligned}
Kinetic\ variable \\
= \beta_1 Heel\ Height + \beta_2 Heel\ Young's\ Modulus + \beta_3\ Interaction \\
+ \beta_4\ Ankle\ Contact\ Angle + \beta_5\ Ankle\ Plantarflexion + \beta_6\ Knee\ Contact\ Angle \\
+ \beta_7\ Knee\ Flexion + ZU + \in
\end{aligned}
$$

The kinetic variables tested in this equation are the same as above. Ankle contact angle, ankle plantarflexion, knee contact angle and knee flexion were continuous variables and measured as described above.

Our second hypothesis was that individuals would generate impact peaks with the longest Δt, slowest F', largest vertical impulse and greatest m_{eff} when wearing footwear that had the highest heels made of materials with the lowest E. This hypothesis requires that we test for the effects of each experimental footwear condition within each participant. The GLMM equation used to test this hypothesis took the following form:

$$Kinetic\ variable = \ \beta_1 Footwear\ condition + ZU + \in$$

The kinetic variables examined were F_{max}, Δt, F', vertical impulse and m_{eff}. Footwear condition refers to the 9 different footwear conditions used in the experiment: 6mm heel height with soft, medium and hard elastic modulus, 14mm heel height with soft, medium and hard elastic modulus, and 20mm heel height with soft, medium and hard elastic modulus.

All kinetic outcome variables and kinematic predictor variables were log-transformed and then converted to Z-scores prior to examination via GLMMs. The GLMMs report statistical results (F-ratio, p-value) for fixed effects. For the first hypothesis, the fixed effects were heel height, heel elastic modulus the interaction between height and elastic modulus, ankle contact angle, ankle plantarflexion, knee contact angle and knee plantarflexion. For the second hypothesis, the fixed effect was the footwear condition. The GLMMs also report parameter estimates (coefficients, standard error, t-ratio and p-value) for each experimental condition relative to a baseline condition. For the first hypothesis, the baseline conditions were the 6mm heel height (for the height conditions) and the hard elastic modulus condition (for the elastic modulus conditions) and t-ratios and p-values are reported relative to these conditions for both GLMMs (Table 3.1, Table 3.2). For the second hypothesis, the baseline condition for the GLMM was the 20mm height-soft elastic modulus condition and t-ratios and p-values are reported relative to this condition (Table 3.3). For all statistical tests, significance was assigned to p-values < 0.05.

Results

Effects of heel height and elastic modulus on impact kinetics

In the first GLMM, we considered the effects of heel height and elastic modulus on F_{max}, Δt, F', vertical impulse and m_{eff}. This section reports the results of that model. The model results are also found in Table 3.1.

Table 3.1: Effects of footwear condition on impact peak kinetic variables

Kinetic Variable	Model Effect	Coefficient estimate	Std. Error	F-ratio	t-value	p-value
F_{max} (BW)	Heel Height			77.0		*<0.0001*
	14 mm	0.162	0.0471		-3.43	*0.0008*
	20 mm	-0.567	0.0471		-12.04	*<0.0001*
	Elastic Modulus			2.80		0.07
	Medium	0.0117	0.0471		0.25	0.80
	Soft	0.09	0.0471		1.91	0.058
	Interactions			3.2		*0.015*
	14* soft	-0.1	0.0666		-1.51	0.14
	14*medium	0.176	0.0666		2.65	*0.009*
	20*soft	0.174	0.0666		2.61	*0.01*
	20*medium	-0.0935	0.0666		-1.4	0.163
Δt (s)	Heel Height			30.1		*<0.0001*
	14 mm	0.00503	0.612		0.08	0.93
	20 mm	0.409	0.612		6.68	*<0.0001*
	Elastic Modulus			4.92		*0.009*
	Medium	-0.159	0.612		-2.61	*0.01*
	Soft	-0.0127	0.612		-0.21	0.83
	Interactions			2.04		0.09
	14* soft	-0.0179	0.0866		-0.21	0.83
	14*medium	-0.102	0.0866		-1.18	0.24
	20*soft	-0.151	0.0866		-1.75	0.084
	20*medium	0.207	0.0866		2.39	*0.0185*
F' (BW/s)	Heel Height			77.2		*<0.0001*
	14 mm	0.296	0.0531		-5.56	*<0.0001*
	20 mm	-0.659	0.0531		-12.4	*<0.0001*
	Elastic Modulus			5.98		*0.003*
	Medium	0.156	0.0531		2.9	*0.005*
	Soft	0.00966	0.0531		0.18	0.86
	Interactions			11.6		*<0.0001*
	14* soft	-0.149	0.0752		-1.98	0.0502
	14*medium	0.376	0.0752		5	*<0.0001*
	20*soft	0.370	0.0752		4.93	*<0.0001*
	20*medium	-0.301	0.0752		-4.01	*0.0001*
Vertical Impulse (BW*ms)	Heel Height			20.9		*<0.0001*
	14 mm	-0.454	0.0765		-5.93	*<0.0001*
	20 mm	0.399	0.0765		5.21	*<0.0001*
	Elastic Modulus			6.02		*0.003*
	Medium	-0.230	0.0765		-3	*0.003*
	Soft	0.230	0.0765		3	*0.003*
	Interactions			7.63		*<0.0001*
	14* soft	0.00389	0.108		0.04	0.97
	14*medium	-0.222	0.108		-2.05	*0.04*
	20*soft	-0.471	0.108		-4.35	*<0.0001*
	20*medium	0.345	0.108		3.18	*0.002*

Table 3.1 (Continued): Effects of footwear condition on impact peak kinetic variables

	Heel Height			10.6		***<0.0001***
	14 mm	-0.342	0.0774		-4.42	***<0.0001***
	20 mm	0.257	0.0774		3.32	***0.001***
	Elastic Modulus			4.34		***0.02***
	Medium	-0.124	0.0774		-1.60	0.11
m_{eff} (%BW)	Soft	0.228	0.0774		2.94	***0.004***
	Interactions			5.76		***0.0003***
	14* soft	-0.0488	0.109		-0.45	0.66
	14*medium	-0.228	0.109		2.08	***0.04***
	20*soft	-0.351	0.109		-3.21	***0.002***
	20*medium	0.327	0.109		2.98	***0.004***

F_{max} was significantly influenced by heel height (F=77.0, p<0.001; Table 3.1). Both the 14mm (p=0.0008) and 20mm (<0.0001) conditions resulted in lower F_{max} than the 6mm condition (Figure 3.2A). F_{max} was not influenced by elastic modulus of the heel (F=2.80, p=0.07). The interaction between height and elastic modulus on F_{max} was statistically significant (F=3.2, p=0.015). In particular, there were significant interactions between the 14mm height condition and the medium elastic modulus condition (p=0.009) and between the 20mm height condition and the soft elastic modulus condition (p=0.01).

Δt was significantly influenced by both heel height (F=30.1, p<0.0001) and E (F=4.92, p=0.009; Table 3.1). The 20mm height condition resulted in longer Δt than the 6mm condition (p<0.0001), while the 14mm condition was not significantly different from the 6mm condition (p=0.93; Figure 3.2B). Among heel elastic modulus conditions, the medium condition resulted in significantly shorter Δt than the hard condition (p=0.01). The soft condition was not significantly different from the hard condition (p=0.83). The interaction between heel height and elastic modulus on Δt was not significant (F=2.04, p=0.09).

F' was significantly affected by heel height (F=77.2, p<0.0001; Figure 3.2C), E (F=5.98, p=0.003) and the interaction between height and E (F=11.6, p<0.0001; Table 3.1). F' was significantly lower in the 20mm and 14mm conditions than in the 6mm condition (p<0.0001, and p<0.0001, respectively). Within

E conditions, F' was greater in the medium condition than the hard condition (p=0.005), but the soft

condition was not significantly different from the hard condition (p=0.86). The 14mm condition

interacted with the medium E condition (p<0.0001) and the 20mm condition had significant interactions

with the soft and medium conditions (p<0.0001, and p=0.0001, respectively).

The vertical impulse of the impact peak was affected by heel height (F=20.9, p<0.0001; Figure

3.2D), E (F=6.02, p=0.003) and the interaction between height and E (F=7.6, p<0.0001; Table 3.1).

Among height conditions, the 14 mm condition resulted in a lower vertical impulse than the 6mm

condition (p<0.0001) and the 20mm condition led to a greater vertical impulse than the 6mm condition

(p<0.0001). Within elastic modulus conditions, vertical impulse in the hard condition was greater than

the medium condition (p=0.003) and less than the soft condition (p=0.003). There was a significant

interaction between the 14mm height condition and the medium E condition (p=0.04), and the 20mm

height condition had significant interactions with the soft (p<0.0001) and medium (p=0.002) E

conditions.

m_{eff} was significantly influenced by heel height (F = 10.6, p<0.0001; Figure 3.2E, Table 3.1)),

with the 6mm condition leading to greater m_{eff} than the 14mm condition (p<0.0001) but lower m_{eff}

than the 20mm condition (p=0.001). m_{eff} was significantly influenced by elastic modulus condition

(F=4.34, p=0.02, Table 3.1). The hard and medium condition were not significantly different from each

other (p=0.110), but m_{eff} was greater in the soft condition than the hard condition (p=0.004). The

interactions between heel height and elastic modulus had significant effects on m_{eff} (F=5.76, p=0.0003,

Table 3.1). The 14mm condition interacted with the medium elastic modulus condition (p=0.04), and the

20mm height condition had significant interactions with both the soft (p=0.002) and medium (p=0.004)

elastic modulus conditions.
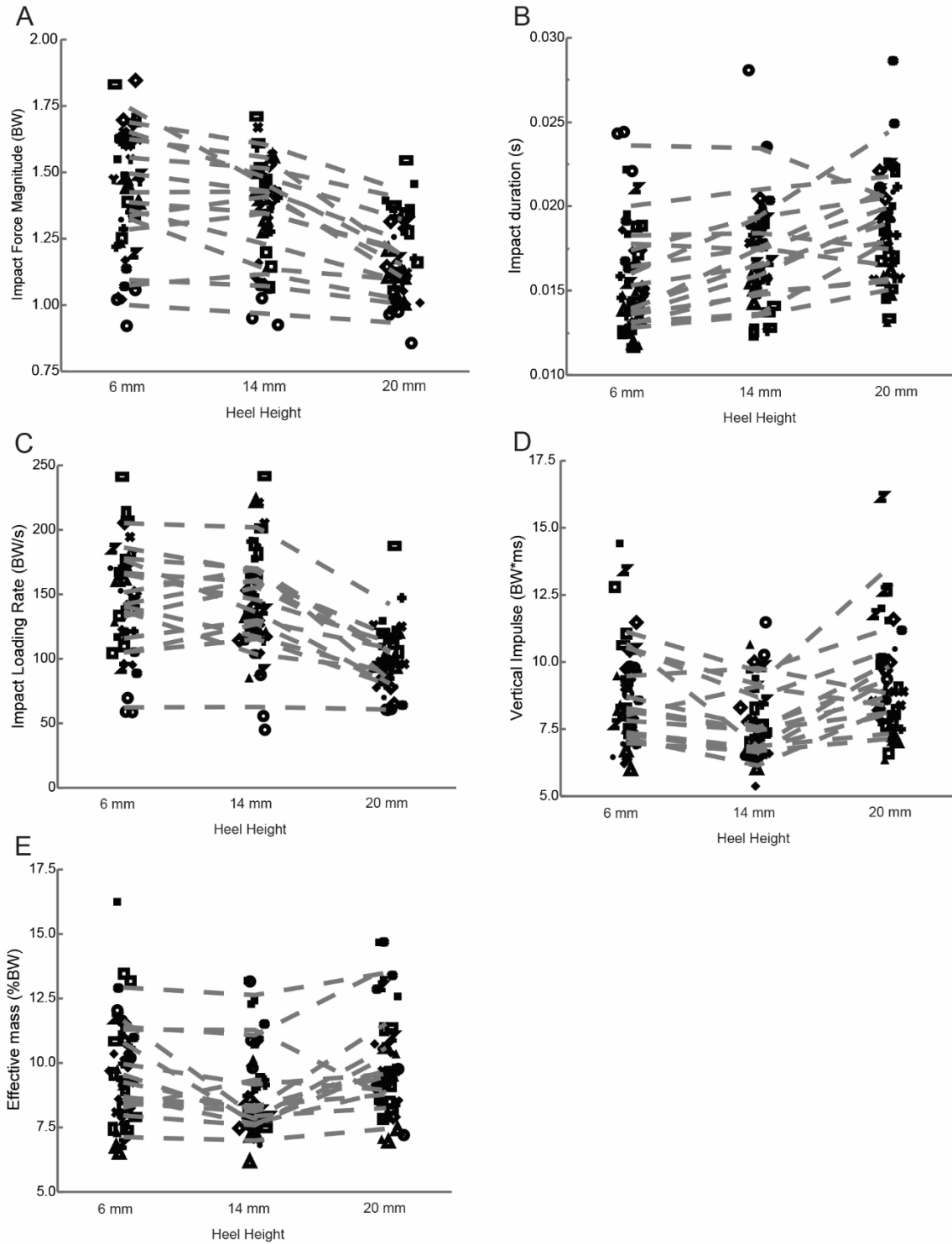
Figure 3.2: F_{max} (A), Δt (B), F' (C), vertical impulse (D) and m_{eff} (E) results for each of the heel height conditions studied. Each subject is represented by a unique symbol and dashed lines connect participants between conditions.

Table 3.2: Effects of footwear condition and lower extremity kinematics on impact peak kinetic variables

Kinetic Variable	Model Effect	Coefficient estimate	Std. Error	F-ratio	t-value	p-value
F_{max} (BW)	Heel Height			37.8		*<0.0001*
	14 mm	0.146	0.457		-3.19	*0.0018*
	20 mm	-0.466	0.0534		-8.68	*<0.0001*
	Elastic Modulus			2.16		0.12
	Medium	-0.0526	0.0484		-1.09	0.28
	Soft	0.0934	0.0450		2.07	*0.0404*
	Interactions			2.39		0.06
	14* soft	-0.0687	0.064		-1.07	0.29
	14*medium	0.108	0.0656		1.66	0.10
	20*soft	0.129	0.0646		2.01	*0.0474*
	20*medium	-0.0104	0.066		-0.16	0.87
	Ankle contact angle	-0.115	0.106	1.17	-1.08	0.28
	Ankle plantarflexion	-0.163	0.0748	4.75	-2.18	*0.0313*
	Knee contact angle	0.00214	0.0736	0.0009	0.03	0.98
	Knee flexion	-0.179	0.0539	11.0	-3.32	*0.001*
Δt (s)	Heel Height			9.92		*0.0001*
	14 mm	0.0201	0.0475		0.42	0.67
	20 mm	0.204	0.0544		3.76	*0.0003*
	Elastic Modulus			0.144		.87
	Medium	-0.018	0.0501		-0.36	0.72
	Soft	-0.00826	0.0469		-0.18	0.86
	Interactions			1.20		0.32
	14* soft	-0.0679	0.0666		-1.02	0.31
	14*medium	0.0408	0.682		0.06	0.55
	20*soft	-0.0749	0.0672		-1.11	0.27
	20*medium	0.0202	0.0686		0.29	0.77
	Ankle contact angle	0.206	0.0926	4.96	2.23	*0.03*
	Ankle plantarflexion	0.190	0.0742	6.58	2.57	*0.01*
	Knee contact angle	0.0315	0.0717	0.193	0.44	0.66
	Knee flexion	0.5002	0.0549	82.9	9.11	*<0.0001*

Table 3.2 (Continued): Effects of footwear condition and lower extremity kinematics on impact peak kinetic variables

	Heel Height			54.8		**<0.0001**
	14 mm	0.278	0.0463		-6.02	**<0.0001**
	20 mm	-0.557	0.0538		-10.3	**<0.0001**
	Elastic Modulus			0.954		0.39
	Medium	0.0538	0.0489		1.10	0.27
	Soft	0.0103	0.0456		0.23	0.82
	Interactions			11.2		**<0.0001**
	14* soft	-0.121	0.0648		-1.87	0.0640
	14*medium	0.287	0.0665		4.32	**<0.0001**
F' (BW/s)	20*soft	0.324	0.0654		4.95	**<0.0001**
	20*medium	-0.179	0.0669		-2.68	**0.009**
	Ankle contact angle	-0.00354	0.101	0.0012	-0.03	0.972
	Ankle plantarflexion	-0.0965	0.0747	1.67	-1.29	0.199
	Knee contact angle	0.0426	0.0731	0.340	0.58	0.56
	Knee flexion	-0.373	0.0543	47.1	-6.86	**<0.0001**
	Heel Height			19.9		**<0.0001**
	14 mm	-0.435	0.0689		-6.30	**<0.0001**
	20 mm	0.237	0.0794		2.99	**0.003**
	Elastic Modulus			5.82		**0.004**
	Medium	-0.102	0.0727		-1.40	.16
	Soft	0.231	0.0679		3.40	**0.0009**
	Interactions			7.32		**<0.0001**
	14* soft	-0.0391	0.0966		-0.40	0.69
	14*medium	-0.0982	0.0989		-0.99	0.32
Vertical Impulse (BW*ms)	20*soft	-0.406	0.0975		-4.16	**<0.0001**
	20*medium	0.185	0.0996		1.86	0.066
	Ankle contact angle	0.0929	0.1407	0.436	0.66	0.512
	Ankle plantarflexion	0.175	0.109	2.58	1.61	0.11
	Knee contact angle	0.0120	0.106	0.0129	0.11	0.91
	Knee flexion	0.435	0.0801	29.4	5.42	**<0.0001**

Table 3.2 (Continued): Effects of footwear condition and lower extremity kinematics on impact peak kinetic variables

				F	t	p
m_{eff} (%BW)	Heel Height			9.45		***0.0002***
	14 mm	-0.0275	0.00643		-4.27	***<0.0001***
	20 mm	0.00912	0.00734		1.24	.21
	Elastic Modulus			5.29		***0.0064***
	Medium	-0.00203	0.00677		-0.30	0.76
	Soft	0.0190	0.00635		3.00	***0.003***
	Interactions			4.54		***0.002***
	14* soft	-0.00843	0.00902		-0.93	0.35
	14*medium	-0.0112	0.00923		-1.21	0.23
	20*soft	-0.0240	0.0091		-2.64	***0.01***
	20*medium	0.0160	0.00929		1.72	0.088
	Ankle contact angle	0.0190	0.0121	2.44	1.56	0.13
	Ankle plantarflexion	0.0199	0.00993	4.0	2.00	0.05
	Knee contact angle	-0.0117	0.00957	1.49	-1.22	0.22
	Knee flexion	0.0312	0.00739	17.7	4.21	***<0.0001***

Effects of heel height, elastic modulus and lower extremity kinematics on impact kinetics

In the second GLMM, we considered the effects of heel height and elastic modulus on F_{max}, Δt, F', vertical impulse and m_{eff}. This section and Table 3.2 report the results of the second GLMM.

F_{max} was significantly influenced by heel height (F=37.8, p<0.0001), ankle plantarflexion during impact (F=4.75, p=0.03) and knee flexion during impact (F=11.0, p=0.001) (Table 3.2). Both the 14mm and 20mm heel height conditions resulted in lower F_{max} than the 6mm condition (p=0.002 and p<0.0001, respectively). Increased ankle plantarflexion was associated with lower F_{max}, as was greater knee flexion during the impact (Figure 3.3A).

Δt was significantly influenced by heel height (F=9.92, p=0.0001; Table 3.2), with the 20mm condition leading to longer Δt than the 6mm condition (p=0.0003). Δt was also significantly affected by ankle contact angle (F=4.96, p=0.03), ankle plantarflexion during the impact (F=6.58, p=0.01) and knee flexion during the impact (F=82.9, p<0.0001). Increased knee flexion was associated with longer Δt within subjects (Figure 3.3B).
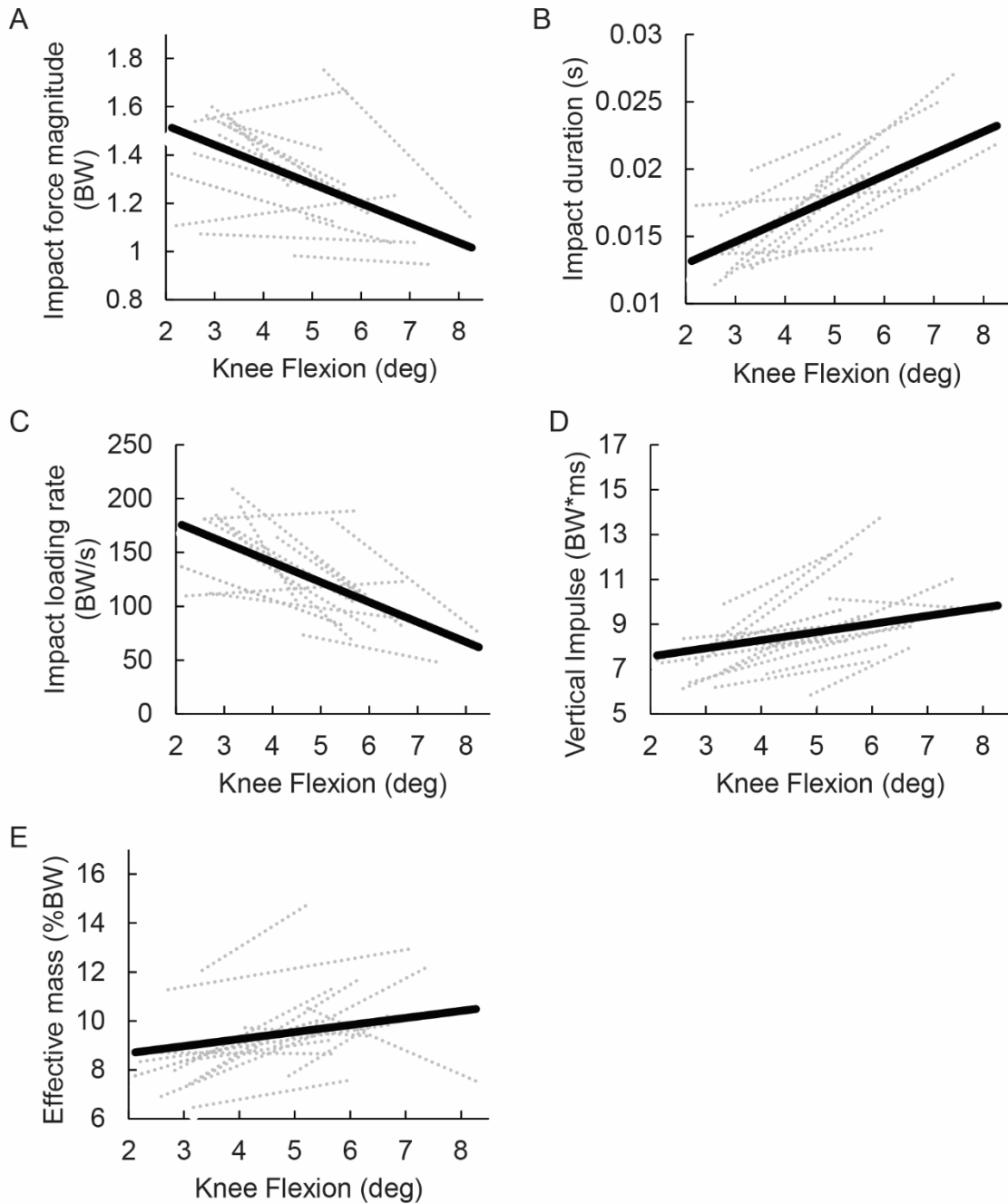
Figure 3.3: F_{max} (A), Δt (B), F' (C), vertical impulse (D) and m_{eff} (E) versus knee flexion during the impact peak. Large, black lines represent the best-fit trend across all participants as fitted by least-squares regression. Grey dotted lines represent the best-fit trends for individual participants as fitted by least squares regression.

Heel height (F=54.8, p<0.0001), the interaction between heel height and E (F=11.2, p<0.0001), and knee flexion during impact (F=47.1, p<0.0001) all had significant effects on F' (Table 3.2). The 14mm and 20mm heel height conditions resulted in slower F' than the 6mm height condition (p<0.0001 and

p<0.0001, respectively; Figure 3.2C). There were significant interactions between the 14mm height and medium elastic modulus condition (p<0.0001), the 20mm height and the soft elastic modulus condition (p<0.0001) and the 20mm height and medium elastic modulus condition (p=0.009). Increased knee flexion during the impact was correlated with decreased F' (Figure 3.3C) within subjects.

Vertical impulse was significantly influenced by heel height (F=19.9, p<0.0001), elastic modulus of the heel (F=5.82, p=0.004), the interaction between heel height and elastic modulus (F=7.32, p<0.0001) and knee flexion during the impact (F=29.4, p<0.0001; Table 3.2). The 6mm heel height condition led to greater vertical impulse than the 14mm condition (p<0.0001) but lower vertical impulse than the 20mm condition (p=0.003, Figure 3.2D). Among elastic modulus condition, the soft condition led to greater vertical impulse than the hard condition (p=0.0009). There was a significant interaction between the 20mm height condition and the soft elastic modulus condition (p<0.0001). Finally, increased knee flexion was associated with greater vertical impulse within individuals (p<0.0001, Figure 3.3D).

m_{eff} within individuals was significantly affected by heel height (F=9.45, p=0.0002), elastic modulus (F=5.29, p=0.006), the interaction between heel height and elastic modulus (F=4.54, p=0.002), and knee flexion (F=17.7, p<0.0001; Table 3.2). The effect of ankle plantarflexion on m_{eff} trended towards statistical significance (F=4.0, p=0.05). Among heel height conditions, the 14mm condition resulted in lower m_{eff} than the 6mm condition (p<0.0001) and among elastic modulus conditions the soft condition led to greater m_{eff} than the hard condition (p=0.003). There was a significant interaction between the 20mm height and soft elastic modulus conditions (p=0.01). Within individuals, increased knee flexion during the impact was correlated with greater m_{eff} (p<0.0001, Figure 3.3E).
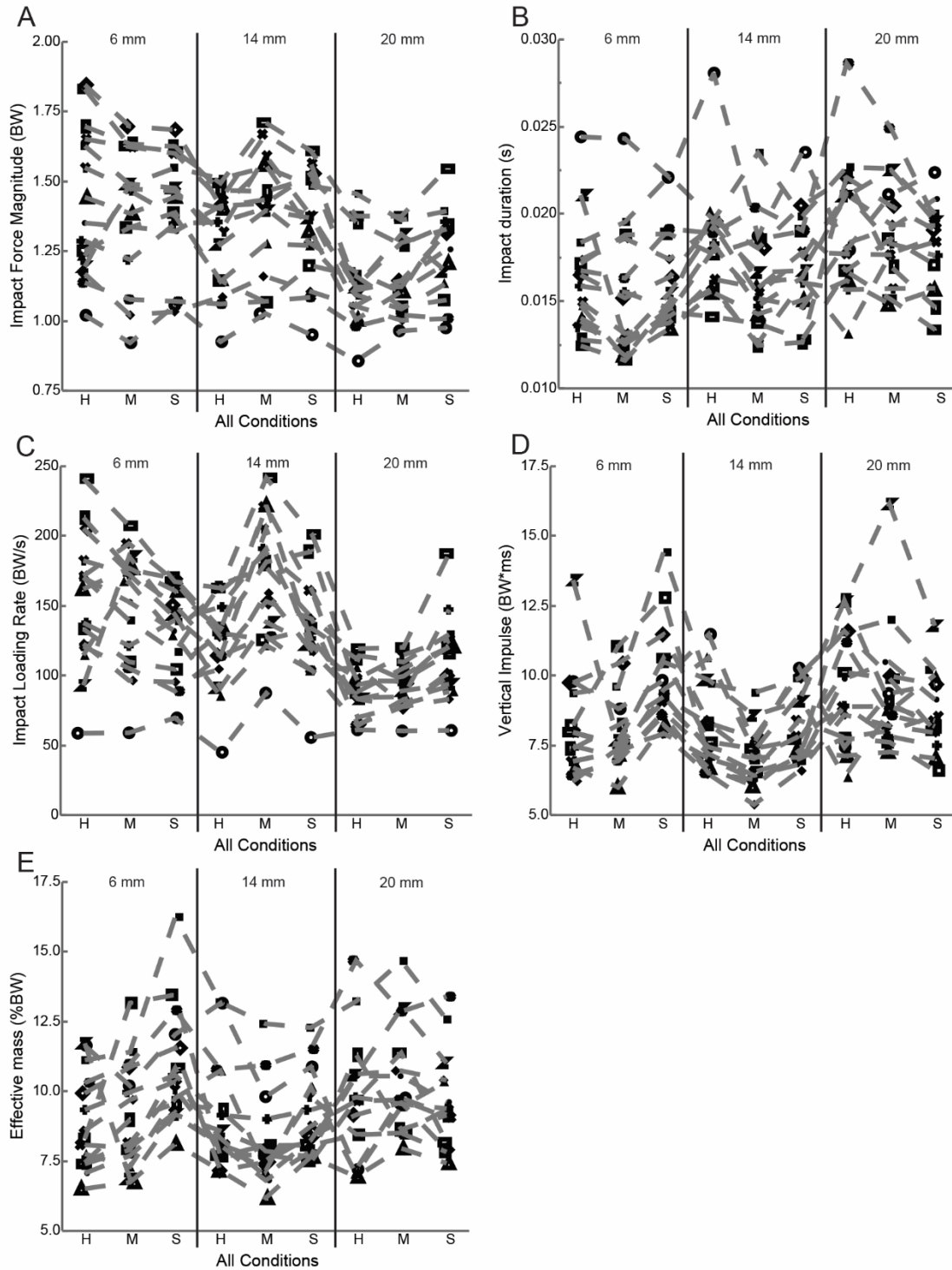
Figure 3.4: F_{max} (A), Δt (B), F' (C), vertical impulse (D) and m_{eff} (E) in each experimental condition. The hard, medium and soft elastic modulus conditions are represented by H, M and S, respectively. Solid vertical lines separate the heel height conditions (from left to right: 6mm, 14mm and 20mm). Each participant is represented by a unique symbol and dashed lines connect participants between conditions.

Effects of individual footwear conditions on impact kinetics

The second hypothesis of this study predicted that individuals would generate impacts with the greatest Δt, slowest F', largest vertical impulse and greatest m_{eff} in footwear with the highest heels made of materials with the lowest E, while F_{max} would remain unaffected. We tested this hypothesis using a GLMM that considered the effects of each of the 9 footwear conditions. The results of this GLMM are reported below and in Table 3.3.

F_{max} within individuals was significantly influenced by shoe condition (F=21.6, p<0.0001; Figure 3.4A, Table 3.3). The 20mm-soft condition resulted in significantly lower F_{max} than either the 6mm-hard, 6mm-medium or 6mm-soft conditions (p<0.0001, p=0.0006, and p<0.0001, respectively). The 20mm-soft condition also had lower F_{max} than the 14mm-medium condition (p=0.0003). However, the 20mm-soft condition resulted in greater F_{max} than the 20mm-hard and 20mm-medium conditions (p<0.0001 and p<0.0001, respectively).

Footwear condition had a significant effect on Δt (F=9.77, p<0.0001; Figure 3.4B, Table 3.3). The 20mm-soft condition resulted in significantly greater Δt compared to the 6mm-hard, medium and soft conditions (p=0.01, p<0.0001 and p=0.04, respectively) and greater Δt compared to the 14mm-hard and medium conditions (p=0.02 and p=0.04, respectively). The 20mm-soft condition led to smaller Δt when compared to the 20mm-hard and 20mm-medium conditions (p<0.0001 and p=0.0003, respectively).

F' was significantly affected by footwear condition (F=26.6, p<0.0001; Figure 3.4C, Table 3.3). The 20mm-soft condition had significantly slower F' than 6mm-hard, 6mm-medium and 14mm-medium conditions (p<0.0001, p<0.0001 and p<0.0001, respectively). However, the 20mm-soft condition had significantly greater F' than the 20mm-hard and 20mm-medium conditions (p<0.0001 and p<0.0001, respectively).

Table 3.3: Effects of each experimental conditions on impact peak kinetic variables

Kinetic Variable	Model Effect	Coefficient estimate	Std. Error	F-ratio	t-ratio	p-value
F_{max} (BW)	All Conditions			21.6		*<0.0001*
	6mm*Hard	0.459	0.094		4.88	*<0.0001*
	6mm*Medium	0.334	0.094		3.55	*0.0006*
	6mm*Soft	0.422	0.094		4.49	*<0.0001*
	14mm*Hard	-0.016	0.094		-0.17	0.86
	14mm*Medium	0.349	0.094		3.71	*0.0003*
	14mm*Soft	0.151	0.094		1.61	0.11
	20mm*Hard	-0.748	0.094		-7.95	*<0.0001*
	20mm*Medium	-0.648	0.094		-6.89	*<0.0001*
Δt (s)	All Conditions			9.77		*<0.0001*
	6mm*Hard	-0.306	0.122		-2.50	*0.01*
	6mm*Medium	-0.678	0.122		-5.54	*<0.0001*
	6mm*Soft	-0.257	0.122		-2.10	*0.04*
	14mm*Hard	0.298	0.122		2.43	*0.02*
	14mm*Medium	-0.257	0.122		-2.10	*0.04*
	14mm*Soft	-0.0256	0.122		-0.21	0.83
	20mm*Hard	-0.525	0.122		4.29	*<0.0001*
	20mm*Medium	0.456	0.122		3.72	*0.0003*
F' (BW/s)	All Conditions			26.6		*<0.0001*
	6mm*Hard	0.495	0.106		4.66	*<0.0001*
	6mm*Medium	0.443	0.106		4.17	*<0.0001*
	6mm*Soft	0.152	0.106		1.43	0.16
	14mm*Hard	-0.0949	0.106		-0.89	0.38
	14mm*Medium	0.825	0.106		7.76	*<0.0001*
	14mm*Soft	0.157	0.106		1.47	0.14
	20mm*Hard	-0.892	0.106		-8.39	*<0.0001*
	20mm*Medium	-0.806	0.106		-7.58	*<0.0001*
Vertical Impulse (BW*ms)	All Conditions			10.6		*<0.0001*
	6mm*Hard	-0.289	0.153		-1.89	0.06
	6mm*Medium	-0.298	0.153		-1.95	0.05
	6mm*Soft	0.752	0.153		4.91	*<0.0001*
	14mm*Hard	-0.236	0.153		-1.54	0.12
	14mm*Medium	-0.906	0.153		-5.91	*<0.0001*
	14mm*Soft	-0.220	0.153		-1.44	0.15
	20mm*Hard	0.526	0.153		3.43	*0.0008*
	20mm*Medium	0.514	0.153		3.36	*0.001*
m_{eff} (%BW)	All Conditions			6.6		*<0.0001*
	6mm*Hard	-0.319	0.154		-2.06	*0.0415*
	6mm*Medium	-0.138	0.154		-0.89	0.37
	6mm*Soft	0.713	0.154		4.60	*<0.0001*
	14mm*Hard	-0.169	0.154		-1.09	0.28
	14mm*Medium	-0.694	0.154		-4.48	*<0.0001*
	14mm*Soft	-0.163	0.154		-1.05	0.29
	20mm*Hard	0.178	0.154		1.15	0.25
	20mm*Medium	0.459	0.154		2.97	*0.0037*

Vertical impulse was significantly affected by footwear condition (F=10.6, p<0.0001, Figure 3.4D, Table 3.3). The vertical impulse of the 20mm-soft condition was significantly greater than only the 14mm-medium condition (p<0.0001). The 6mm-soft, 20mm-hard and 20mm-medium conditions each resulted in significantly greater vertical impulse than the 20mm-soft condition (p<0.0001, p=0.0008 and p=0.001, respectively).

Footwear condition had a significant effect on m_{eff} (F=6.6, p<0.0001; Figure 3.4E, Table 3.3). m_{eff} was greater in the 20mm-soft condition than in the 6mm-hard and 14mm-medium conditions (p=0.04 and p<0.0001, respectively). However, the 20mm-soft condition resulted in significantly lower m_{eff} than the 6mm-soft and 20-mm medium conditions (p<0.0001 and p=0.004, respectively).

Discussion

This study investigated how variations in heel height affect several kinetic aspects of heel strike running impact peaks and how impact peaks are influenced by simultaneous changes in height and E of the heel using a within-participant study design. Our first hypothesis was that increasing heel height would lead to longer Δt, slower F', increased m_{eff}, and increased vertical impulse for a given individual, but that F_{max} would remain unaffected. Our results provide at minimum partial support for these hypotheses except for F_{max}. The 20mm height condition (the highest heel used in this study) resulted in individuals generating impact peaks with greater Δt, vertical impulse and m_{eff} than in the 6mm condition (the lowest heel used in this study). However, the 14mm height condition resulted in significantly lower vertical impulse and m_{eff} than the 6mm condition, suggesting a complicated relationship between heel height and these kinetic variables. F_{max} significantly decreased with increasing heel height, with both the 14mm and 20mm height conditions leading to lower F_{max} than the 6mm condition.

We also hypothesized that individuals would generate impact peaks with the longest Δt, slowest F', greatest m_{eff}, and largest vertical impulse in the highest footwear heels made of materials with the lowest E (the 20mm height-soft elastic modulus condition), but that F_{max} would remain unaffected. These hypotheses were not supported by our data. Instead, we found that F_{max} was significantly affected by footwear condition and that significant interactions occurred between heel height and E for several variables. We found that the 20mm-hard and 20mm-medium conditions had greater Δt and vertical impulse than the 20mm-soft condition, and that the 20mm-medium and 6mm-soft condition resulted in greater m_{eff} than the 20mm-soft condition. Greater values of F' were observed in the 20mm-hard and 20mm-medium conditions than in the 20mm-soft condition.

This study has several limitations. Instrumented treadmills, like the one used in this study, may influence kinematics, kinetics and muscle activation relative to over-ground studies using embedded force plates (Nigg et al. 1995; Wank et al. 1998). In addition, measuring the start of the impact peak when the vertical force exceeds 50 N likely has a small influence on the values of Δt, Δv, F', m_{eff} and the vertical impulse. However, our values of Δt and F' are comparable to other studies that have used embedded force plates or have used different definitions of the beginning of the impact peak (Gill and O'Connor 2003; Chi and Schmitt 2005; Lieberman et al. 2010). In addition, the values of m_{eff} measured in this study (an average of 9.46 %BW across all shoe conditions) are large compared to values found for barefoot runners (5.3 to 6.8 %BW), but comparable to heel strike runners wearing experimental footwear (8.2 to 10.3 %BW) (Chi and Schmitt 2005; Lieberman et al. 2010; Addison and Lieberman 2015). These findings therefore suggest that our methodology does not confound the results. A final limitation is that we did not measure muscle activity in this study. Experimental conditions may have altered participants' lower limb muscle activity patterns therefore influencing kinetic and kinematic variables. Future research into the influence of heel height and E on impact peaks should include EMG measurements to quantify lower extremity muscle activation patterns.

Despite these limitations, the results from this study demonstrate the importance of heel height and lower extremity kinematics, particularly knee flexion, on the generation of heel strike running impact peaks. Heel height significantly influenced each kinetic variable measured in this study, even when lower extremity kinematics were accounted for (Figure 3.2A-E, Table 3.2). This was not true for the elastic modulus of the heel. Heel elastic modulus had no effect on F_{max}, and had significant effects on Δt and F' only when lower extremity kinematics were not included in the GLMM (Table 3.1 and Table 3.2). Of the lower extremity kinematic variables measured, knee flexion during the impact had strong effects on F_{max} Δt, F', vertical impulse, m_{eff}. Notwithstanding the interactions between heel height and E, increased knee flexion during impact was correlated with lower F_{max} and F' and greater Δt, vertical impulse and m_{eff} within individuals (Figure 3.3A-E). These results suggest that heel height and knee flexion during the impact play a crucial role in the generation of impact peaks, perhaps more-so than the elastic modulus of the heel material. This implication is important because most prior studies on heel strike running impact peaks have considered solely the effects of elastic modulus of the substrate or footwear (Light et al. 1980; Clarke et al. 1983; Nigg et al. 1987; Nigg et al. 1988; Lafortune and Hennig 1992; Hennig et al. 1993; Addison and Lieberman 2015). Clearly, other factors such as heel height and knee flexion are relevant and influential, and more research is necessary to consider the effects of these variables.

The statistical interactions between heel height and heel elastic modulus on impact kinetics have potentially important implications for hypotheses about the relationship between variations in shoe construction and the generation of heel strike running impact peaks. We hypothesized that the effects of increasing heel height on impact peaks would be multiplied by lower E, such that individuals would generate impact peaks with the lowest F', greatest vertical impulse and largest m_{eff} in footwear with the highest heels made of materials with the lowest E. However, we found that E had significant but complicated effects on several aspects of the impact peak that differ in interesting ways with prior

findings. For instance, several studies have found that F' declines as interface modulus decreases (Lafortune et al. 1996; Wakeling et al. 2003; Addison and Lieberman 2015). Our results are consistent with these findings when we consider E variation in the 6mm height condition only: F' tended to decline from the hard to the medium to the soft condition (Figure 3.4C; GLMM equation (6mm height only): $F' = \beta_1 Elastic\ Modulus + ZU + \epsilon$: F=4.28, p=0.02). However, within the 20mm height condition, F' increased from the soft to medium to hard condition (Figure 3.4C; GLMM equation (20mm height only): $F' = \beta_1 Elastic\ Modulus + ZU + \epsilon$: F=14.6, p<0.0001). In other words, while higher heels led to lower F' overall (Figure 3.2C), decreasing heel E led to higher loading rates within the 20mm height condition. This finding suggests that additional research is necessary to uncover the mechanism behind the interactions between heel height and heel modulus during heel strike running.

The results presented here raise the hypothesis that human lower limb musculature is adapted to regulate F_{max} in response to variation in E, but not to variation in heel height. Similar to prior studies, we found that F_{max} did not change in response to variations in E (Clarke et al. 1983; Nigg et al. 1988; Wakeling et al. 2003; Kersting and Bruggemann 2006; Addison and Lieberman 2015). One hypothesized reason for the insensitivity of F_{max} across interfaces of varying stiffness (either due to changes in heel height or changes in E) is that the lower extremity musculature alters activity patterns to regulate F_{max} (Zadpoor and Nikooyan 2010). However, we found that F_{max} decreased as heel height increased. If increased heel height reduces the stiffness of the heel-ground interface, as our model suggests, then our finding that F_{max} declines in higher heeled footwear is consistent with results from modeling studies that show that F_{max} declines in less stiff footwear when lower extremity muscle activity is not accounted for (Zadpoor et al 2007). Therefore, our findings suggest that lower extremity muscles regulate F_{max} when heel elastic modulus varies but have a relatively reduced capacity to regulate F_{max} when heel height varies. While we did not measure muscle activity in this study, the result that F_{max} is sensitive to heel height but not E indicates that lower limb muscles may respond differently to

variations in E than they do to variations in heel height (Wakeling et al. 2002). The finding that F_{max} is unregulated across heel heights may be rooted in human evolutionary history. Although humans have had hundreds of thousands, possibly millions of years to adapt to running on natural surfaces that vary in elastic modulus, humans began running in footwear with elevated, cushioned heels only recently. To test this hypothesis future work should investigate how activity patterns of the lower extremity muscles vary in response to heel height versus heel E in heel strike runners.

References

Addison, B. J. and D. E. Lieberman (2015). "Tradeoffs between impact loading rate, vertical impulse and effective mass for walkers and heel strike runners wearing footwear of varying stiffness." Journal of Biomechanics **48**(7): 1318-1324.

Alexander, R. (2003). Principles of Animal Locomotion. Princeton, NJ., Princeton University Press.

Bonacci, J., P. U. Saunders, et al. (2013). "Running in a minimalist and lightweight shoe is not the same as running barefoot: a biomechanical study." British Journal of Sports Medicine **47**(6): 387-392.

Cavanagh, P. R. (1990). Biomechanics of distance running. Champaign, Human Kinetics Publishers.

Chi, K. J. and D. Schmitt (2005). "Mechanical energy and effective foot mass during impact loading of walking and running." Journal of Biomechanics **38**(7): 1387-1395.

Clarke, T. E., E. C. Frederick, et al. (1983). "Effects of shoe cushioning upon ground reaction forces in running." International Journal of Sports Medicine **4**(4): 247-251.

Clarke, T. E., E. C. Frederick, et al. (1983). "The effects of shoe design parameters on rearfoot control in running." Medicine and Science in Sports and Exercise **15**(5): 376-381.

Collins, J. J. and M. W. Whittle (1989). "Impulsive forces during walking and their clinical implications." Clinical Biomechanics **4**(3): 179-187.

Daoud, A. I., G. J. Geissler, et al. (2012). "Foot Strike and Injury Rates in Endurance Runners: A Retrospective Study." Medicine and Science in Sports and Exercise **44**(7): 1325-1334.

Davis, I., C. E. Milner, et al. (2004). "Does increased loading during running lead to tibial stress fractures? A prospective study." Medicine and Science in Sports and Exercise **36**(5): S58-S58.

Derrick, T. R. (2004). "The effects of knee contact angle on impact forces and accelerations." Medicine and Science in Sports and Exercise **36**(5): 832-837.

Esenyel, M., K. Walsh, et al. (2003). "Kinetics of high-heeled gait." Journal of the American Podiatric Medical Association **93**(1): 27-32.

Ferris, D. P., M. Louie, et al. (1998). "Running in the real world: adjusting leg stiffness for different surfaces." Proceedings of the Royal Society B-Biological Sciences **265**(1400): 989-994.

Folman, Y., J. Wosk, et al. (1986). "Cyclic impacts on heel strike - a possible biomechanical factor in the etiology of degenerative disease of the human locomotor system." Archives of Orthopaedic and Trauma Surgery **104**(6): 363-365.

Gerritsen, K. G. M., A. J. Vandenbogert, et al. (1995). "Direct dynamics simulation of the impact phase in heel-toe running." Journal of Biomechanics **28**(6): 661-668.

Gill, H. S. and J. J. O'Connor (2003). "Heelstrike and the pathomechanics of osteoarthrosis: a pilot gait study." Journal of Biomechanics **36**(11): 1625-1631.

Gill, H. S. and J. J. O'Connor (2003). "Heelstrike and the pathomechanics of osteoarthrosis: a simulation study." Journal of Biomechanics **36**(11): 1617-1624.

Hennig, E. M., T. L. Milani, et al. (1993). "Use of ground reaction force parameters in predicting peak tibial accelerations in running." Journal of Applied Biomechanics **9**(4): 306-314.

Hong, W. H., Y. H. Lee, et al. (2005). "Influence of heel height and shoe insert on comfort perception and biomechanical performance of young female adults during walking." Foot & Ankle International **26**(12): 1042-1048.

Hume, P., W. Hopkins, et al. (2008). "Effectiveness of foot orthoses for treatment and prevention of lower limb injuries - A review." Sports Medicine **38**(9): 759-779.

Kerdok, A. E., A. A. Biewener, et al. (2002). "Energetics and mechanics of human running on surfaces of different stiffnesses." Journal of Applied Physiology **92**(2): 469-478.

Kersting, U. G. and G.-P. Bruggemann (2006). "Midsole material-related force control during heel-toe running." Research in sports medicine (Print) **14**(1): 1-17.

Lafortune, M. A. and E. M. Hennig (1992). "Cushioning properties of footwear during walking - accelerometer and force platform measurements." Clinical Biomechanics **7**(3): 181-184.

Lafortune, M. A., E. M. Hennig, et al. (1996). "Dominant role of interface over knee angle for cushioning impact loading and regulating initial leg stiffness." Journal of Biomechanics **29**(12): 1523-1529.

Larson, P. (2014). "Comparison of foot strike patterns of barefoot and minimally shod runners in a recreational road race." Journal of Sport and Health Science **3**(2): 137-142.

Lieberman, D. E., M. Venkadesan, et al. (2010). "Foot strike patterns and collision forces in habitually barefoot versus shod runners." Nature **463**(7280): 531-U149.

Light, L. H., G. E. McLellan, et al. (1980). "Skeletal transients on heel strike in normal walking with different footwear." Journal of Biomechanics **13**(6): 477-480.

McCulloch, C. E. and S. R. Searle (2001). Generalized, Linear and Mixed Models. New York (NY), John Wiley.

McKenzie, D. C., D. B. Clement, et al. (1985). "Running shoes, orthotics, and injuries." Sports Medicine **2**(5): 334-347.

Milner, C. E., R. Ferber, et al. (2006). "Biomechanical factors associated with tibial stress fracture in female runners." Medicine and Science in Sports and Exercise **38**(2): 323-328.

Nigg, B. M. (2001). "The role of impact forces and foot pronation: A new paradigm." Clinical Journal of Sport Medicine **11**(1): 2-9.

Nigg, B. M. (2010). "Biomechanics of Sport Shoes. Calgary, Alberta, Canada.".

Nigg, B. M., H. A. Bahlsen, et al. (1987). "The influence of running velocity and midsole hardness on external impact forces in heel toe running." Journal of Biomechanics **20**(10): 951-959.

Nigg, B. M., R. W. Deboer, et al. (1995). "A kinematic comparison of overground and treadmill running." Medicine and Science in Sports and Exercise **27**(1): 98-105.

Nigg, B. M., W. Herzog, et al. (1988). "Effect of viscoelastic shoe insoles on vertical impact forces in heel-toe running." American Journal of Sports Medicine **16**(1): 70-76.

Nigg, B. M. and W. Liu (1999). "The effect of muscle stiffness and damping on simulated impact force peaks during running." Journal of Biomechanics **32**(8): 849-856.

Pohl, M. B., J. Hamill, et al. (2009). "Biomechanical and Anatomic Factors Associated with a History of Plantar Fasciitis in Female Runners." Clinical Journal of Sport Medicine **19**(5): 372-376.

Reinschmidt, C. and B. M. Nigg (1995). "Snfluence of heel height on ankle joint moments in running." Medicine and Science in Sports and Exercise **27**(3): 410-416.

Snow, R. E. and K. R. Williams (1994). "High heeled shoes - their effect on center-of-mass position, posture, 3-dimensional kinematics, rearfoot motion, and ground reaction forces." Archives of Physical Medicine and Rehabilitation **75**(5): 568-576.

Squadrone, R. and C. Gallozzi (2009). "Biomechanical and physiological comparison of barefoot and two shod conditions in experienced barefoot runners." Journal of Sports Medicine and Physical Fitness **49**(1): 6-13.

van der Worp, M. P., D. S. M. ten Haaf, et al. (2015). "Injuries in Runners; A Systematic Review on Risk Factors and Sex Differences." Plos One **10**(2).

Voloshin, A., J. Wosk, et al. (1981). "Force wave transmission through the human locomotor system." Journal of Biomechanical Engineering-Transactions of the Asme **103**(1): 48-50.

Voloshin, A. S. and D. J. Loy (1994). "Biomechanical evaluation and management of the shock waves resulting from high-heel gait: I - temporal domain study." Gait & Posture **2**: 117-122.

Wakeling, J. M., A. M. Liphardt, et al. (2003). "Muscle activity reduces soft-tissue resonance at heel-strike during walking." Journal of Biomechanics **36**(12): 1761-1769.

Wakeling, J. M., S. A. Pascual, et al. (2002). "Altering muscle activity in the lower extremities by running with different shoes." Medicine and Science in Sports and Exercise **34**(9): 1529-1532.

Wank, V., U. Frick, et al. (1998). "Kinematics and electromyography of lower limb muscles in overground and treadmill running." International Journal of Sports Medicine **19**(7): 455-461.

Wen, D. (2007). "Risk factors for overuse injuries in runners." Current Sports Medicine Reports **6**(5): 307-313.

Williams, D. S., I. S. McClay, et al. (2000). "Lower extremity mechanics in runners with a converted forefoot strike pattern." Journal of Applied Biomechanics **16**(2): 210-218.

Zadpoor, A. A. and A. A. Nikooyan (2010). "Modeling muscle activity to study the effects of footwear on the impact forces and vibrations of the human body during running." Journal of Biomechanics **43**(2): 186-193.

Zadpoor, A. A. and A. A. Nikooyan (2011). "The relationship between lower-extremity stress fractures and the ground reaction force: A systematic review." Clinical Biomechanics **26**(1): 23-28.

Zadpoor, A. A., A. A. Nikooyan, et al. (2007). "A model-based parametric study of impact force during running." Journal of Biomechanics **40**(9): 2012-2021.

Chapter 4 – Patterns of variation in trabecular bone volume fraction in the calcaneus and C2

vertebra of *Gorilla gorilla, Pan troglodytes and Homo sapiens*

Introduction

Many of the postcranial skeletal differences among humans and between *H. sapiens*, other

hominins and hominoids reflect differences in locomotion and other behaviors. One well-documented

type of skeletal variation concerns cortical bone robusticity in *Homo* (Lovejoy and Trinkaus 1980; Ruff et

al. 1993; Cowgill 2010). A second but less studied type of skeletal variation concerns trabecular bone

volume fraction (BVF), a structural variable that is strongly linked to trabecular bone stiffness and

strength (Carter and Hayes 1977, Rice et al. 1988). Several studies of BVF in joints of the appendicular

skeleton find lower trabecular BVF among Holocene *H. sapiens* compared to Pleistocene *Homo* and

extant hominoids (Griffin et al. 2010; Scherf et al. 2013; Tsegai et al. 2013; Chirchir et al. 2015; Ryan and

Shaw 2015)*.* Since many lines of evidence suggest that increased mechanical loading, either in terms of

magnitude, rate or number of loading events, increases trabecular BVF (Simkin et al. 1987; Davee et al.

1990; Joo et al. 2003; Pontzer et al. 2006; Barak et al. 2011), it is reasonable to hypothesize that reduced

levels of mechanical loading caused by more sedentary lifestyles explain the trend towards lower

trabecular BVF in modern humans (Chirchir et al. 2015; Ryan and Shaw 2015).

One limitation to the inference that decreased mechanical loading is the primary cause of lower

trabecular BVF in recent *H. sapiens* is that the trabecular structures so far examined mostly come from

bones and joints in which mechanical loading is complex and highly variable (Brand et al. 1982; Hodge et

al. 1986; Li et al. 1999; Boutroy et al. 2008). It is therefore difficult to assess the extent to which these

joints experienced decreased mechanical loading. This study focuses on trabecular structure in the

human calcaneus to test whether variations in mechanical loading have affected trabecular BVF in *H.*

sapiens because the mechanical loading regimes of this bone are simpler and better understood than

most of the rest of the human skeleton (Giddings et al. 2000; Gefen and Seliktar 2004). The human

calcaneus primarily deals with two types of forces: impact forces generated at foot strike during walking

and heel strike running, and bending forces generated during the propulsive parts of stance. These

forces differ not only between humans but also between humans and other hominoids in terms of

magnitude and repetitiveness. The calcaneus is the first bone in the human body to experience impact

forces during walking and heel strike running, generating forces anywhere from 0.6 to 1.0 body weights

(BW) during walking and from 1.0 to 3.0 BW during heel strike running (Nigg et al. 1995; Whittle 1999).

Impact forces at the human heel also occur at very high loading rates, especially during barefoot heel

strike running (400-500 BW/second) (Lieberman et al. 2010). Chimpanzee heel strikes, on the other

hand, do not always produce measureable impact peaks, particularly during quadrupedal locomotion

(Pontzer et al. 2014). Another difference is daily travel distances and physical activity levels. Modern

human hunter-gatherers and farmers have higher daily physical activity levels than industrialized

humans, and modern human hunter-gatherers typically walk between 9 and 15 kilometers per day,

while humans in industrialized societies walk 4 to 8 km/day and chimpanzees walk only 1.5 to 3 km/day

(Pontzer and Wrangham 2004; Marlowe 2005; Bassett et al. 2010; Pontzer et al. 2012). These

differences likely expose the calcaneus of non-industrial humans to millions more impact and bending

forces per year compared to industrialized humans or hominoids. Available evidence suggests that

humans have lower calcaneal trabecular BVF than other apes; however these studies are based only on

relatively sedentary *H. sapiens* populations, raising the possibility that trabecular BVF in the modern

human calcaneus may have also declined relative to earlier *H. sapiens* (Latimer and Lovejoy 1989; Maga

et al. 2006; Zeininger 2013). In sum, the evidence suggests that humans in general experience greater

mechanical loading of the calcaneus than apes and that non-industrial *H. sapiens* experience greater

mechanical loading of the calcaneus than industrialized *H. sapiens.*

Another limitation to the available BVF data is that BVF is typically measured in regions of

appendicular bones such as the femoral head that experience mechanical stimulus from locomotor

forces, as opposed to bones of the axial skeleton that experience locomotor forces less directly (CITE). It

is therefore difficult to assess to what extent declines in BVF are due to variation in mechanical loading

or caused by some other more systemic phenomena. This study also examines BVF in C2 vertebrae, a

bone less likely to be influenced by variation in mechanical loading. While physical activity can have

systemic effects on cortical bone robusticity, evidence suggests that applied forces can have localized

effects on both cortical and trabecular bone tissue (Lieberman 1996; Adami et al. 1999; Haapasalo et al.

2000; Bogenschutz et al. 2011). Reports on cortical robusticity have noted declines in femoral robusticity

but not humeral robusticity in Holocene *H. sapiens*, presumably because of the greater locomotor

demand placed on the human lower extremity relative to the upper limb (Ruff et al. 1993). Further,

greater applied forces to the dominant arm likely explains bi-lateral asymmetry in humeral cortical

robusticity of tennis players (Haapasalo et al. 2000). These findings suggest that if lack of mechanical

stimulus due to increased sedentism is the cause of declines in trabecular BVF in recent *H. sapiens*, then

the effects should be localized to regions of the skeleton that most directly experience mechanical

stimulus from locomotion, such as the calcaneus, and bones such as C2 vertebrae that experience less

locomotor loading should be relatively unaffected.

Another important concern is the question of whether decreases in trabecular BVF among

recent *H. sapiens* populations are caused by lower mechanical stimuli from more sedentary lifestyles.

Available data is mixed in regard to this interpretation. Ryan and Shaw (2015) found that Holocene

foragers (5,000-7,000 years BP) have greater femoral head BVF than presumably less active

agriculturalists (700-900 years BP). On the other hand, Chirchir et al (2015) found lower BVF in the

appendicular joints of Holocene *H. sapiens* compared to Pleistocene *Homo* and found no appendicular

joint BVF differences between modern industrialized Americans and presumably more active Native

American farmers. The results from Chirchir et al (2015) are consistent with trends from long-bone

diaphyses that show the largest decreases in femoral cortical robusticity occur between Pleistocene and

Holocene *H. sapiens*, compared to relatively smaller differences among Holocene populations (Ruff et al. 1993). Trabecular bone is influenced by factors other than mechanical loading, and while it is unclear how variations in genes, diet and hormones have interacted with mechanical loading to affect *H. sapiens* trabecular BVF, there is evidence for a major, widespread systemic decline in trabecular BVF in *H. sapiens* sometime after the Pleistocene regardless of the presumed activity levels of the populations (Bouxsein et al. 2004; Wiren et al. 2012; Devlin et al. 2013; Chirchir et al. 2015). A finer-scale investigation of several *H. sapiens* populations that vary in geologic time and activity level is necessary to establish more carefully these patterns of variation and test whether declines in physical activity may be the cause of low trabecular BVF in recent *H. sapiens* and whether the patterns are systemic.

This study accordingly uses structural data obtained from micro CT scans in apes and several human populations to test whether variations in mechanical loading influenced trabecular BVF. We examine BVF in the calcaneus of several *H. sapiens* populations and African apes, and in C2 vertebrae of three *H. sapiens* populations. We test three specific hypotheses relevant to the general hypothesis that variations in mechanical loading are a primary cause of the patterns of variation observed in *H. sapiens* trabecular BVF. First, we predict that modern sedentary Americans should have lower calcaneal trabecular BVF than more active, non-industrial *H. sapiens* populations. Second, we predict that *H. sapiens,* particularly those from non-industrial populations, have greater calcaneal trabecular BVF than African apes. Finally, if variations in BVF are primarily a result of direct mechanical loading then we predict that trabecular BVF in C2 vertebrae should be unchanged across human populations. Alternatively, if systemic declines in BVF occurred after the Pleistocene then we should observe a decline in both calcaneal and C2 vertebral trabecular BVF.

Materials and Methods

Materials

<u>Sample populations</u>

The calcanei sample consists of *Gorilla gorilla, Pan troglodytes* and Pleistocene and Holocene *H. sapiens*, while the C2 sample consists of one Pleistocene and two Holocene *H. sapiens* populations. The wild-collected gorilla (n=10) and chimpanzee (n=7) calcanei sample includes adult males and females obtained from the Museum of Comparative Zoology, Harvard University. The Pleistocene human sample is comprised of adult males and females from the Natufian culture (calcanei n=10; C2 n=10), a population of semi-sedentary hunter-gatherers in the Levant from between 15 to 12 Kya (Unger-Hamilton 1989; Lieberman 1993).The Natufian samples were obtained from the Peabody Museum, Harvard University. In addition, we examined three Holocene *H. sapiens* populations. The Point Hope sample is composed of adult males and females (calcanei n=19; C2 n=19) from the Ipiutak and Tiagara cultures located in present-day Point Hope, Alaska. The Ipiutak culture lasted from roughly 2100 to 1500 BP, while the Tiagara culture lasted from roughly 800 to 300 years BP. Ipiutak and Tiagara individuals were Inuit hunter-gatherers that subsisted in large part on walrus, seal and caribou (Larsen and Rainey 1948). The Point Hope sample was obtained from the American Museum of Natural History, New York. A second Holocene human sample is from the site of Mistihalj dated from 1400 to 1475 AD and located on the border between modern-day Bosnia-Herzegovina and Montenegro; these individuals are associated with the Vlakh ethnic group, a population indigenous to the Balkans that have traditionally been nomadic pastoralists (Alexeeva et al. 2003). The Mistihalj sample, which includes adult males and females (calcanei n=15; C2 n=12) was obtained from the Peabody Museum, Harvard University. Finally, we used a calcanei sample (10 males and 10 females) of contemporary American cadavers obtained from MedCure (www.medcure.org; Portland, OR), an anatomical gifts program. The modern American

sample did not include C2 vertebrae. All modern American individuals were free from metabolic bone diseases and had died between June 2013 and July 2014.

Methods

Micro-CT scanning

All specimens were scanned individually using an X-Tek micro-CT scanner, model HMXST225 at the Center for Nanoscale Systems at Harvard University. All calcanei and C2 vertebrae were scanned with a source energy of 75 kV at a current of 130 microA. For calcanei, scan resolution was 39, 45 and 46 microns for the chimpanzee, human and gorilla calcanei, respectively. Scan resolution was 45 microns for human C2 vertebrae. Calcanei were mounted in the microCT scanner with the long axis of the bone placed vertically, and C2 vertebrae were mounted so that the cranial-caudal axis was positioned vertically. All calcanei and C2 vertebrae scans were collected with 3142 projections, with 1 frame per projection. 3D volumes were reconstructed from the raw data using CT PRO software (Nikon Metrology Inc.).

Image Processing

Reconstructed volumes were initially processed in VGStudioMax v2.2 software (Volume Graphics, Heidelberg, Germany). Two 3D cubic volumes of interest (VOIs) were created: one in the calcaneal tuberosity and the other beneath the posterior articular facet (PAF) in the calcaneus. The edge-length of the tuberosity VOI and the PAF VOI were scaled to $1/7^{th}$ and $1/10^{th}$ of total bone length, respectively (tuberosity VOI edge length range across all species: 6.88 – 12.74 mm; PAF VOI edge length range across all species: 4.82-8.92mm). These dimensions were chosen because they were the largest that could reliably fit within the gorilla calcanei. The posterior surface of the tuberosity VOI was positioned at 15% of bone length anterior to the posterior aspect of the calcaneal tuberosity, and then placed as close to the center of the coronal plane cross-section as possible (Figure 4.1A). The superior surface of the calcaneal PAF VOI was positioned at 5% of bone length inferior to the surface of the PAF,

and then positioned as close to the center of the coronal plane cross-section as possible (Figure 4.1A). Edge length of 3D cubic VOIs in the C2 vertebrae were scaled to 25% of vertebral body height (C2 VOI edge length across all human populations: 4.01 to 6.30mm). The inferior surface of C2 VOs were positioned at 20% of vertebral body height superior to the caudal surface of the vertebral body, and then positioned towards the posterior of the vertebral body to avoid areas of disrupted trabecular architecture due to blood and nervous supply, and then finally positioned as close to the center of the coronal plane cross-section as possible (Figure 4.1B). VOIs were then saved as stacks of 16-bit RGB color TIFF images.
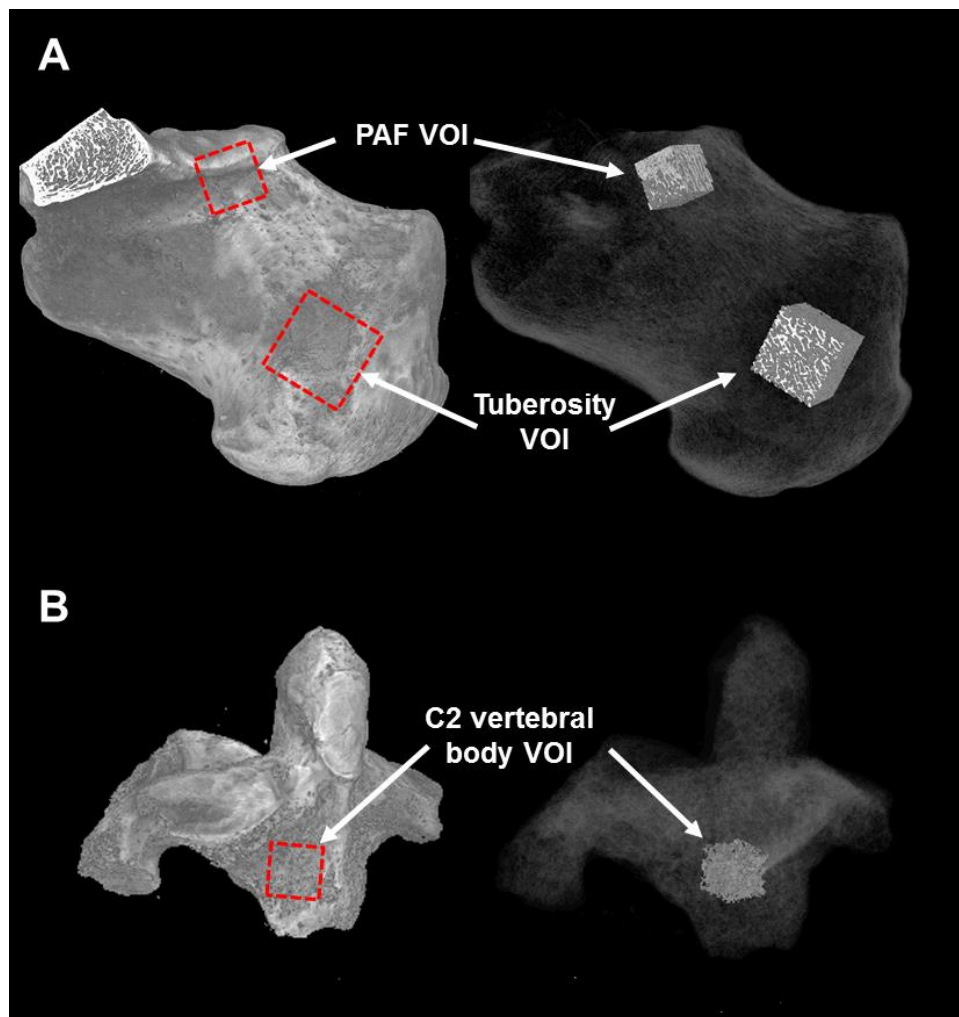

Figure 4.1: VOIs created for each bone in the A) Calcaneal PAF and calcaneal tuberosity and in the B) C2 vertebral body

ImageJ software was used for the remainder of image processing. 16-bit RGB color TIFF image stacks were converted to 8-bit images for compatibility with Image J's thresholding algorithm and the proper length scale was set for each VOI. Pixel resolution was 21.7, 25.6 and 22.2 pixels per mm for gorilla, chimpanzees and human image stacks. A modified half-maximum height method was used to set the threshold for bone versus air pixels (Spoor et al. 1993; Fajardo et al. 2002). First, a line 10 pixels in length was drawn across a random bone-air interface in a random image slice in the VOI TIFF stack. The grey-scale values along this line were recorded and the maximum and minimum grey values were averaged. This process was performed a total of 10 times per VOI. Then, the 10 averages from the maximum and minimum grey values were themselves averaged, and this value was set as the threshold to differentiate bone from air pixels.

Thresholding samples from the Natufian population was more difficult because of post-mortem alteration of the trabecular tissue that could affect the quantification of trabecular structure, including the presence of high-density mineral inclusions, the possible deposition of material onto the surface of trabeculae and the overlap in density values between the bone and the depositional material (Ryan and Ketcham 2002). To deal with these potential sources of error, we created two threshold values for each Natufian tuberosity VOI. One threshold calculation counted the depositional material as bone, while a second threshold calculation removed these inclusions from the bone material. We then determined trabecular BVF in the tuberosity of the Natufians using these two different threshold methods and compared the BVF values. On average, there was less than 1% difference in trabecular BVF values between the two thresholding methods. This value was deemed insignificant and thus the thresholding calculation that counted mineral inclusions as bone was used to process and analyze all VOIs.

The BoneJ plugin for ImageJ was used to calculate the BVF, trabecular thickness (Tb.Th), trabecular separation (Tb.Sp), DA, structure model index (SMI) and connectivity density (ConnD) of all VOIs (Doube et al. 2010). Trabecular BVF was determined by a voxel-based algorithm that counts bone

and non-bone voxels in a TIFF image stack. BoneJ calculates Tb.Th. and Tb.Sp. using an algorithm that

defines thickness at a point as the diameter of the largest sphere that fits within the structure and which

contains the point. DA is calculated using the mean intercept length (MIL) method (Harrigan and Mann

1984; Odgaard 1997). Briefly, the MIL method builds an ellipsoid with an orientation and dimensions

that correspond to the orientations of trabeculae in a sample. DA is calculated as 1-(length of the

shortest axis of the ellipsoid/length of the longest axis of the ellipsoid). Thus, DA values range from 0 to

1, with larger values indicate greater anisotropy. BoneJ uses a method developed by Hildebrand and

Ruegsegger (1997) to calculate SMI, which is a measure of the rod versus plate-like geometry of

trabecular structures. Briefly, this method uses the change in trabecular surface area per change in

volume to estimate the value of SMI. Perfectly plate-shaped trabeculae have an SMI value of 0, while

perfectly rod-shaped trabecular have a value of 3 (Hildebrand and Ruegsegger 1997). Finally,

connectivity is estimate of the number of connected trabeculae in a volume, and BoneJ calculates

ConnD as the number of connected trabeculae divided by the volume of the sample. Larger numbers

indicated larger connectivity densities. A detailed list of BVF, Tb.Th., Tb.Sp., DA, SMI and ConnD for each

VOI is provided in the appendix.

Statistical analyses

MicroCT scanning revealed damaged trabeculae in a small number of specimens. One Natufian

sample and two Mistihalj samples had damaged trabeculae in the tuberosity region and were not

included in the statistical analysis. In addition, one Natufian sample had a tuberosity BVF 2 standard

deviations greater than the mean and was not included in statistical analyses. Thus, analyses on the

tuberosity were performed with eight Natufian samples and 13 Mistihalj samples, while analyses on the

PAF were performed with the full sample sizes (Natufian n=10; Mistihalj n=15).

One-way ANOVA was used to compare trabecular bone variables between groups, with

statistical significance set to $p < 0.05$. For tests on trabecular BVF we tested for differences in species

level means (pooling all human populations) as well as population level means (splitting human populations) in the two calcaneal VOIs. For the remainder of the trabecular structural variables we tested only for population level differences. When ANOVA tests indicated significance, we tested for differences between two particular groups using the Tukey-HSD method to account for multiple comparisons. Statistical analyses were performed in JMP v. 11 software (SAS, North Carolina, USA).

Results

Trabecular BVF

Calcaneal Tuberosity VOI

One-way ANOVA revealed significant differences between populations in calcaneal tuberosity trabecular BVF (Figure 4.2; F(5,75)=9.32, p<0.0001). Tukey-HSD tests showed significant differences in BVF between chimpanzees (average BVF=0.259 +/- 0.04) and each Holocene human population and between Natufians (average BVF=0.255 +/- 0.05) and each Holocene population. Chimpanzees had 38%, 48% and 48% greater trabecular BVF than Point Hope, Mistihalj and Americans, respectively, but were not statistically different from Natufians. BVF was 36%, 46% and 46% greater in Natufians than in Point Hope, Mistihalj and Americans, respectively. There were no differences in trabecular BVF between the three Holocene *H. sapiens* populations (Table 4.1, Table 4.2).

Calcaneal PAF VOI

One-way ANOVA showed significant differences between populations in trabecular BVF in the calcaneal PAF (Figure 4.3; F(5,78)=11.3, p<0.0001). Multiple comparison tests showed significant differences in BVF between chimpanzees (average BVF=0.523 +/- 0.06) and each Holocene human population and between Natufians (average BVF=0.573 +/- 0.07) and each Holocene human population. Chimpanzees had 33%, 17% and 26% greater trabecular BVF than Point Hope, Mistihalj and Americans, respectively, but were not significantly different from Natufians. Natufians had 37%, 21% and 29% greater trabecular BVF than Point Hope, Mistihalj and Americans, respectively. There were no significant

69

differences between the three Holocene *H. sapiens* populations. In addition, BVF was 25% and 18% greater in gorillas than in Point Hope and Americans, respectively (Table 4.3, Table 4.4).
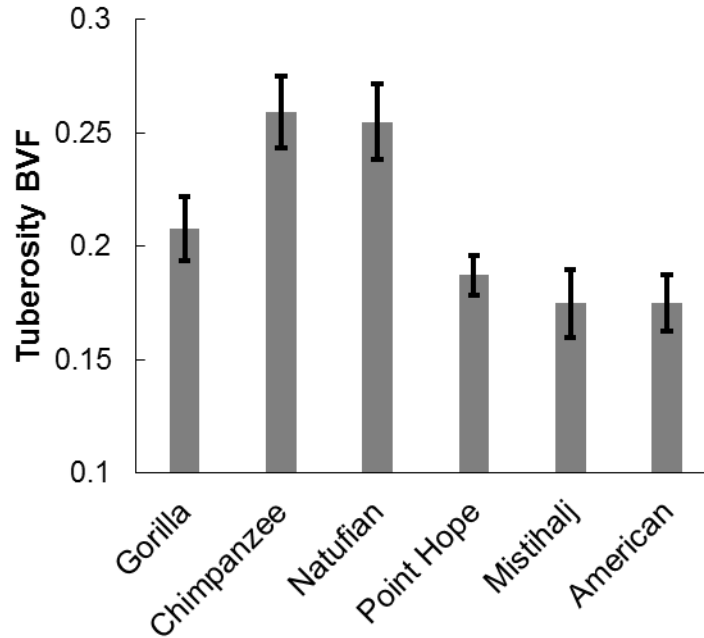
Figure 4.2: Trabecular BVF in the calcaneal tuberosity. Height of bars represent average BVF for the populations and error bars represent standard error.

C2 vertebrae VOI

One-way ANOVA showed significant differences between human populations in trabecular BVF (Figure 4.4; $F_{(2,27)}=12.1$, $p<0.0001$). Trabecular BVF was significantly greater in the Natufian population than the Point Hope and Mistihalj populations by 53% and 25%, respectively. Trabecular BVF was 23% greater in Mistihalj than in Point Hope ($p=0.056$) (Table 4.5, Table 4.6).

Table 4.1: Calcaneal tuberosity - summary statistics (Average +/- SD)

Species	N	BVF					
Gorilla	10	.21 (0.05)					
Chimpanzee	7	.26 (0.04)					
H. sapiens	60	.19 (0.06)					
Population	**N**	**BVF**	**Tb.Th**	**Tb.Sp**	**DA**	**SMI**	**Conn.D**
Gorilla	10	0.21 (0.05)	0.27 (0.06)	1.01 (0.26)	0.58 (0.09)	1.64 (0.34)	2.39 (1.34)
Chimpanzee	7	0.26 (0.04)	0.23 (0.04)	0.71 (0.06)	0.63 (0.04)	1.11 (0.50)	4.14 (1.39)
Natufian	8	0.26 (0.05)	0.27 (0.02)	0.76 (0.13)	0.64 (0.04)	1.36 (0.53)	3.14 (0.81)
Point Hope	19	0.19 (0.04)	0.20 (0.02)	0.76 (0.14)	0.71 (0.07)	2.21 (0.50)	4.52 (2.09)
Mistihalj	13	0.18 (0.05)	0.18 (0.03)	0.70 (0.09)	0.64 (0.07)	2.62 (0.67)	6.15 (1.69)
American	20	0.18 (0.06)	0.20 (0.03)	0.72 (0.14)	0.70 (0.06)	2.51 (0.59)	4.69 (1.78)

Other structural variables

Calcaneal Tuberosity VOI

There were several significant differences in other trabecular structural variables between populations in the tuberosity VOI. The most noteworthy trends are that the Holocene *H. sapiens* populations generally had the lowest Tb.Th values and the highest SMI values, indicating thinner, rod-shaped trabeculae. In addition, gorillas had larger Tb.Sp. values than either chimpanzees or any of the *H. sapiens* populations (Table 4.1, Table 4.2).

Calcaneal PAF VOI

Trends in other structural variables observed in the tuberosity were also evident in the calcaneal PAF. Tb.Th. was generally lower in the Holocene *H. sapiens* populations than in either Natufians or gorillas, and Holocene *H. sapiens* had the largest SMI values. Gorillas also tended toward greater Tb.Sp. than other populations. Two other noteworthy trends appeared in the calcaneal PAF VOI: DA values

were larger in all human populations than in chimpanzees, and ConnD values in gorillas and Natufians were less than chimpanzees or any of the Holocene *H. sapiens* populations (Table 4.3, Table 4.4).

<u>C2 body VOI</u>

Tb.Th was greater and SMI lower in the Natufians when compared to either Point Hope or Mistihalj. The Point Hope population tended to have the largest Tb.Sp values. Finally, the Mistihalj group showed greater ConnD than either the Point Hope or Natufian populations (Table 4.5, Table 4.6).

Table 4.2: Calcaneal tuberosity - Tukey HSD Test p-values for multiple comparisons (significant differences are in bold and italics)

| Species Comparison	BVF					
Gorilla v. Chimpanzee	0.13					
Gorilla v. *H. sapiens*	0.58					
Chimpanzee v. *H. sapiens*	*0.004*					
Population Comparison	**BVF**	**Tb.Th**	**Tb.Sp**	**DA**	**SMI**	**Conn.D**
Gorilla v. Chimpazee	0.27	0.17	*0.0014*	0.47	0.38	0.30
Gorilla v. Natufian	0.32	0.99	*0.01*	0.55	0.89	0.94
Gorilla v. Point Hope	0.89	*0.0002*	*0.0009*	0.24	0.10	*0.024*
Gorilla v. Mistihalj	0.59	*<0.0001*	*<0.0001*	0.28	*0.0007*	*<0.0001*
Gorilla v. American	0.51	*<0.0001*	*<0.0001*	*0.0004*	*0.001*	*0.01*
Chimpanzee v. Natufian	0.99	0.09	0.98	0.99	0.95	0.86
Chimpanzee v. Point Hope	*0.02*	0.72	0.96	0.24	*0.0003*	0.99
Chimpanzee v. Mistihalj	*0.005*	0.12	0.99	0.99	*<0.0001*	0.13
Chimpanzee v. American	*0.002*	0.50	0.99	0.41	*<0.0001*	0.98
Natufian v. Point Hope	*0.02*	*0.0001*	0.99	0.13	*0.006*	0.40
Natufian v. Mistihalj	*0.006*	*<0.0001*	0.92	0.99	*<0.0001*	*0.003*
Natufian v. American	*0.002*	*<0.0001*	0.98	0.25	*<0.0001*	0.27
Point Hope v. Mistihalj	0.98	0.60	0.81	0.09	0.29	0.09
Point Hope v. American	0.97	0.99	0.93	0.99	0.51	0.99
Mistihalj v. American	0.99	0.83	0.99	0.20	0.99	0.16
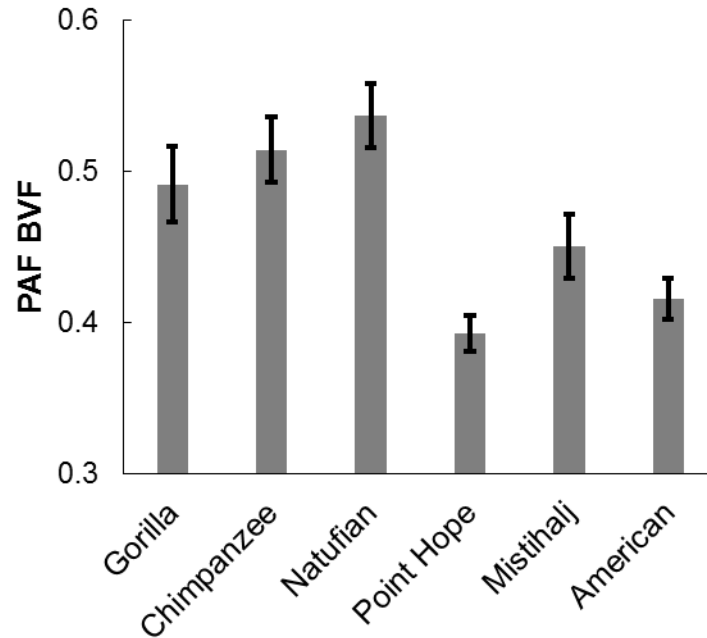
Figure 4.3: Trabecular BVF values in the calcaneal PAF. Height of bars represent average BVF for the populations and error bars represent standard error.

Table 4.3: Calcaneal PAF - summary statistics (Average +/- SD)

Species	N	BVF					
Gorilla	10	0.49 (0.08)					
Chimpanzee	7	0.52 (0.07)					
H. sapiens	64	0.43 (0.08)					
Population	**N**	**BVF**	**Tb.Th**	**Tb.Sp**	**DA**	**SMI**	**Conn.D**
Gorilla	10	0.49 (0.08)	0.50 (0.12)	0.79 (0.15)	0.70 (0.08)	-0.96 (0.9)	1.16 (0.45)
Chimpanzee	7	0.52 (0.07)	0.39 (0.07)	0.60 (0.10)	0.53 (0.07)	-0.96 (0.9)	3.59 (1.70)
Natufian	10	0.54 (0.07)	0.53 (0.08)	0.68 (0.10)	0.79 (0.04)	-0.89 (0.54)	1.14 (0.39)
Point Hope	19	0.39 (0.05)	0.35 (0.05)	0.68 (0.07)	0.82 (0.03)	0.24 (0.87)	2.59 (0.75)
Mistihalj	15	0.45 (0.07)	0.38 (0.06)	0.60 (0.07)	0.69 (0.10)	0.46 (0.56)	3.91 (1.13)
American	20	0.42 (0.062)	0.35 (0.05)	0.60 (0.10)	0.75 (0.06)	0.43 (0.51)	3.72 (1.35)

Table 4.4: Calcaneal PAF - Tukey HSD Test p-values for multiple comparisons (significant differences are in bold and italics)

Species Comparison	BVF					
Gorilla v. Chimpanzee	0.82					
Gorilla v. *H. sapiens*	0.10					
Chimpanzee v *H. sapiens*	*0.038*					
Population Comparison	**BVF**	**Tb.Th**	**Tb.Sp**	**DA**	**SMI**	**Conn.D**
Gorilla v. Chimpazee	0.98	*0.018*	*0.0013*	*<0.0001*	0.99	*0.0002*
Gorilla v. Natufian	0.65	0.90	0.11	*0.025*	0.99	0.99
Gorilla v. Point Hope	*0.004*	*<0.0001*	0.052	*0.0002*	<0.0001	*0.01*
Gorilla v. Mistihalj	0.67	*0.0008*	*<0.0001*	0.99	0.0008	*<0.0001*
Gorilla v. American	0.052	*<0.0001*	*<0.0001*	0.37	*<0.0001*	*<0.0001*
Chimpanzee v. Natufian	0.98	*0.0008*	0.48	*<0.0001*	0.99	*0.0001*
Chimpanzee v. Point Hope	*0.0013*	0.82	0.34	*<0.0001*	*0.0003*	0.28
Chimpanzee v. Mistihalj	0.30	0.99	0.99	*<0.0001*	*0.004*	0.98
Chimpanzee v. American	*0.015*	0.86	0.99	*<0.0001*	*0.0002*	0.99
Natufian v. Point Hope	*<0.0001*	*<0.0001*	0.99	0.91	*<0.0001*	*0.009*
Natufian v. Mistihalj	*0.026*	*<0.0001*	0.31	*0.008*	*0.002*	*<0.0001*
Natufian v. American	*0.0002*	*<0.0001*	0.32	0.54	*<0.0001*	*<0.0001*
Point Hope v. Mistihalj	0.14	0.81	0.13	*<0.0001*	0.97	*0.007*
Point Hope v. American	0.88	0.99	0.12	*0.019*	0.99	*0.016*
Mistihalj v. American	0.66	0.86	0.99	0.18	0.93	0.99

Discussion

This study investigated whether variations in mechanical loading account for recent declines in trabecular BVF by examining trabecular structure in the calcaneus and C2 vertebrae of different human populations as well as in two species of great apes. We predicted that if declines in mechanical stimulus to bone from more sedentary lifestyles precipitated declines in trabecular BVF, then calcaneal trabecular BVF should be lower in modern Americans than earlier *H. sapiens* populations who were presumably more active. We also predicted that calcaneal trabecular BVF would be greater in hunter-gatherer *H. sapiens* than African apes. Finally, we predicted that trabecular BVF in C2 vertebrae would be unchanged across human populations. These hypotheses were not supported by the comparative data.

Instead, the results suggest that trabecular BVF declined systemically in *H. sapiens* after the Pleistocene. The Pleistocene Natufians showed greater calcaneal trabecular BVF in the calcaneus than any of the three Holocene human populations. Natufians also had greater BVF in C2 vertebrae than Point Hope or Mistihalj. Moreover, there were no significant differences in calcaneal BVF among the three Holocene human populations.
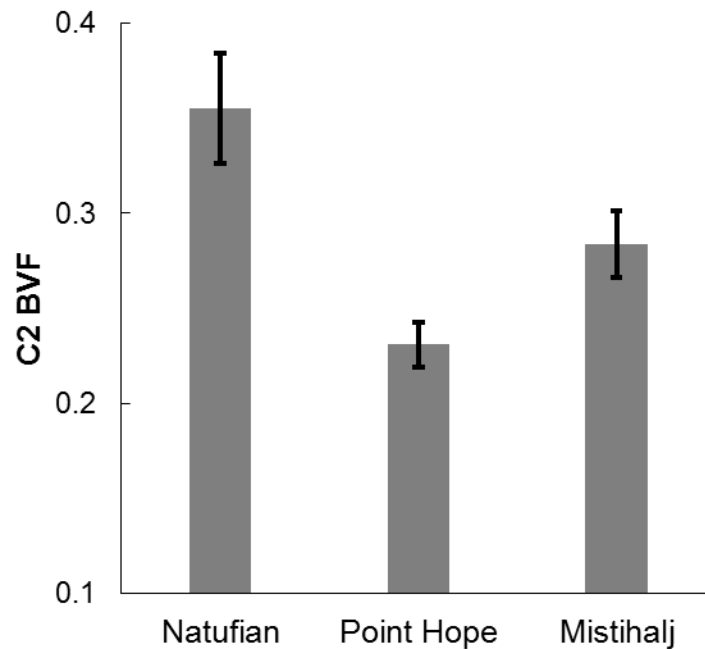
Figure 4.4: Trabecular BVF in C2 vertebrae. Height of bars represent average BVF for the populations and error bars represent standard error.

Before considering the meaning of these results, it is worth noting several limitations of this study. One potential drawback is that we lack data on physical activity levels of the human populations studied. We presumed due to the complete lack of agriculture in Point Hope and the lack of plant domestication in Mistihalj that these populations had somewhat comparable physical activity levels to the Natufians and greater physical activity levels than the modern Americans studied. While levels of physical activity between the non-industrial Holocene groups and Natufians are unknown, several researchers have argued that both Point Hope and Misithalj populations had relatively high physical activity levels compared to other Holocene groups because of their high degree of femoral cortical bone

robusticity (Trinkaus 1976; Cowgill 2010). Thus, Point Hope and Mistihalj are ideal populations for examining variation in bone structure between Holocene groups and for testing if increases in physical inactivity in some Holocene *H. sapiens* populations resulted in lower trabecular BVF.

Table 4.5: C2 - summary statistics (Average +/- SD)

Population	N	BVF	Tb.Th	Tb.Sp	DA	SMI	Conn.D
Natufian	9	0.36 (0.09)	0.36 (0.08)	0.80 (0.09)	0.27 (0.12)	1.10 (0.53)	2.84 (1.29)
Point Hope	19	0.23 (0.05)	0.27 (0.04)	0.94 (0.19)	0.33 (0.10)	1.76 (0.35)	3.63 (1.25)
Mistihalj	12	0.29 (0.06)	0.24 (0.03)	0.67 (0.09)	0.21 (0.07)	1.52 (0.40)	6.95 (1.77)

Although age and sex influence trabecular bone structural variables, this study did not analyze the effects of these variables due to study design and constraints with sample populations. For instance, several calcanei from the Natufian population had no or few associated skeletal elements, making it difficult to estimate age or sex for these individuals. We used only adult specimens (as judged by closure of femoral epiphyses for specimens, and by calcaneal epiphyses when other skeletal elements were not available), and attempted to balance sex ratios within populations. Despite these efforts, the Point Hope population was largely comprised of males (calcaneus: 15 males, 4 females, 1 unidentified, C2: 14 males, 4 females, 2 unidentified) and the American sample was likely biologically older (average age 57 years) than the other samples due to age-related constraints on availability of cadaver specimens. If variations in physical activity were the primary cause of variations in BVF, the bias towards males in the Point Hope sample would be expected to elevate the population-level BVF because evidence suggests hunter-gather males are more physically active than females (Marlowe 2005; Pontzer et al. 2012). Further, the bias towards older individuals in the American sample would be expected to decrease the BVF of this population because BVF declines with age. Despite biases in the Point Hope and American populations that would be expected to enhance BVF differences in these populations, we found no BVF differences between the Holocene populations.

Table 4.6: C2 body - Tukey HSD Test p-values for multiple comparisons (significant differences are in bold and italics)

Comparison	BVF	Tb.Th	Tb.Sp	DA	SMI	Conn.D
Natufian v. Point Hope	*<0.0001*	*<0.0001*	0.06	0.28	*0.001*	0.37
Natufian v. Mistihalj	*0.048*	*<0.0001*	0.12	0.41	0.07	*<0.0001*
Point Hope v. Mistihalj	0.056	0.33	*<0.0001*	*0.007*	0.28	*<0.0001*

Another concern is body size differences between species and populations and its potential effects on trabecular BVF values. While previous studies have found no correlation between femoral head diameter and trabecular BVF, we investigated the relationship between calcaneal size and trabecular BVF to further test whether body size may be confounding our results (Doube et al. 2011). Across all species in this study, trabecular BVF in the tuberosity was weakly inversely correlated with total calcaneus length in the anterior-posterior direction (r=-0.31, p = 0.0043, n=80). When only the human populations were considered, there was no relationship between tuberosity trabecular BVF and total calcaneus length (r=-0.01, p=0.93, n=60). Further, there were no differences in total calcaneus length among the human populations (one-way ANOVA – F(3,56)=0.99, p=0.41). These data suggest that body size differences between human populations do not influence variations in calcaneal BVF.

Despite the above limitations, the results of this study add to prior findings by documenting trabecular structural variables (such as DA, Tb.Th., Tb.Sp., SMI and ConnD) that influence mechanical properties of trabecular tissue and vary with body size. Low BVF, low Tb.Th. and high SMI are linked to reduced stiffness and strength in trabecular tissue, and larger values of DA increase stiffness and strength of trabecular tissue along the axis of primary trabecular strut orientation (Carter and Hayes 1977; Silva and Gibson 1997; Augat et al. 1998; Mittra et al. 2005). Our findings suggest that since the Holocene, Tb.Th generally declined and SMI increased, while DA has an inconsistent pattern of change. This result suggests that lower Tb.Th and higher SMI paralleled the declines in BVF since the Holocene. Both lower Tb.Th and greater SMI are associated with reduced trabecular bone stiffness and strength,

therefore suggesting that the combined mechanical effect of changes in BVF, Tb.Th and SMI is a reduction in stiffness and strength in calcaneal and C2 trabecular structures Holocene compared to Pleistocene *H. sapiens* (Carter and Hayes 1977; Rice et al. 1988; Silva and Gibson 1997; Mittra et al. 2005). Further, gorillas have the smallest ConnD and largest Tb.Sp. of the populations examined in our study, which is consistent with prior results indicating that Tb.Sp increases and ConnD decreases with increasing body size in mammals (Doube et al. 2011). These findings suggest that variations in Tb.Sp and ConnD amongst closely related taxa reflect differences in body size, while differences in BVF, Tb.Th. and SMI are a functional signal of trabecular tissue stiffness and strength.

The results from this study add to our understanding of the mechanism and timing of the declines in trabecular BVF in *H. sapiens*. For one, we studied trabecular structure in the calcaneus, a bone in which the mechanical loading regime is better understood than other bones in human skeleton and is thus better suited to testing hypotheses relating mechanical stimulus to BVF (Giddings et al. 2000; Gefen and Seliktar 2004). The human calcaneus experiences impact forces at the moment of heel-ground contact and then large bending forces during the push-off phase of gait. Reductions in daily travel ranges and physical activity levels, as seen between modern human societies, would undoubtedly reduce the mechanical stimulus to the calcaneus (Pontzer et al. 2009; Bassett et al. 2010; Hallal et al. 2012; Pontzer et al. 2012). However, there were no differences in calcaneal BVF between the Arctic hunter-gatherers of Point Hope and modern Americans. Rather, a drastic decline in calcaneal BVF was observed between the Pleistocene Natufians and the Holocene *H. sapiens* populations.

Additionally, our study adds to our understanding of variation in trabecular BVF in *H. sapiens* by examining trabecular structure in C2 vertebrae, a bone likely to be less affected by the forces generated by locomotion. Even so, we found significant declines in BVF in C2 vertebrae between the Natufians and the Holocene *H. sapiens* populations. Moreover, the magnitude of the decline in C2 BVF (25% between Natufians and Mistihalj, 53% between Natufians and Point Hope) was comparable to the declines

observed in the calcaneus (21% between Natufians and Mistihalj in the PAF and 61% between Natufians and Point Hope in the tuberosity). The finding that BVF declines in C2 followed the same pattern as the calcaneus despite lower locomotor forces suggests a systemic decline in BVF that may be unrelated to variations in physical activity levels.

Finally, our study advances knowledge of variation in *H. sapiens* trabecular BVF by examining populations that vary widely in time, geographic location and subsistence strategy. We examined Pleistocene and Holocene hunter-gatherers (Natufians and Point Hope, respectively), nomadic pastoralists (Mistihalj) and modern Americans, making this the largest comparative study on *H. sapiens* trabecular BVF to date. Altogether, the evidence from this study points to a systemic decline in *H. sapiens* BVF sometime after the Pleistocene, which is consistent with prior findings (Chirchir et al. 2015; Ryan and Shaw 2015). We also find no differences in BVF among Holocene *H. sapiens* populations despite varying subsistence strategies. While declines in physical activity after the Pleistocene may have played a role in the observed decline in BVF, the lack of association between presumed physical activity level and calcaneal BVF in Holocene populations suggests that phenomena other than or in addition to variations in physical activity are responsible for declines in trabecular BVF. For instance, environmental factors such as nutrition, hormones and infectious disease prevalence are known to influence skeletal morphology and thus could have played a role in shaping BVF in Holocene populations (New et al. 2000; Eshed et al. 2010; Wiren et al. 2012; Devlin et al. 2013). It is also possible that selection, perhaps through pleiotropic effects, worked to reduce BVF in Holocene *H. sapiens* (Trut et al. 2006). Regardless of the proximate and ultimate causes of variation in trabecular BVF, our results are consistent with prior findings and provide strong evidence for a systemic decline in *H. sapiens* trabecular BVF after the Pleistocene. Future work should examine other *H. sapiens* populations to further document the patterns of variation in BVF and should investigate the environmental and genetic influences that have shaped the modern human skeleton.

79

Acknowledgements

References

Adami, S., D. Gatti, et al. (1999). "Site-specific effects of strength training on bone structure and geometry of ultradistal radius in postmenopausal women." J Bone Miner Res **14**(1): 120-124.

Alexeeva, T., D. Bogatenkov, et al. (2003). "Anthropology of medieval Vlakhs in comparative study: on date of Mistikhalj burial site." Moskva: Scientific World (in Russian, summary in English.

Augat, P., T. Link, et al. (1998). "Anisotropy of the elastic modulus of trabecular bone specimens from different anatomical locations." Med Eng Phys **20**(2): 124-131.

Barak, M. M., D. E. Lieberman, et al. (2011). "A Wolff in sheep's clothing: Trabecular bone adaptation in response to changes in joint loading orientation." Bone **49**(6): 1141-1151.

Bassett, D. R., H. R. Wyatt, et al. (2010). "Pedometer-Measured Physical Activity and Health Behaviors in U. S. Adults." Medicine and Science in Sports and Exercise **42**(10): 1819-1825.

Bogenschutz, E. D., H. D. Smith, et al. (2011). "Mid-humerus adaptation in fast pitch softballers and the impact of throwing mechanics." Medicine and Science in Sports and Exercise **43**(9): 1698-1706.

Boutroy, S., B. Van Rietbergen, et al. (2008). "Finite element analysis based on in vivo HR-pQCT images of the distal radius is associated with wrist fracture in postmenopausal women." Journal of Bone and Mineral Research **23**(3): 392-399.

Bouxsein, M. L., T. Uchiyama, et al. (2004). "Mapping quantitative trait loci for vertebral trabecular bone volume fraction and microarchitecture in mice." J Bone Miner Res **19**(4): 587-599.

Brand, R. A., R. D. Crowninshield, et al. (1982). "Forces on the Femoral Head During Activities of Daily Living." The Iowa Orthopaedic Journal **2**: 43-49.

Carter, D.R. and W.C. Hayes (1977). "The compressive behavior of bone as a two-phase porous structure." Journal of Bone and Joint Surgery American **59**(7): 954-962.

Chirchir, H., T. L. Kivell, et al. (2015). "Recent origin of low trabecular bone density in modern humans." Proceedings of the National Academy of Sciences of the United States of America **112**(2): 366-371.

Cotter, M. M., D. A. Loomis, et al. (2011). "Human Evolution and Osteoporosis-Related Spinal Fractures." Plos One **6**(10).

Cowgill, L. W. (2010). "The Ontogeny of Holocene and Late Pleistocene Human Postcranial Strength." American Journal of Physical Anthropology **141**(1): 16-37.

Davee, A. M., C. J. Rosen, et al. (1990). "Exercise patterns and trabecular bone-density in college-women." Journal of Bone and Mineral Research **5**(3): 245-250.

Devlin, M. J., C. Grasemann, et al. (2013). "Maternal perinatal diet induces developmental programming of bone architecture." J Endocrinol **217**(1): 69-81.

Doube, M., M. M. Klosowski, et al. (2010). "BoneJ Free and extensible bone image analysis in ImageJ." Bone **47**(6): 1076-1079.

Doube, M., M. M. Klosowski, et al. (2011). "Trabecular bone scales allometrically in mammals and birds." Proceedings of the Royal Society B-Biological Sciences **278**(1721): 3067-3073.

Eshed, V., A. Gopher, et al. (2010). "Paleopathology and the origin of agriculture in the Levant." Am J Phys Anthropol **143**(1): 121-133.

Fajardo, R. J., T. M. Ryan, et al. (2002). "Assessing the accuracy of high-resolution X-ray computed tomography of primate trabecular bone by comparisons with histological sections." American Journal of Physical Anthropology **118**(1): 1-10.

Gefen, A. and R. Seliktar (2004). "Comparison of the trabecular architecture and the isostatic stress flow in the human calcaneus." Medical Engineering & Physics **26**(2): 119-129.

Giddings, V. L., G. S. Beaupre, et al. (2000). "Calcaneal loading during walking and running." Medicine and Science in Sports and Exercise **32**(3): 627-634.

Griffin, N. L., K. D'Aout, et al. (2010). "Comparative forefoot trabecular bone architecture in extant hominids." Journal of Human Evolution **59**(2): 202-213.

Haapasalo, H., S. Kontulainen, et al. (2000). "Exercise-induced bone gain is due to enlargement in bone size without a change in volumetric bone density: A peripheral quantitative computed tomography study of the upper arms of male tennis players." Bone **27**(3): 351-357.

Hallal, P. C., L. B. Andersen, et al. (2012). "Global physical activity levels: surveillance progress, pitfalls, and prospects." Lancet **380**(9838): 247-257.

Harrigan, T. P. and R. W. Mann (1984). "Characterization of microstructural anisotropy in orthotropic materials using a 2nd rank tensor." Journal of Materials Science **19**(3): 761-767.

Hildebrand, T. and P. Ruegsegger (1997). "Quantification of Bone Microarchitecture with the Structure Model Index." Comput Methods Biomech Biomed Engin **1**(1): 15-23.

Hodge, W. A., R. S. Fijan, et al. (1986). "Contact pressures in the human hip-joint measured invivo." Proceedings of the National Academy of Sciences of the United States of America **83**(9): 2879-2883.

Joo, Y. I., T. Sone, et al. (2003). "Effects of endurance on three-dimensional trabecular bone microarchitecture in young growing rats." Bone **33**(4): 485-493.

Larsen, H. and F. Rainey (1948). "Ipiutak and the Arctic whale hunting culture." Anthropological Papers of the American Museum of Natural History **42**: 1-276.

Latimer, B. and C. O. Lovejoy (1989). "The calcaneus of australopithecus-afarensis and its implications for the evolution of bipedality." American Journal of Physical Anthropology **78**(3): 369-386.

Li, G., J. Gil, et al. (1999). "A validated three-dimensional computational model of a human knee joint." Journal of Biomechanical Engineering-Transactions of the Asme **121**(6): 657-662.

Lieberman, D. E. (1993). "The rise and fall of seasonal mobility among hunter-gatherers - the case of the southern levant." Current Anthropology **34**(5): 599-631.

Lieberman, D. E. (1996). "How and why humans grow thin skulls: Experimental evidence for systemic cortical robusticity." American Journal of Physical Anthropology **101**(2): 217-236.

Lieberman, D. E., M. Venkadesan, et al. (2010). "Foot strike patterns and collision forces in habitually barefoot versus shod runners." Nature **463**(7280): 531-U149.

Lovejoy, C. O. and E. Trinkaus (1980). "Strength and robusticity of the neandertal tibia." American Journal of Physical Anthropology **53**(4): 465-470.

Maga, M., J. Kappelman, et al. (2006). "Preliminary observations on the calcaneal trabecular microarchitecture of extant large-bodied hominoids." American Journal of Physical Anthropology **129**(3): 410-417.

Marlowe, F. W. (2005). "Hunter-gatherers and human evolution." Evolutionary Anthropology **14**(2): 54-67.

Mittra, E., C. Rubin, et al. (2005). "Interrelationship of trabecular mechanical and microstructural properties in sheep trabecular bone." Journal of Biomechanics **38**(6): 1229-1237.

New, S. A., S. P. Robins, et al. (2000). "Dietary influences on bone mass and bone metabolism: further evidence of a positive link between fruit and vegetable consumption and bone health?" Am J Clin Nutr **71**(1): 142-151.

Nigg, B. M., G. K. Cole, et al. (1995). "Impact forces during heel toe running." Journal of Applied Biomechanics **11**(4): 407-432.

Odgaard, A. (1997). "Three-dimensional methods for quantification of cancellous bone architecture." Bone **20**(4): 315-328.

Pontzer, H., D. E. Lieberman, et al. (2006). "Trabecular bone in the bird knee responds with high sensitivity to changes in load orientation." Journal of Experimental Biology **209**(1): 57-65.

Pontzer, H., D. A. Raichlen, et al. (2014). "Bipedal and quadrupedal locomotion in chimpanzees." Journal of Human Evolution **66**: 64-82.

Pontzer, H., D. A. Raichlen, et al. (2009). "The metabolic cost of walking in humans, chimpanzees, and early hominins." Journal of Human Evolution **56**(1): 43-54.

Pontzer, H., D. A. Raichlen, et al. (2012). "Hunter-Gatherer Energetics and Human Obesity." Plos One **7**(7).

Pontzer, H. and R. W. Wrangham (2004). "Climbing and the daily energy cost of locomotion in wild chimpanzees: implications for hominoid locomotor evolution." Journal of Human Evolution **46**(3): 317-335.

Rice, J. C., S. C. Cowin, et al. (1988). "On the dependence of the elasticity and strength of cancellous bone on apparent density." Journal of Biomechanics **21**(2): 155-168.

Ruff, C. B., E. Trinkaus, et al. (1993). "Postcranial robusticity in homo .1. Temporal trends and mechanical interpretation." American Journal of Physical Anthropology **91**(1): 21-53.

Ryan, T. M. and R. A. Ketcham (2002). "Femoral head trabecular bone structure in two omomyid primates." Journal of Human Evolution **43**(2): 241-263.

Ryan, T. M. and C. N. Shaw (2015). "Gracility of the modern Homo sapiens skeleton is the result of decreased biomechanical loading." Proceedings of the National Academy of Sciences of the United States of America **112**(2): 372-377.

Scherf, H., K. Harvati, et al. (2013). "A comparison of proximal humeral cancellous bone of great apes and humans." Journal of Human Evolution **65**(1): 29-38.

Silva, M. J. and L. J. Gibson (1997). "Modeling the mechanical behavior of vertebral trabecular bone: Effects of age-related changes in microstructure." Bone **21**(2): 191-199.

Simkin, A., J. Ayalon, et al. (1987). "Increased trabecular bone-density due to bone-loading exercises in postmenopausal osteoporotic women." Calcified Tissue International **40**(2): 59-63.

Spoor, C. F., F. W. Zonneveld, et al. (1993). "Linear measurements of cortical bone and dental enamel by computed-tomography - applications and problems." American Journal of Physical Anthropology **91**(4): 469-484.

Trinkaus, E. (1976). "The evolution of the hominid femoral diaphysis during the Upper Pliestocene in Europe and the Near East." Zietschrift fur Morphologie und Anthropologie **67**(3): 291-319.

Trut, L., A. Kharlamova, et al., Eds. (2006). Morphology and behavior: are the coupled at the genome level? In: The Dog and its Genome. Woodbury, New York, Cold Spring Harbor Laboratory Press.

Tsegai, Z. J., T. L. Kivell, et al. (2013). "Trabecular Bone Structure Correlates with Hand Posture and Use in Hominoids." Plos One **8**(11).

Unger-Hamilton, R. (1989). "The epi-palaeolithic southern levant and the origins of cultivation." Current Anthropology **30**(1): 88-103.

Whittle, M. W. (1999). "Generation and attenuation of transient impulsive forces beneath the foot: a review." Gait & Posture **10**(3): 264-275.

Wiren, K. M., X. W. Zhang, et al. (2012). "Androgen prevents hypogonadal bone loss via inhibition of resorption mediated by mature osteoblasts/osteocytes." Bone **51**(5): 835-846.

Zeininger, A. (2013). <u>Ontogeny of Bipedalism: Pedal Mechanics and Trabecular Bone Morphology</u>. PhD, University of Texas, Austin.

Chapter 5 – Testing hypotheses about bony resistance to impact forces in human calcaneal trabecular bone

Introduction

The human calcaneus (the heel bone) must resist millions of impact forces per year due to repetitive heel-ground impacts during walking and heel strike running, and trabecular bone tissue is thought to play an important role in resisting impact forces (Radin et al. 1972; Currey 2002; Dong et al. 2004; Passi and Gefen 2005). However, opinions differ about how variations in trabecular BVF in humans and between humans and other species function to resist impacts. Some researchers argue that increased elastic modulus, strength and toughness via larger trabecular BVF are adaptations to resist impacts (Currey 2002), while others suggest that lower trabecular BVF is an adaptation for dissipating energies and shielding cartilage from damage (Radin et al 1972; Goodwin and Horner 2004; Latimer 2005). How variations in trabecular bone structure resist impacts may also be relevant to the etiology of diseases such as osteoarthritis (OA) that have been linked to both high trabecular BVF and to repetitive impact forces (Radin et al. 1972).

Differing opinions about how trabecular tissue would be shaped to resist impact forces can be summarized with two competing hypotheses. One hypothesis is that trabecular structures with greater BVF are better adapted to resist impact forces because larger BVF increases the elastic modulus (E), yield strength (σ_y) and work-to-failure (W_f - the energy absorbed before trabecular tissue fracture, Figure 5.1A) of trabecular tissue (Currey 2002). If so, then trabecular structures with larger BVF improve bone resistance to impacts because they are stiffer, stronger and absorb more energy before fracture. An alternative hypothesis is that structures with lower BVF are better adapted to resist impact forces because they dissipate more mechanical energy (Latimer 2005). When an external force is applied cyclically, the energy dissipated upon unloading and is measured as the area between the loading and unloading curves (Figure 5.1B). Compared to E, σ_y and W_f, relatively little is known about energy

86

dissipation in trabecular tissue. Early reports suggested that energy dissipation in trabecular tissue was

so small as to be unmeasurable more recent studies have shown that energy dissipation decreases with

the rate of applied strains (Pugh et al. 1973; Dong et al. 2004). Efforts to relate variations in trabecular

structure to energy dissipation have yielded partly contradictory conclusions. Linde et al (1989) found a

weak inverse correlation between trabecular tissue apparent density (a function of trabecular BVF and

the density of the trabecular bone material) and the fraction of energy dissipated in trabecular samples

from the human proximal tibia under cyclic loading to 0.6% strain. In contrast, Lambers et al (2013)

found no relationship between human vertebral trabecular BVF and the total amount of energy

dissipated under cyclic compression to 0.35% strain. Toyras et al (2002) found that in bovine trabecular

bone under stress-controlled cyclic compression (strains less than 0.2%) the fraction of energy

dissipated increased in samples of lower bone mineral density as measured by DXA. While these

investigations have provided valuable information about energy dissipation in trabecular tissue, these

studies used different measurements of energy dissipation (fraction vs. total amount of energy

dissipated) under experimental conditions that varied widely in terms of applied strains and stresses,

making it difficult to draw general conclusions about the relationship between trabecular BVF and

energy dissipation (Linde et al. 1989; Toyras et al. 2002; Lambers et al. 2013).

One way to think about how trabecular bone dissipates energy is to begin with the premise that

energy dissipation in trabecular tissue is primarily caused by microdamage (Fantner et al. 2005; Lambers

et al. 2013). Microdamage in trabecular tissue increases with strain magnitude (ε), and in turn, energy

dissipation per unit volume (W_d) is positively correlated with strain magnitude (Lambers et al. 2013):

Equation 1: $\varepsilon \sim W_d$

Using classic solid mechanics, strain is equal to the stress (σ) applied to trabecular tissue divided by the

elastic modulus (E):

Equation 2: $\varepsilon = \dfrac{\sigma}{E}$

Studies find that E of human trabecular tissue is proportional to BVF squared (Rice et al. 1988; Keaveny et al. 2001). Substituting this relationship and equation 1 into equation 2 yields:

Equation 3: $W_d \sim \dfrac{\sigma}{BVF^2}$

A

Stress — σ_y — W_f

Strain

B

Stress — loading — unloading — W_d
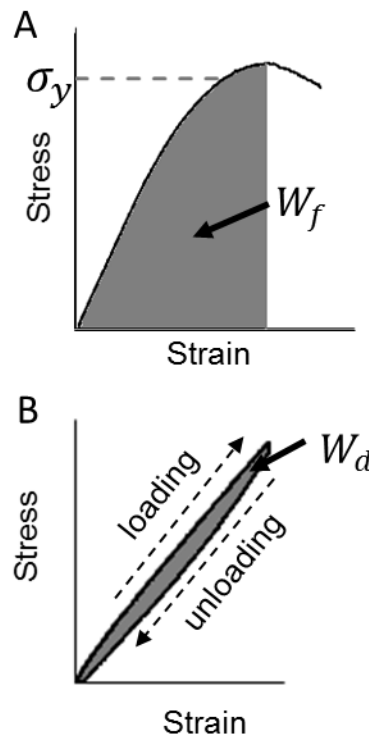
Strain

Figure 5.1: Materials testing measurements. A: Work-to-failure (W_f) was measured as the area beneath the stress-strain curve from 0 strain to the strain at which the stress is maximized. Yield stress (σ_y) was measured using the 0.2% offset method and is generally less than the maximum stress. B: Energy dissipation (W_d) was measured as the area between the loading and unloading curves during cyclic loading.

Equation 3 indicates an inverse relationship between energy dissipation and BVF - trabecular structures with lower BVF will dissipate more energy when stress across specimens is constant. Specifically, we hypothesize that W_d in trabecular bone tissue will scale with the inverse of BVF squared under stress-controlled conditions.

The positive relationships between BVF and E, σ_y and W_f (E, σ_y and W_f will be collectively termed the 'bone strength variables') and the inverse relationship between W_d and BVF suggest that there is a trade-off between the bone strength variables and W_d as mediated by BVF. In practical terms, decreasing BVF will increase energy dissipation at the expense of each of the bone strength variables. Thus, we hypothesize that trabecular BVF mediates a trade-off between the bone strength variables and W_d.

Further, the hypothesized trade-off between the bone strength variables and W_d may help explain how the human calcaneus evolved to resist repetitive impacts from walking and heel strike running. Modern human hunter-gatherers from tropical environments walk on average between 9 and 15 km/day and it is thought that humans used to run regularly to hunt, thus exposing the human calcaneus to millions of impact forces per year (Marlowe 2005, Bramble and Lieberman 2004). Scholars have interpreted the relatively lower calcaneal BVF values in modern humans compared to apes as beneficial for dissipating energy from impacts (Latimer and Lovejoy 1989; Latimer 2005). Other lines of evidence, however, show that human calcaneal trabecular BVF was greater in the Pleistocene, perhaps indicating larger E, σ_y and W_f relative to modern humans (Addison et al., in prep). Alternatively, human calcaneal trabecular BVF may be shaped to optimize W_d and one or more of the bone strength variables. However, with several outstanding hypotheses and little data, it is clear that in order to understand how the human calcaneus evolved to resist repetitive impacts we must compare structural data from human calcaneal trabecular bone to actual mechanical data on the relationships between trabecular BVF and the mechanical variables W_d, E, σ_y and W_f.

This study therefore tests the following hypotheses. First, W_d is predicted to scale with the inverse of trabecular BVF squared under stress-controlled conditions. Second, we predict tradeoffs between W_d and each of the bone strength variables, mediated by BVF. We test these hypotheses in

89

trabecular tissue samples taken from human calcanei loaded in cyclic compression. We then compare

previously collected data on human calcaneal BVF from several populations to the experimental data in

order to explore how variations in calcaneal BVF resist repetitive impact forces. Specifically, we

hypothesize that if human calcanei resist impacts by one or more of the bone strength variables, then

human calcaneal trabecular tissue will have relatively greater E, σ_y and W_f compared to W_d when

experimental data is converted to a normalized scale. Alternatively, if human calcanei resist impacts by

dissipating mechanical energy, then human calcaneal trabecular tissue will have relatively greater W_d

than any of the bone strength variables. Finally, if human calcaneal trabecular tissue is shaped to

optimize W_d and one or more of the bone strength variables, then human calcaneal trabecular BVF will

have equivalent relative values of W_d and the bone strength variables.

Methods

Sample Preparation

Human cadaver calcanei were obtained from an anatomical gifts program (MedCure, Portland,

Oregon, USA). The sample consisted of 13 donors with no medical history of metabolic bone disease or

cancer (Female: 7 donors, average age=57.1; Male: 6 donors, average age=57.2). All calcanei were first

microCT scanned at the Center for Nanoscale Systems at Harvard University using an XTEK micro-CT

scanner, model HMXST225 (Nikon Metrology) at a resolution of 45 microns with a tungsten target and a

source energy of 75 kV and current of 130 microA. Scans revealed no evidence of bone damage or

pathologies, and showed that the primary orientation of trabeculae was aligned with the long axis of the

calcaneal tuberosity.

We followed the general procedure outlined in prior studies to obtain trabecular bone cores

from cadaver calcanei and perform mechanical tests (Keaveny et al. 1997). Subsequent to microCT

scanning, two cuts 35 mm apart were made perpendicular to the long axis of the calcaneal tuberosity

using an Isomet low-speed saw with a diamond tipped blade (Beuhler, Lake Bluff, IL, USA), leaving a slab

of trabecular bone from which cylindrical cores were extracted. Cores of trabecular bone were removed

using a 7.6 mm diameter diamond tipped coring bit (Starlite Industries, Bryn Mawr, PA, USA). Specimens

were kept hydrated during coring and subsequently wrapped in saline-soaked gauze and stored

individually in air-tight containers at -20 C. A total of 29 trabecular cores were used for mechanical

testing, with between 1 and 3 cores from each donor.

Prior to mechanical testing, specimens were again microCT scanned using the same parameters

described above. 3D volumes of trabecular cores were reconstructed from the raw data using CT PRO

software (Nikon Metrology). Reconstructed volumes were initially processed in VGStudioMax v2.2

software (Volume Graphics, Heidelberg, Germany). 3D cylindrical volumes of interest encompassing the

entire bone core were created and exported as stacks of 16-bit TIFF images. 16-bit images were

converted to 8-bit images in ImageJ software (image resolution was 22.2 pixels per mm), and we used a

modified half-maximum height method to separate bone versus non-bone pixels (Fajardo et al. 2002).

Briefly, a line 10 pixels in length was drawn across a random bone to non-bone interface in a random

image slice in the TIFF stack. The grey-scale values along this line were recorded and the maximum and

minimum grey values were averaged. This process was repeated 10 times per cylindrical core. The 10

averages from the maximum and minimum greyscale values were then averaged to compute a

threshold used to differentiate bone versus non-bone pixels. The BoneJ plugin for ImageJ was used to

calculate trabecular BVF (Doube et al. 2010).

Specimens were wrapped in saline-soaked gauze and stored at -20 C after micro-CT scanning.

Prior to the day of testing, specimen ends were mounted in brass endcaps with adhesive (Locktite 401)

following the method described by Keaveny et al 1997. Specimens measured an average (SD) of 15.0 +/-

0.28 mm between the endcaps. The effective length of the each specimen was calculated as the

exposed length plus half of the total length minus the exposed length (Keaveny et al. 1997). The average

(SD) effective length (in mm) of the specimens was 23.4 +/- 0.7. Following mounting, specimens were re-wrapped in saline soaked gauze and allowed to thaw at room temperature overnight.

Mechanical Testing

Specimens were tested in cyclic compression using an Instron model 8511 (8800 controller). Specimens were gripped at the endcaps and a two-axis positioning table was used to align the specimens vertically. An extensometer (Instron model 2620-826) was attached to the endcaps using elastic bands. All testing was performed at room temperature. All specimens were first preconditioned by loading for 10 cycles in position control. A set strain across all specimens was not achieved during the preconditioning cycles due to varying specimen lengths and equipment limitations (see Appendix A), so the lowest strain reached by all specimens (0.154%) was used to calculate elastic modulus. The compressive modulus (E) of each specimen was measured by taking the slope of the best linear fit of the tenth loading cycle from 0.0% to 0.154% ε.

Next, 28 of the original 29 specimens were loaded in cyclic compression in position control mode for 10 cycles with lower and upper load limits (30 N and 0 N, respectively; 1 specimen failed below 30 N and thus was not used) imposed on the test so that the motion of the machine actuator reversed direction when a load limit was breached (see Appendix B). The rate of displacement of the crosshead was set to 0.022 mm/s. This methodology effectively created a cyclic, stress-controlled experiment but at similar strain rate across specimens, and was chosen because previous research has indicated that mechanical properties of trabecular bone are sensitive to strain rate (Carter and Hayes 1977; Linde et al. 1991; Dong et al. 2004). Finally, 6 specimens (other specimens were lost due to operator error) were loaded in compression to failure at a crosshead displacement rate of 0.022 mm/s.

We used the raw stress and strain data from the cyclic and failure tests to calculate W_d, W_f and σ_y. We first measured the energy absorbed during the loading cycle, W_a, by calculating the area

beneath the loading curve and calculated W_d by subtracting the area beneath the unloading curve from

the area beneath the loading curve. In both stress and strain controlled protocols, W_d and W_a from the

first five loading-unloading cycles were averaged to obtain mean values for each specimen. For the

failure tests, σ_y was calculated using the 0.2% offset method and W_f was calculated as the area beneath

the stress-strain curve from 0% ε to the failure strain, which was defined as the strain at which stress

was maximized (Linde et al. 1989).

Comparative trabecular morphology

We collected trabecular bone structural data from the calcaneus using microCT scanning from 4

human populations spanning the Pleistocene and Holocene geological periods, including hunter-

gatherers from the Levant dated to 12,000 years ago (Natufian, n=10; Pleistocene), Inuit hunter-

gatherers from Alaska (Point Hope, n=19; Holocene), medieval European pastoralists from modern-day

Serbia (Mistihalj, n=15; Holocene) and a modern Americans (n=20; Holocene). The samples from the

American population were the same samples used in the materials testing described above; for more

details on the archaeological populations, see Addison et al (in prep). All bones were scanned at 45

microns. We examined cubic volumes of interest (VOIs) in the calcaneal tuberosity and used a process

identical to the one described above to threshold VOIs and determine trabecular BVF. Because the

Natufian population had greater calcaneal BVF than the other populations and there were no significant

differences in calcaneal BVF between Point Hope, Mistihalj or modern Americans, we separated the

populations into "Pleistocene" (consisting only of Natufians) and "Holocene" (consisting of Point Hope,

Mistihalj and Americans) groups, denoting the geologic age of the populations.

Data Analyses

JMP v11 software was used to perform least-squares regression analyses between trabecular

BVF and E, σ_y, W_d, W_a and W_f. The specimen that failed below 30 N was used in the σ_y and W_f

analyses because the rates of crosshead displacement during the stress-controlled test and the failure

test were the same, giving a total of 7 specimens for the σ_y and W_f analyses. In addition, we analyzed

the relationships between strain and W_d and between W_a and W_d using log base 10 transformations to

account for potential heteroscedasticity. Further, we analyzed the relationship between BVF and W_d for

specimens that experienced strains equal to or less than 0.2% to understand how energy dissipation

relates to BVF for strains in the physiologic range (see Appendix C). We used ANOVA to compare

calcaneal BVF between Pleistocene and Holocene *H. sapiens.* Relationships between variables were

considered significant at p-values < 0.05. Finally, we performed bootstrapping analyses on the BVF vs.

σ_y and BVF vs. W_f relationships to understand how the limited sample size influenced the confidence of

the result (see Appendix D).

Tradeoff models

We tested the hypothesized tradeoff models by normalizing the experimentally obtained values

of W_d and the bone strength variables from 0 to 100 (%). We then regressed the normalized E, σ_y, W_f,

and W_d values against BVF and created tradeoff plots comparing normalized W_d to each of the

normalized bone strength variables. Because the bone strength variables were hypothesized to increase

with BVF while W_d was predicted to decrease with BVF, the intersection of the regression lines would

identify the BVF value that optimized W_d and either E, σ_y or W_f. Next, we compared Pleistocene and

Holocene *H. sapiens* calcaneal BVF population means to the optimum points on each tradeoff model.

Finally, we performed bootstrapping analyses on the scaled values of E, σ_y and W_f to calculate

confidence intervals (see Appendix D).

Results

The trabecular cores used for E and W_d analyses had a greater than 4-fold range in trabecular

BVF (range: 0.08 to 0.38; average=0.204, standard deviation=0.073), while the samples used for σ_y and

W_f analyses had a 3.5 fold range (range: 0.08 to 0.28; average=0.204, standard deviation = 0.064).

Trabecular BVF was a strong predictor of E (r = 0.91, p < 0.0001), σ_y (r = 0.91, p =0.001) and W_f (r = 0.84, p=0.0035) (Table 5.1).

Table 5.1: Relationships between trabecular BVF and elastic modulus, yield stress and work-to-failure

Independent variable	Dependent variable	Equation	r	p-value
BVF	E (MPa)	$y = 17568x^{2.14}$	0.91	p < 0.0001
BVF	σ_y (MPa)	$y = 159.6x^{2.43}$	0.95	p = 0.001
BVF	W_f (Pa)	$y = 866597x^{2.14}$	0.92	p =0.0035

Stress Control tests

Trabecular BVF was a significant predictor of W_d (r = -0.80 p < 0.0001; Figure 5.2A; Table 5.2) and W_a (r = -.90, p < 0.0001; Figure 5.2B; Table 5.2). Log(W_d) was also correlated with log(ε) (r = 0.94, p < 0.0001; Figure 5.2C; Table 5.2) and log(W_a) (r = 0.95, p < 0.0001; Figure 5.2D; Table 5.2). See Appendix C for regression relationships between BVF and W_d for strains less than 0.2%.

Table 5.2: Regression relationships for the stress controlled test

Independent variable	Dependent variable	Equation	r	p-value
BVF	W_d (Pa)	$y = 1.73x^{-2.11}$	-0.80	p < 0.0001
BVF	W_a (Pa)	$y = 21.65x^{-1.92}$	-0.90	p < 0.0001
Log(ε(%))	Log(W_d (Pa))	$y = 1.1x + 0.49$	0.94	p < 0.0001
Log(W_a (Pa))	Log(W_d (Pa))	$y = 1.16x - 1.40$	0.95	p < 0.0001

Comparative Trabecular Morphology

Pleistocene *H. sapiens* calcaneal BVF (average: 0.26, SD: 0.05) was significantly greater than Holocene *H. sapiens* (average: 0.18, SD: 0.05; F(1,58)=16.5, p=0.0001).
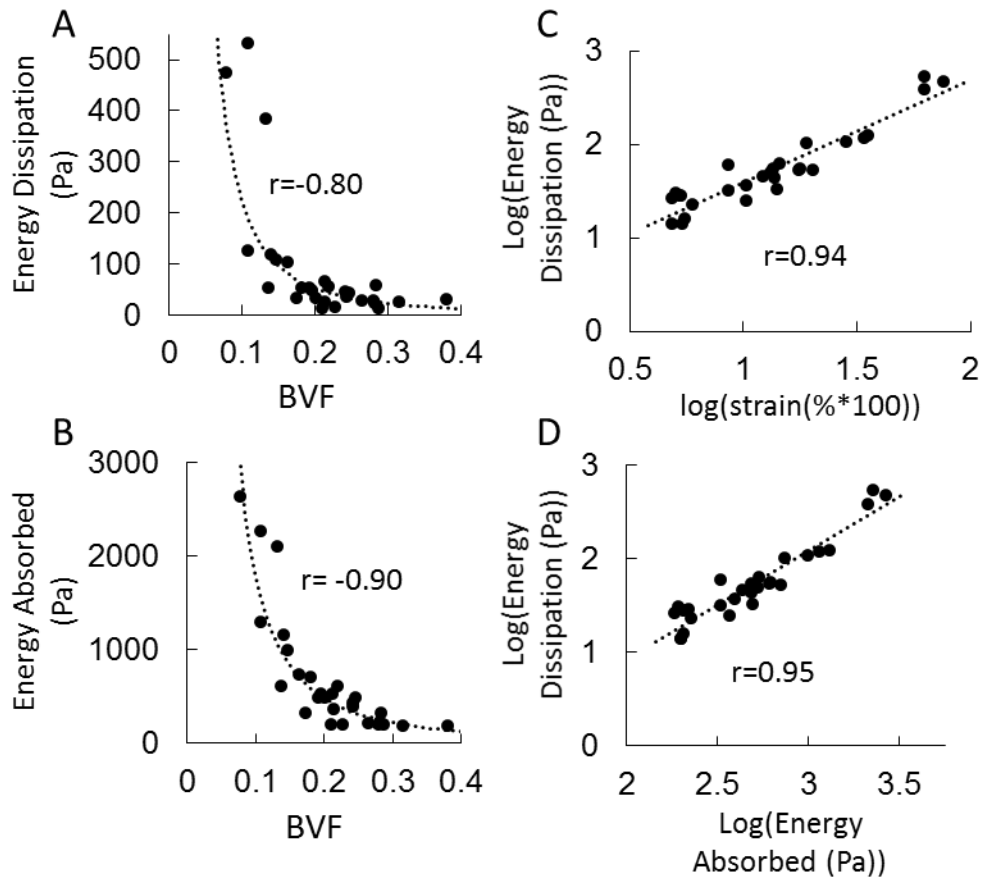
Figure 5.2: Regression results between variables. A: Trabecular BVF versus W_d, B: Trabecular BVF versus W_a, C: log_{10}(strain) versus log_{10} (W_d), D: $log_{10}(W_a)$ versus $log_{10}(W_d)$.

Tradeoff models

The tradeoff models using the best-fit regression equations of BVF vs. normalized W_d and each of the bone strength variables plotted in Figure 5.3A-C indicate that a BVF of 0.15 optimizes W_d and each of the bone strength variables.

Figure 5.4A-C plots the best-fit regression equations of BVF vs. normalized W_d and each of the bone strength variables (the raw data points have been removed for clarity), and the mean calcaneal BVF of the Holocene and Pleistocene populations. The Holocene and Pleistocene population mean BVF (0.18 and 0.26, respectively) are 20% and 73% greater than the optimum BVF (0.15). The optimum BVF

96

falls within one standard deviation (0.05) of the mean Holocene BVF and falls outside of two standard deviations (0.05) of the mean Pleistocene BVF.

Discussion

We predicted that W_d would scale with the inverse of BVF squared and that there would be a tradeoff between W_d and each of the bone strength variables mediated by BVF. Both hypotheses were supported by the experimental data. We found that lower BVF values correlated significantly with greater W_d. We also correctly predicted a trade-off between W_d and the bone strength variables mediated by BVF: specimens with larger BVF had greater E, σ_y and W_f but lower W_d under stress controlled conditions (Figure 5.3). The tradeoff model indicated that a BVF of 0.15 optimized W_d and each of the bone strength variables.

Next, we evaluated Pleistocene and Holocene calcaneal trabecular BVF population means in the context of the tradeoff models to test hypotheses about how calcaneal trabecular tissue resists impacts. Average calcaneal BVF values in Pleistocene and Holocene *H. sapiens* were greater than the optimum BVF of 0.15, indicating that trabecular tissue from the human calcaneus has proportionally greater E, σ_y and W_f than W_d, thus supporting the hypothesis that human calcaneal trabecular tissue resists impacts by being stiff, strong and absorbing energy before fracture, particularly for the Pleistocene samples (Figure 5.4).

This study has several limitations. The strain rate of the cyclic waveform used in this study was slightly variable because of varying specimen lengths and equipment limitations, and both E and σ_y are sensitive to strain rate (Carter and Hayes 1977; Linde et al. 1991). However, the variability in strain rate (940 +/- 27.2 $\frac{\mu\varepsilon}{s}$) is small compared to studies that have investigated the phenomena and there was no relationship between strain rate and W_d (r = 0.14, p=0.50) (Carter and Hayes 1977). Further, the strain rate of the cyclic waveform used in this study is an order of magnitude slower than physiologically
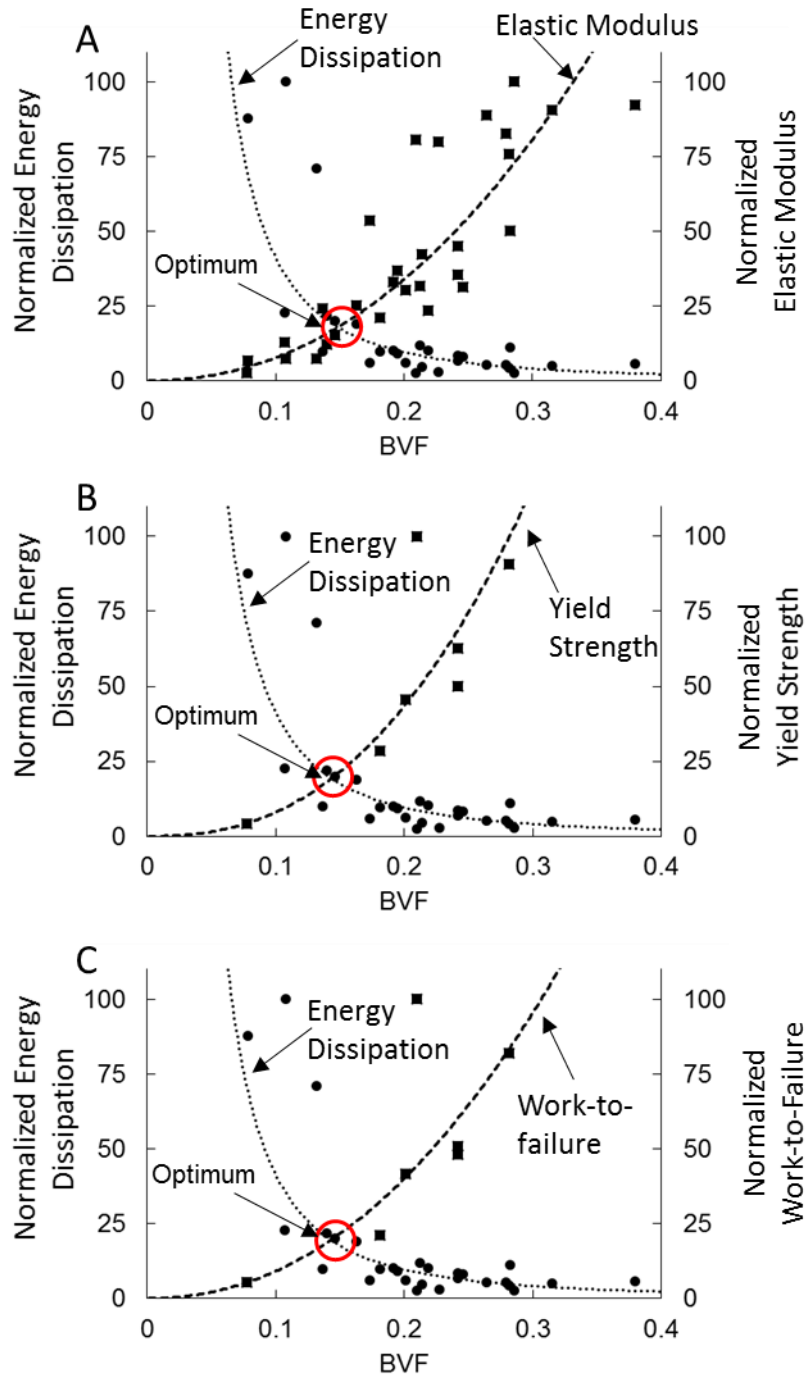
Figure 5.3: Tradeoff models with raw data points shown. The BVF that optimizes W_d with E, σ_y or W_f is circled. A: Tradeoff model of W_d and E, B: Tradeoff model of W_d and σ_y, C: Tradeoff model of W_d and W_f.

relevant impact strain rates (roughly 10,000 $\mu\dot{\varepsilon}$; measured in the human tibia) (Burr et al. 1996) due to

constraints of experimental equipment. Previous studies have shown that E, σ_y and W_f would be

greater had we used a faster strain rate (Carter and Hayes 1977; Linde et al. 1991). It is unclear how higher strain rates would affect W_d; however it is likely that W_d would decrease with strain rate because the fraction of energy dissipated is inversely related to strain rate (Dong et al. 2004). Thus we should view the W_d values as an upper bound on energy dissipation and the values of E, σ_y and W_f as lower bounds on elastic modulus, yield strength and work-to-failure, respectively, for trabecular tissue under impact loading. In addition, other aspects of trabecular architecture, such as anisotropy or structure model index, influence E, σ_y and W_f and likely W_d as well (Ulrich et al. 1999; Mittra et al. 2005). We considered the effects of BVF only in this study because most prior hypotheses concerning impacts and trabecular structure focus on variations in BVF (Latimer and Lovejoy 1989; Currey 2002; Latimer 2005). The strong relationships between BVF and E, σ_y, W_f and W_d suggest that our regression analyses were not confounded by lack of inclusion of other trabecular structural variables in our regression models. Future work should investigate the relative contribution of other aspects of trabecular structure to W_f and W_d.

An additional limitation is that we used prior observations and inferences about trabecular microdamage to predict that W_d would vary with BVF^{-2}, but we did not quantify microdamage in the samples. Therefore we cannot be certain whether microdamage is the cause of variations in W_d values observed here. Microdamage has been shown to increase rapidly when strains outside the physiologic range are imposed (Moore and Gibson 2002; Nagaraja et al. 2005). Evidence that W_d is more strongly associated with strain when specimens loaded outside the physiologic strain range are considered (see Figure 5.2 and Appendix C) suggests that microdamage is involved in energy dissipation.

Results from this study suggest that the primary function of human calcaneal trabecular tissue under impact forces is to be stiff, strong and tough rather than to dissipate mechanical energy because the average calcaneal BVF values for both human groups indicate a large E, σ_y and W_f relative to W_d.

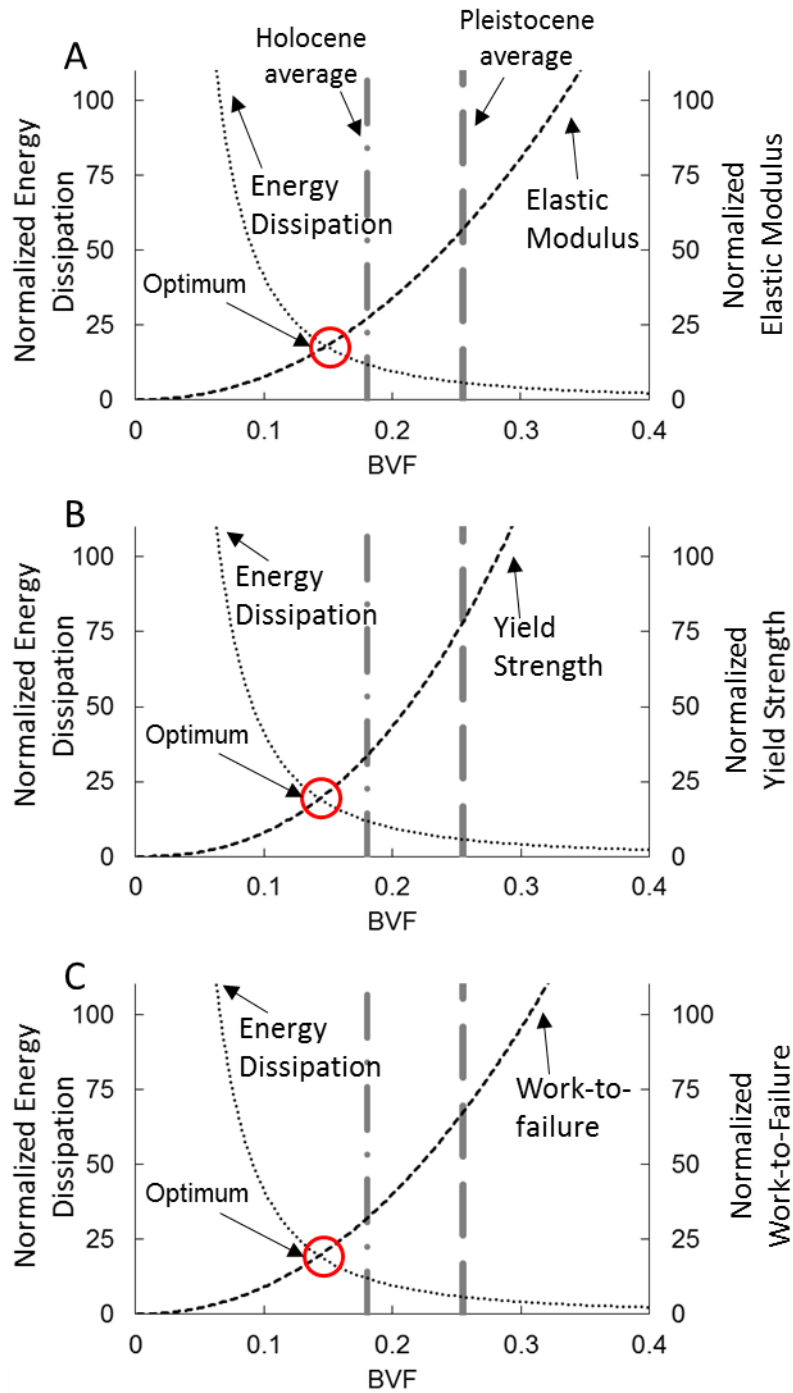**Figure 5.4**: Tradeoff models with average Pleistocene and Holocene calcaneal tuberosity BVF indicated as dashed lines. A: Tradeoff model of W_d and E, B: Tradeoff model of W_d and σ_y, C: Tradeoff model of W_d and W_f.

This result is especially true if we consider only the Pleistocene group, which is likely more

representative of the ancestral condition of trabecular BVF because of their geological age and

subsistence strategies (Unger-Hamilton 1989; Lieberman 1993). This finding has important implications for how the human musculo-skeletal system resists impacts from walking and heel-strike running. Impact energy not dissipated by the calcaneus is transferred through the lower extremity, thus placing increased emphasis on other mechanisms to dissipate energy, notably eccentric muscle contractions or passive damping in cartilage. Available data suggest that energy dissipation in young bovine cartilage under shear varies depending on the depth from the cartilage surface, and that human ankle muscles dissipate energy on the order of 0.5 J/kg from drop-heights of 30 cm (Zhang et al. 2000; Buckley et al. 2013). However, varying study goals and experimental conditions obscure the relative contributions of bone, cartilage and muscles to dissipating energy from heel strike impacts, and additional research is necessary to uncover how these tissues work in concert to dissipate impact energies.

The results from this study may be relevant to the incidence and prevalence of OA. One longstanding hypothesis is that subchondral trabecular bone of elevated BVF contributes to the incidence of OA because high-BVF trabecular tissue has an increased elastic modulus and reduced capacity to absorb and dissipate mechanical energies (Radin et al. 1972). In turn, the surrounding cartilage deteriorates under excessive shear stresses (Radin et al. 1972). Under this hypothesis, we might expect OA incidence (controlled for biological age) to be greater in Pleistocene vs. Holocene *H. sapiens* because evidence suggests systemically higher trabecular BVF in Pleistocene populations (Chirchir et al. 2015; Addison et al, in prep). However, this prediction is complicated by a number of factors. First, there is contradictory evidence as to whether the elastic modulus of subchondral trabecular bone influences the stresses in articular cartilage (Brown et al. 1984; Burgin and Aspden 2008). Second, paleopathological studies on OA incidence suffer from limitations such as lack of strict controls for biological age and anatomical location, as well as using proxies for OA incidence (such as the presence of osteophytes) or pitting eburnation. Unsurprisingly, then, some studies find OA incidence is greater in forager populations than in either agriculturalists or industrial populations (Jurmain 1977;

Jurmain 1980; Larsen 1981), while others find greater incidence in agriculturalists (Goodman et al. 1984;

Bridges 1992). Finally, the use of soft, heeled footwear in modern human populations alters the

mechanical energy associated with heel strike impacts, complicating any direct relationships between

trabecular BVF, energy dissipation and OA prevalence between modern humans and their ancestors

(Addison and Lieberman 2015). These findings, of course, say nothing about other putative causes of OA

such as biological age, inflammation and 'abnormal' mechanical forces (Anderson and Loeser 2010;

Berenbaum 2013; Felson 2013). Clearly, more research is required in order to establish patterns of OA

incidence in *H. sapiens* populations and to understand the interplay between biological and

environment risk factors in the etiology of the disease.

References

Addison, B.J., M.J. Senter-Zapata and D.E. Lieberman (in prep). "Patterns of variation in trabecular bone volume fraction in the calcaneus and C2 vertebra of *Gorilla gorilla, Pan troglodytes and Homo sapiens.*"

Addison, B. J. and D. E. Lieberman (2015). "Tradeoffs between impact loading rate, vertical impulse and effective mass for walkers and heel strike runners wearing footwear of varying stiffness." Journal of Biomechanics **48**(7): 1318-1324.

Anderson, S. and R. F. Loeser (2010). "Why is osteoarthritis an age-related disease?" Best practice & research. Clinical rheumatology **24**(1): 15-26.

Berenbaum, F. (2013). "Osteoarthritis as an inflammatory disease (osteoarthritis is not osteoarthrosis!)." Osteoarthritis and Cartilage **21**(1): 16-21.

Bramble, D. M. and D. E. Lieberman (2004). "Endurance running and the evolution of Homo." Nature **432**(7015): 345-352.

Bridges, P. S. (1992). "Prehistoric arthritis in the america." Annual Review of Anthropology **21**: 67-91.

Brown, T. D., E. L. Radin, et al. (1984). "Finite-element studies of some juxtarticular stress changes due to localized subchondral stiffening." Journal of Biomechanics **17**(1): 11-&.

Buckley, M. R., L. J. Bonassar, et al. (2013). "Localization of Viscous Behavior and Shear Energy Dissipation in Articular Cartilage Under Dynamic Shear Loading." Journal of Biomechanical Engineering-Transactions of the Asme **135**(3): 9.

Burgin, L. V. and R. M. Aspden (2008). "Impact testing to determine the mechanical properties of articular cartilage in isolation and on bone." Journal of Materials Science-Materials in Medicine **19**(2): 703-711.

Burr, D. B., C. Milgrom, et al. (1996). "In vivo measurement of human tibial strains during vigorous activity." Bone **18**(5): 405-410.

Carter, D. R. and W. C. Hayes (1977). "Compressive behavior of bone as a 2-phase porous structure." Journal of Bone and Joint Surgery-American Volume **59**(7): 954-962.

Chirchir, H., T. L. Kivell, et al. (2015). "Recent origin of low trabecular bone density in modern humans." Proceedings of the National Academy of Sciences of the United States of America **112**(2): 366-371.

Currey, J. D. (2002). Bones: Structure and Mecanics. Princeton, Princeton University Press.

Dong, X. N., Y. N. Yeni, et al. (2004). "Effects of end boundary conditions and specimen geometry on the viscoelastic properties of cancellous bone measured by dynamic mechanical analysis." Journal of Biomedical Materials Research Part A **68A**(3): 573-583.

Doube, M., M. M. Klosowski, et al. (2010). "BoneJ Free and extensible bone image analysis in ImageJ." Bone **47**(6): 1076-1079.

Fajardo, R. J., T. M. Ryan, et al. (2002). "Assessing the accuracy of high-resolution X-ray computed tomography of primate trabecular bone by comparisons with histological sections." American Journal of Physical Anthropology **118**(1): 1-10.

Fantner, G. E., T. Hassenkam, et al. (2005). "Sacrificial bonds and hidden length dissipate energy as mineralized fibrils separate during bone fracture." Nature Materials **4**(8): 612-616.

Felson, D. T. (2013). "Osteoarthritis as a disease of mechanics." Osteoarthritis and Cartilage **21**(1): 10-15.

Goodman, A., J. Lallo, et al. (1984). "Health Changes at Dickson Mounds, Illinois (A.D. 950-1300)." Paleopathology at the Origins of Agriculture: 271-305.

Goodwin, M. B. and J. R. Horner (2004). "Cranial histology of pachycephalosaurs (Ornithischia : Marginocephalia) reveals transitory structures inconsistent with head-butting behavior." Paleobiology **30**(2): 253-267.

Jurmain, R. D. (1977). "Stress and etiology of osteoarthritis." American Journal of Physical Anthropology **46**(2): 353-365.

Jurmain, R. D. (1980). "The pattern of involvement of appendicular degenerative joint disease." American Journal of Physical Anthropology **53**(1): 143-150.

Keaveny, T. M., E. F. Morgan, et al. (2001). "Biomechanics of trabecular bone." Annual Review of Biomedical Engineering **3**: 307-333.

Keaveny, T. M., T. P. Pinilla, et al. (1997). "Systematic and random errors in compression testing of trabecular bone." Journal of Orthopaedic Research **15**(1): 101-110.

Lambers, F. M., A. R. Bouman, et al. (2013). "Microdamage Caused by Fatigue Loading in Human Cancellous Bone: Relationship to Reductions in Bone Biomechanical Performance." Plos One **8**(12).

Larsen, C. S. (1981). "Functional implications of postcranial size-reduction on the prehistoric georgia coast, usa." Journal of Human Evolution **10**(6): 489-502.

Latimer, B. (2005). "The perils of being bipedal." Annals of Biomedical Engineering **33**(1): 3-6.

Latimer, B. and C. O. Lovejoy (1989). "The calcaneus of australopithecus-afarensis and its implications for the evolution of bipedality." American Journal of Physical Anthropology **78**(3): 369-386.

Lieberman, D. E. (1993). "The rise and fall of seasonal mobility among hunter-gatherers - the case of the southern levant." Current Anthropology **34**(5): 599-631.

Linde, F., I. Hvid, et al. (1989). "Energy absorptive properties of human trabecular bone specimens during axial-compression." Journal of Orthopaedic Research **7**(3): 432-439.

Linde, F., P. Norgaard, et al. (1991). "Mechanical-properties of trabecular bone - dependency on strain rate." Journal of Biomechanics **24**(9): 803-809.

Marlowe, F. W. (2005). "Hunter-gatherers and human evolution." Evolutionary Anthropology **14**(2): 54-67.

Mittra, E., C. Rubin, et al. (2005). "Interrelationship of trabecular mechanical and microstructural properties in sheep trabecular bone." Journal of Biomechanics **38**(6): 1229-1237.

Moore, T. L. A. and L. J. Gibson (2002). "Microdamage accumulation in bovine trabecular bone in uniaxial compression." Journal of Biomechanical Engineering-Transactions of the Asme **124**(1): 63-71.

Nagaraja, S., T. L. Couse, et al. (2005). "Trabecular bone microdamage and microstructural stresses under uniaxial compression." Journal of Biomechanics **38**(4): 707-716.

Passi, N. and A. Gefen (2005). "Trabecular bone contributes to strength of the proximal femur under mediolateral impact in the avian." Journal of Biomechanical Engineering-Transactions of the Asme **127**(1): 198-203.

Pugh, J. W., R. M. Rose, et al. (1973). "Elastic and viscoelastic properties of trabecular bone - dependence on structure." Journal of Biomechanics **6**(5): 475-&.

Radin, E. L., R. M. Rose, et al. (1972). "Role of mechanical factors in pathogenesis of primary osteoarthritis." Lancet **1**(7749): 519-&.

Rice, J. C., S. C. Cowin, et al. (1988). "On the dependence of the elasticity and strength of cancellous bone on apparent density." Journal of Biomechanics **21**(2): 155-168.

Toyras, J., M. T. Nieminen, et al. (2002). "Bone mineral density, ultrasound velocity, and broadband attenuation predict mechanical properties of trabecular bone differently." Bone **31**(4): 503-507.

Ulrich, D., B. Van Rietbergen, et al. (1999). "The ability of three-dimensional structural indices to reflect mechanical aspects of trabecular bone." Bone **25**(1): 55-60.

Unger-Hamilton, R. (1989). "The epi-palaeolithic southern levant and the origins of cultivation." Current Anthropology **30**(1): 88-103.

Zhang, S. N., B. T. Bates, et al. (2000). "Contributions of lower extremity joints to energy dissipation during landings." Medicine and Science in Sports and Exercise **32**(4): 812-819.

Chapter 6 - Discussion

In this chapter I first summarize the major results and conclusions from Chapters 2 through 5. I then discuss the broader implications of the study findings by specifically addressing their relevance to theories of impact resistance in bone tissue, the generation and resistance of impact forces in Pleistocene vs. Holocene *H. sapiens* and the etiology of osteoarthritis.

Chapter Summaries

Chapter 2 examined how variation in foot-ground interface stiffness affects the generation of walking and heel strike running impact forces. I focused on variables such as impact loading rate and vertical impulse that have been implicated in the etiology of various repetitive stress injuries. I tested the hypotheses that less stiff interfaces result in lower impact loading rates but greater vertical impulses, and that there is a tradeoff between impact loading rate and vertical impulse for walkers and heel strike runners. Both of these hypotheses were supported by the experimental data. I concluded that footwear which reduces the stiffness of the heel-ground interface may decrease impact loading rates at the expense of greater vertical impulses, and therefore walking or heel strike running in less stiff footwear may decrease injury risk from impact loading rates but increase injury risk from larger vertical impulses.

I studied how variation in the height and the elastic modulus of shoe heels affected heel strike running impact peaks in Chapter 3. I tested the hypothesis that increased heel height would increase the duration of impact, the vertical impulse and the effective mass of the foot while decreasing impact loading rates in heel strike runners. I also hypothesized that the effects of high heels and low elastic modulus heels would multiply such that the highest heels made of the least stiff material would lead to impact peaks with the longest impact durations, vertical impulses and effective masses, but the slowest impact loading rates. The final hypothesis was that the impact force magnitude would remain

unaffected by heel height. The results showed that higher heels lengthened the duration of impact and slowed impact loading rates, but also led to decreased impact force magnitude. Contrary to our second hypothesis, we found complex interactions between heel height and heel elastic modulus on the generation of impact forces. The results indicate that heel height alters heel strike running impact forces in predictable ways, but suggest that the effects of elastic modulus on impact peaks cannot be determined without accounting for heel height. Results also show that knee flexion during the impact peak is a strong predictor of impact force magnitude, impact time duration, F', vertical impulse and m_{eff}.

Chapter 4 investigated variation in trabecular BVF in the calcaneus and in C2 vertebrae among several *H. sapiens* populations, chimpanzees and gorillas. I tested the hypothesis that variations in mechanical loading due to physical activity are a primary cause of the patterns of variation observed in trabecular BVF. I found that Pleistocene *H. sapiens* had calcaneal trabecular BVF indistinguishable from both chimpanzees and gorillas, and that Pleistocene *H. sapiens* had greater calcaneal BVF than any Holocene *H. sapiens* population. Further, there were no differences in calcaneal BVF between the Holocene *H. sapiens* populations despite widely varying subsistence strategies. I also found that C2 vertebrae trabecular BVF was greater in Pleistocene than Holocene *H. sapiens*. I concluded that *H. sapiens* trabecular BVF declined systemically sometime after the Pleistocene and that phenomena other than or in addition to variation in mechanical loading from physical activity are related to the decline.

Chapter 5 considered how variation in *H. sapiens* calcaneal trabecular BVF affects the mechanical function of trabecular tissue. I hypothesized that energy dissipation would vary with the inverse of BVF squared under stress controlled conditions. I also hypothesized that trabecular BVF mediates a tradeoff between energy dissipation and each of three mechanical properties: elastic modulus, yield strength and work to failure. I then used the experimental results and the tradeoffs between mechanical properties to understand how variations in calcaneal trabecular bone in *H. sapiens*

resists impact forces. The results indicate that energy dissipation scales with the inverse of BVF squared under stress controlled conditions, and that increasing BVF results in larger elastic modulus, yield strength and work to failure at the expense of energy dissipation. The tradeoff models indicated a BVF of 0.15 optimized energy dissipation and each of elastic modulus, yield strength and work-to-failure. Calcaneal trabecular bone of Pleistocene *H. sapiens* (average BVF: 0.26) thus had a relatively greater values of elastic modulus, yield strength and toughness, while calcaneal trabecular bone from Holocene *H. sapiens* (average BVF: 0.18) was closer to the optimum point of the mechanical variables. These findings suggest that BVF in the calcaneus of *H. sapiens* originally favored mechanical properties such as stiffness, strength and toughness in order to resist repetitive impacts to the heel.

Implications

Addressing theories of impact resistance in trabecular bone

One of the major motivations for this thesis was to evaluate differing models of how bone tissue resists repetitive impact forces. Several researchers have advanced an idea that I call the 'bone energy dissipation hypothesis' (Latimer and Lovejoy 1989; Currey 2002; Goodwin and Horner 2004; Latimer 2005). Under this model, bone tissue is adapted to resist impacts by absorbing and dissipating mechanical energy. Because these mechanical properties would be especially useful in cases where impacts affect joints because the subchondral trabecular bone may shield articular cartilage from excessive loads, researchers have hypothesized that energy absorption and dissipation would increase as the volume fraction of bone (BVF) decreased (Radin et al. 1972; Latimer 2005). Thus, the bone energy dissipation hypothesis predicts that trabecular tissue of low BVF would be favored to resist impact forces. The other hypothesis, which I call the 'bone strength hypothesis', predicts that mechanical properties such as a high elastic modulus, yield strength and work-to-failure would be favorable for resisting impacts (Currey 2002). With larger values of elastic modulus, yield strength and work-to-failure, bone tissue would be stronger and tougher and thus increase its resistance to fracture. Elastic

108

modulus, yield strength and work to failure all increase as trabecular BVF increases, and thus the strength hypothesis predicts that trabecular tissue of high BVF would be favored to resist impacts (Rice et al. 1988; Linde et al. 1989). Note that these two models have competing predictions about how trabecular tissue would be shaped structurally to resist impacts: the bone energy dissipation hypothesis suggests that lower BVF would be favored, while the bone strength hypothesis suggests that greater BVF would be favored.

In Chapter 5 I tested several aspects of these competing hypotheses. First, I tested whether energy dissipation increased as trabecular BVF decreased in calcaneal trabecular bone under cyclic loading to a constant stress. This hypothesis was supported by the experimental data. I then tested whether there would be a tradeoff in terms of energy dissipation between BVF and the three 'bone strength variables' (elastic modulus, yield strength and work-to-failure) and hypothesized that there would be a BVF that optimized energy dissipation and each of the bone strength variables. These hypotheses were also supported by experimental data. I then compared population averages in calcaneal BVF from Chapter 4 to the tradeoff models to understand how the human calcaneus resists impacts. The tradeoff models showed that the average calcaneal BVF from the Pleistocene *H. sapiens* population (BVF=0.26) was 42% greater than the BVF that optimized each of the bone strength variables and energy dissipation (BVF=0.15) and that the optimal BVF fell 2 standard deviations below the average Pleistocene *H. sapiens* calcaneal BVF. The finding that the average BVF from Pleistocene *H. sapiens* was 42% greater than the optimum BVF suggests that *H. sapiens* calcaneal trabecular bone originally favored large values of E, σ_y and W_f to resist impacts during walking and heel strike running.

Results from Chapter 5 have several implications for the bone energy dissipation and bone strength hypotheses. First, the results confirm the conjecture from the bone energy dissipation hypothesis that energy dissipation is increased in trabecular tissue with low BVF. The results also suggest that the energy dissipation strategy was not the favored strategy in the human calcaneus to resist repetitive impacts to

the heel despite the inverse relationship between BVF and energy dissipation. Rather, results suggest that the human calcaneus resists impacts by being stiff, strong and tough.

The human calcaneus is an especially interesting location to find evidence in support of the bone strength hypothesis because the articular cartilage in the lower extremity is potentially at risk from the energies imparted by repetitive impacts at heel strike (Radin et al. 1972; Radin et al. 1991; Whittle 1999). Impact energies from walking and heel strike running begin at the foot but propagate up the leg and through the axial skeleton, and some researchers have linked heel strike impacts with degenerative changes in joints and joint pain (Radin et al. 1973; Folman et al. 1986; Radin et al. 1991). Because articular cartilage may be at risk from repetitive heel strikes, one might expect to find evidence for an energy dissipation strategy or an optimized strategy in trabecular bone in order to dissipate energy and thus shield cartilage from being overloaded from impact forces. However, the evidence from this study suggests that a trabecular structure that increased stiffness, strength and toughness at the expense of energy dissipation was originally favored to resist impacts in the human calcaneus.

Another important implication is that the tradeoff between energy dissipation and the bone strength variables found in human calcaneal trabecular bone likely also exists in trabecular tissue from other anatomical locations in both humans and other organisms. Thus the trade-off framework established in this thesis can be used to evaluate impact resistance in bones of other organisms such as beaks of woodpeckers and skulls of bighorn sheep. While several studies have attempted to correlate cranial shape to the ability to resist impact forces in head-butting animals, future work can use the trade-off model presented in this thesis as a means to investigate the role of trabecular tissue in resisting impact forces (Farke 2008; Snively and Theodor 2011).

Generating and resisting impacts: Yesterday and today

The results from this study imply that the generation and resistance of impact forces during walking and heel strike running has changed during recent human evolution, and is different for modern industrialized *H. sapiens* than for hunter-gatherers or possibly even pre-industrial humans. To summarize briefly, the use of cushioned footwear worn by many people today decreases impact loading rates while increasing the vertical impulse and mechanical energy imparted to the body during impact. At the same time, the lower trabecular BVF in the Holocene *H. sapiens* calcaneus likely reduces trabecular tissue stiffness, strength and toughness while increasing energy dissipation during impacts.

To explore these implications further, it is useful to remember that the results from Chapters 2 and 3 indicate that the impact force itself has likely changed in modern industrialized humans compared to early *H. sapiens* because of footwear. The soft, compliant shoe heels frequently worn by industrialized humans alter the walking and running heel strike impact force in a manner that decreases impact loading rates while increasing the vertical impulse and mechanical energy (Addison and Lieberman 2015). In addition, the elevated heels of modern footwear act to decrease impact force magnitude and loading rate while increasing vertical impulse compared to minimal footwear. Thus, footwear commonly used by humans in industrial societies act to decrease impact loading rates and impact force magnitudes but result in larger impact energies applied to the skeleton at the heel. Larger impact energies at heel strike due to footwear may be relevant to the etiology of various musculoskeletal injuries such as osteoarthritis, which will be discussed below.

In addition, the results from Chapter 4 indicate that trabecular BVF may have declined systemically sometime after the Pleistocene and those from Chapter 5 show how variation in BVF affects the mechanical properties of calcaneal trabecular bone. The average Holocene calcaneal tuberosity trabecular BVF (0.18) is 31% lower than the average Pleistocene calcaneal tuberosity trabecular BVF (0.26). The best-fit regression equations between trabecular BVF and elastic modulus, yield strength,

work-to-failure and energy dissipation can be used to estimate the degree to which the decline in calcaneal BVF from Pleistocene to Holocene affects its mechanical properties. The 31% decline in calcaneal BVF from Pleistocene to Holocene *H. sapiens* results in an estimated 54% decline in elastic modulus, a 59% decline in yield strength and a 55% decline in work-to-failure, while increasing energy dissipation under a given load by 54%. These results imply that the ways in which calcaneal trabecular bone resists heel strike impacts during walking and running has changed from Pleistocene to Holocene *H. sapiens*, with Pleistocene calcaneal trabecular bone being stiffer, stronger and tougher and Holocene calcaneal trabecular bone better able to dissipate the mechanical energy imparted by the impact.

Osteoarthritis

The results from this thesis are relevant to improving our understanding of the ultimate and proximate causes of osteoarthritis (OA). Although the causes of OA are complex and multifactorial involving both inflammatory, genetic and mechanical risk factors, the incidence of the disease is linked to high bone density (Berenbaum 2013; Felson 2013; Reynard and Loughlin 2013; Hardcastle et al. 2015). In particular, high bone density (as assessed by single-photon absorptiometry and/or DXA; both measurement techniques calculate bone mineral density values that include contributions from both cortical and trabecular bone) has been associated with the incidence of radiographic OA, and repetitive impact forces leading to larger trabecular BVF (via bone remodeling) has been associated with cartilage degeneration and joint pain in the knee (Radin et al. 1973; Radin et al. 1991; Nevitt et al. 1995; Nevitt et al. 2010; Hardcastle et al. 2015). Because this thesis dealt explicitly with both trabecular bone density (in the form of BVF) and walking and heel strike running impacts, the data may be helpful in evaluating ongoing debates about the causes and progression of OA.

Many studies have noted an association between high bone density and radiographic OA in modern *H. sapiens*, although the causality is still unknown (Peel et al. 1995; Sowers et al. 1999; Chaganti et al. 2010; Nevitt et al. 2010; Hardcastle et al. 2015). Among several hypotheses relating high bone

density to OA, one longstanding hypothesized mechanism is that subchondral trabecular bone tissue of elevated density (or larger BVF) has a larger elastic modulus, reducing its ability to absorb and dissipate energy imparted by mechanical forces (Radin et al. 1970; Radin et al. 1972). In turn, the surrounding cartilage degenerates under excessive shear stresses (Radin et al. 1972; Radin and Rose 1986). It is important to note that experimental evidence has both supported this hypothesis (Radin et al. 1973) and suggested that it is too simplistic because subchondral trabecular BVF doesn't affect stresses in cartilage (Brown et al. 1984). Further, researchers have offered other mechanisms linking bone density to OA, including irregular joint shapes caused by variations in bone density and reactivation of endochondral ossification (Baker-LePain and Lane 2010; Burr and Gallant 2012).

Under the hypothesis that elevated trabecular BVF is a risk factor for OA, one might predict that the incidence of OA would have decreased in Holocene compared to Pleistocene *H. sapiens* because of data that suggests systemic declines in trabecular BVF after the Pleistocene. However, available evidence is inconclusive on the incidence of OA among populations and how it has changed over time. Most studies that have tried to measure OA in past *H. sapiens* populations focus on how OA incidence differs between populations with varying subsistence strategies. The results of these studies are largely mixed; some studies find declines in OA incidence from foragers to agriculturalists, while others find the opposite pattern (Jurmain 1977; Jurmain 1980; Larsen 1981; Goodman et al. 1984; Bridges 1992). In terms of temporal trends in OA, Jurmain (1977) compared OA incidence in appendicular joints between pre-historic arctic hunter-gatherers, Holocene agriculturalists and modern industrial Americans, finding that the hunter-gatherers had the greatest incidence of OA followed by modern Americans and finally by agriculturalists. However, paleopathological studies of OA prevalence often suffer from limitations such as using proxies of the disease (such as presence of osteophytes, pitting or eburnation) for diagnosis and lack of specificity when controlling for biological age and anatomical location. Further, it is not clear if some of the skeletal proxies used to diagnose OA is human skeletons accurately predict

symptoms of the disease. More research is clearly needed to better establish the relationship between bone density and temporal trends in OA in *H. sapiens.*

If repetitive impulsive forces contribute to the incidence of OA, one might predict that OA may be reduced in modern industrial populations because industrialized individuals are less physically active and thus experience fewer heel strike impacts. This conjecture, however, is complicated by the use of compliant footwear by modern industrialized *H. sapiens*. Modern footwear elevates the heel and introduces a compliant interface between the heel and the ground, which increases the vertical impulse and mechanical energy of the impact relative to minimalist footwear that mimics barefoot locomotion (Addison and Lieberman 2015). Larger values of mechanical energy at heel strike may increase the mechanical energy that joints of the lower extremity must resist, which in turn may lead to cartilage degeneration. Accordingly, one might expect that OA risk would increase in industrial shod populations. Further, runners are more likely to land on the heel when wearing any type of footwear than when barefoot (Larson 2014; Lieberman 2014; Lieberman et al. 2015). This suggests that modern shod humans may experience more frequent heel strike impacts during running than their ancestors. If the frequency of repetitive impulsive forces contribute to OA, then we might expect greater risk of OA in modern industrial populations relative to pre-historic unshod or minimally shod populations. However, as noted above, more research is necessary to establish temporal trends in OA incidence and its associations with subsistence strategy in *H. sapiens*.

It is clear that even within the realms of bone density and impact forces there are several hypothesized mechanisms and confounding factors which might lead to differentials in OA incidence between *H. sapiens* populations. Of course, this says nothing about other putative factors that affect the etiology of OA such as age, genetic predisposition, injury, and either local or systemic inflammation (Anderson and Loeser 2010; Berenbaum 2013; Felson 2013; Reynard and Loughlin 2013). It is evident that more OA incidence data that controls for age and skeletal location from a broader range of

populations is necessary in order to establish relationships between OA and bone density and/or impact

forces. In terms of the association between trabecular BVF and OA, one way forward would be to

compare OA incidence in specific joints between *H. sapiens* populations that are likely to differ in

trabecular BVF at the given joint (such as the populations used in this study). As for the role of impulsive

forces in the etiology of OA, future studies should attempt to better understand what aspects of

mechanical loading are risk factors for cartilage degeneration. For instance, what constitutes 'abnormal'

mechanical loading and what (if any) aspects of the impact force during human walking and heel strike

running are abnormal (Radin et al. 1991; Felson 2013)? Available evidence linking heel strike impacts to

symptomatic or radiographic OA in *H. sapiens* is mixed (Folman et al. 1986; Lane et al. 1986; Panush et

al. 1986; Eichner 1989; Radin et al. 1991) and future work should attempt to disentangle the relative

contributions of impact force magnitude, rate, and environmental factors such as frequency of physical

activity and use of modern footwear to the etiology of OA.

References

Addison, B. J. and D. E. Lieberman (2015). "Tradeoffs between impact loading rate, vertical impulse and effective mass for walkers and heel strike runners wearing footwear of varying stiffness." Journal of Biomechanics **48**(7): 1318-1324.

Anderson, S. and R. F. Loeser (2010). "Why is osteoarthritis an age-related disease?" Best practice & research. Clinical rheumatology **24**(1): 15-26.

Baker-LePain, J. C. and N. E. Lane (2010). "Relationship between joint shape and the development of osteoarthritis." Current Opinion in Rheumatology **22**(5): 538-543.

Berenbaum, F. (2013). "Osteoarthritis as an inflammatory disease (osteoarthritis is not osteoarthrosis!)." Osteoarthritis and Cartilage **21**(1): 16-21.

Bridges, P. S. (1992). "Prehistoric arthritis in the Americas." Annual Review of Anthropology **21**: 67-91.

Brown, T. D., E. L. Radin, et al. (1984). "Finite-element studies of some juxtaarticular stress changes due to localized subchondral stiffening." Journal of Biomechanics **17**(1): 11-&.

Burr, D. B. and M. A. Gallant (2012). "Bone remodelling in osteoarthritis." Nature Reviews Rheumatology **8**(11): 665-673.

Chaganti, R. K., N. Parimi, et al. (2010). "Bone mineral density and prevalent osteoarthritis of the hip in older men for the Osteoporotic Fractures in Men (MrOS) Study Group." Osteoporosis International **21**(8): 1307-1316.

Currey, J. D. (2002). Bones: Structure and Mecanics. Princeton, Princeton University Press.

Eichner, E. R. (1989). "An epidemiologic perspective – does running cause osteo-arthritis." Physician and Sportsmedicine **17**(3): 147-&.

Farke, A. A. (2008). "Frontal sinuses and head-butting in goats: a finite element analysis." Journal of Experimental Biology **211**(19): 3085-3094.

Felson, D. T. (2013). "Osteoarthritis as a disease of mechanics." Osteoarthritis and Cartilage **21**(1): 10-15.

Folman, Y., J. Wosk, et al. (1986). "Cyclic impacts on heel strike – a possible biomechanical factor in the etiology of degenerative disease of the human locomotion system." Archives of Orthopaedic and Trauma Surgery **104**(6): 363-365.

Goodman, A., J. Lallo, et al. (1984). "Health Changes at Dickson Mounds, Illinois (A.D. 950-1300)." Paleopathology at the Origins of Agriculture: 271-305.

Goodwin, M. B. and J. R. Horner (2004). "Cranial histology of pachycephalosaurs (Ornithischia : Marginocephalia) reveals transitory structures inconsistent with head-butting behavior." Paleobiology **30**(2): 253-267.

Hardcastle, S. A., P. Dieppe, et al. (2015). "Individuals with high bone mass have an increased prevalence of radiographic knee osteoarthritis." Bone **71**: 171-179.

Hardcastle, S. A., P. Dieppe, et al. (2015). "Osteoarthritis and bone mineral density: are strong bones bad for joints?" BoneKEy reports **4**: 624.

Jurmain, R. D. (1977). "Stress and etiology of osteoarthritis." American Journal of Physical Anthropology **46**(2): 353-365.

Jurmain, R. D. (1980). "The pattern of involvement of appendicular degenerative joint disease." American Journal of Physical Anthropology **53**(1): 143-150.

Lane, N. E., D. A. Bloch, et al. (1986). "Long-distance running, bone-density and osteoarthritis." Jama-Journal of the American Medical Association **255**(9): 1147-1151.

Larsen, C. S. (1981). "Functional implications of postcranial size-reduction on the prehistoric Georgia coast, USA." Journal of Human Evolution **10**(6): 489-502.

Larson, P. (2014). "Comparison of foot strike patterns of barefoot and minimally shod runners in a recreational road race." Journal of Sport and Health Science **3**(2): 137-142.

Latimer, B. (2005). "The perils of being bipedal." Annals of Biomedical Engineering **33**(1): 3-6.

Latimer, B. and C. O. Lovejoy (1989). "The calcaneus of *Australopithecus* afarensis and its implication for the evolution of bipedality." American Journal of Physical Anthropology **78**(3): 369-386.

Lieberman, D. E. (2014). "Strike type variation among Tarahumara Indians in minimal sandals versus conventional running shoes." Journal of Sport and Health Science **3**(2): 86-94.

Lieberman, D. E., E. R. Castillo, et al. (2015). "Variation in Foot Strike Patterns among Habitually Barefoot and Shod Runners in Kenya." Plos One **10**(7): 17.

Linde, F., I. Hvid, et al. (1989). "Energy absorptive properties of human trabecular bone specimens during axial-compression. Journal of Orthopaedic Research **7**(3): 432-439.

Nevitt, M. C., N. E. Lane, et al. (1995). "Radiographic osteoarthritis of the hip and bone-mineal density." Arthritis and Rheumatism **38**(7): 907-916.

Nevitt, M. C., Y. Zhang, et al. (2010). "High systemic bone mineral density increases the risk of incident knee OA and joint space narrowing, but not radiographic progression of existing knee OA: the MOST study." Annals of the Rheumatic Diseases **69**(1): 163-168.

Panush, R. S., C. Schmidt, et al. (1986). "Is running associated with degenerative joint disease?" Jama-Journal of the American Medical Association **255**(9): 1152-1154.

Peel, N. F. A., N. A. Barrington, et al. (1995). "Bone-mineral density and bone turnover in spinal osteoarthrosis." Annals of the Rheumatic Diseases **54**(11): 867-871.

Radin, E. L., H. G. Parker, et al. (1973). "Respone of joints to impact loading 3: relationship between trabecular microfractures and cartilage degeneration." Journal of Biomechanics **6**(1): 51-&.

Radin, E. L., I. L. Paul, et al. (1970). "Subchondral bone changes in patients with early degenerative joint disease." Arthritis and Rheumatism **13**(4): 400-&.

Radin, E. L. and R. M. Rose (1986). "Role of subchondral bone in the initiation and progression of cartilage damage." Clinical Orthopaedics and Related Research(213): 34-40.

Radin, E. L., R. M. Rose, et al. (1972). "Role of mechanical factors in pathogenesis of primary osteoarthritis." Lancet **1**(7749): 519-&.

Radin, E. L., K. H. Yang, et al. (1991). "Relationship between lower-limb dynamics and knee-joint pain." Journal of Orthopaedic Research **9**(3): 398-405.

Reynard, L. N. and J. Loughlin (2013). "Insights from human genetic studies into the pathways involved in osteoarthritis." Nature Reviews Rheumatology **9**(10): 573-583.

Rice, J. C., S. C. Cowin, et al. (1988). "On the dependence of the elasticity and strength of cancellous bone on apparent density." Journal of Biomechanics **21**(2): 155-168.

Snively, E. and J. M. Theodor (2011). "Common Functional Correlates of Head-Strike Behavior in the Pachycephalosaur Stegoceras validum (Ornithischia, Dinosauria) and Combative Artiodactyls." Plos One **6**(6).

Sowers, M., L. Lachance, et al. (1999). "The associations of bone mineral density and bone turnover markers with osteoarthritis of the hand and knee in pre- and perimenopausal women." Arthritis and Rheumatism **42**(3): 483-489.

Whittle, M. W. (1999). "Generation and attenuation of transient impulsive forces beneath the foot: a review." Gait & Posture **10**(3): 264-275.

Appendix 1 – Supplementary Data for Chapter 2

Mechanical Energy

While Chapter 2 focused on variables of the impact peak that have been implicated in repetitive stress injuries such as F_{max}, F' and vertical impulse, it may also be important to consider the mechanical energy imparted to the body during the impact. Here, I include a brief analysis of how mechanical energy of the impact is altered by the experimental conditions.

Experimental data confirmed the hypothesis that m_{eff} would increase in less stiff footwear. It is reasonable, then, to expect that the total mechanical energy of the impact would be greater in less stiff footwear because m_{eff} is greater. Following Chi and Schmidt (2005), the total mechanical energy of m_{eff} immediately prior to impact is calculated as (Chi and Schmitt 2005):

Mechanical Energy = $\frac{1}{2}m_{eff}v_i^2 - m_{eff}g\Delta z$

where Δz is the change in vertical distance of the lateral malleolus marker during the impact peak.

Results from ANOVA show that there were significant differences in mechanical energy of the impact between conditions in both walking and running (Walking: F(2,54) = 21.5, p < 0.0001; Running: F(2,54)=12.1, p < 0.0001). Appendix Table 1.1 shows the mean (SD) of the mechanical energy of the impact during walking and heel strike running. During walking, the mechanical energy increased by 19.5% between the control and hard pad and by 37.2% between the hard pad and the soft pad (control vs. hard: p < 0.0001; hard v. soft: p < 0.0001). In heel strike running, the mechanical energy increased by 20.8% and 38.8% between the control and hard pad and between the hard and soft pad, respectively (control vs. hard: p = 0.02; hard vs. soft: p < 0.0001) (Appendix Table 1.1, Appendix Figure 1.1).

Appendix Table 1.1: Mean (SD) of mechanical energy during the impact during walking and heel strike running for each experimental condition. P-values from ANOVA are shown.

	WALKING				RUNNING			
	Mean (SD)			p-value	Mean (SD)			p-value
	Control	Hard	Soft		Control	Hard	Soft	
Mechanical Energy (J)	0.91 (0.19)	1.08 (0.27)	1.49 (0.35)	<0.0001	1.84 (0.46)	2.22 (0.83)	3.08 (1.00)	<0.0001
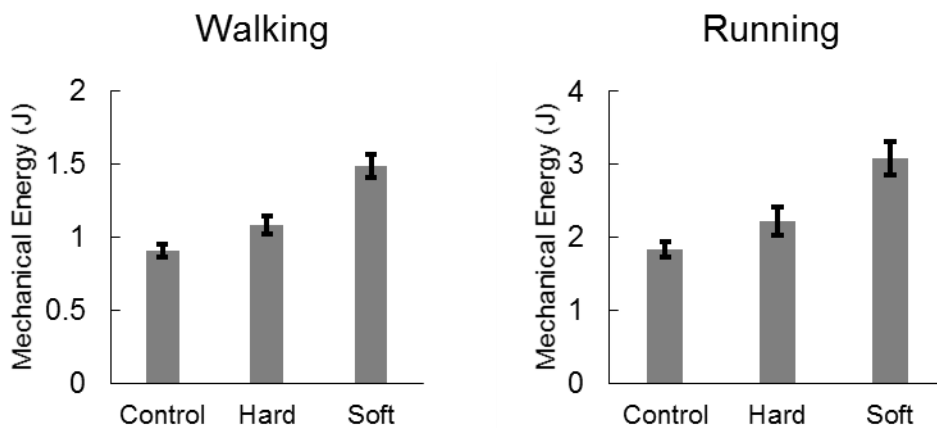
Appendix Figure 1.1: Mechanical energy of the impact in each condition during walking and running. Error bars represent standard error

References

Chi, K. J. and D. Schmitt (2005). "Mechanical energy and effective foot mass during impact loading of walking and running." Journal of Biomechanics **38**(7): 1387-1395.

Appendix 2 – Supplementary data for Chapter 3

Measurement of elastic modulus for heel materials

Elastic modulus for each of the three heel materials was measured in compression between 0 and 50% strain. The stress-strain curves in this range were reasonably linear and thus the Young's modulus of each material was calculated as the slope of the best-fit least-squares regression line of the raw data.

Appendix table 2.1: Regression equations and elastic moduli for heel materials

Material	Regression equation	R^2	Elastic Modulus (MPa)
Soft	y=2.43x − 0.082	0.91	2.4
Medium	y=31.8x − 0.63	0.98	32
Hard	y=44.7x − 1.78	0.97	45
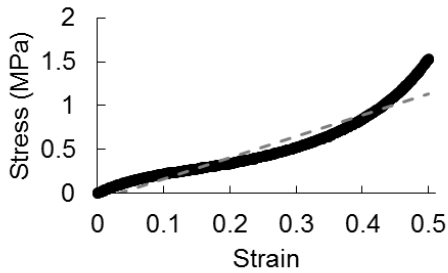
Appendix Figure 2.1: Stress vs. strain relationship for the soft heel material. Black dots are the raw data and dashed grey line is the best-fit least-squares regression line.
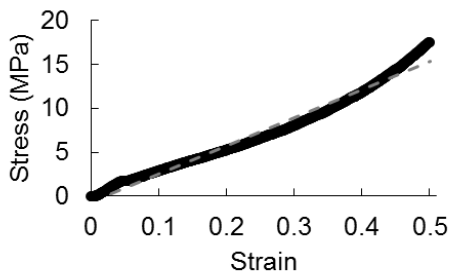
Appendix Figure 2.2: Stress vs. strain relationship for the medium heel material. Black dots are the raw data and dashed grey line is the best-fit least-squares regression line.
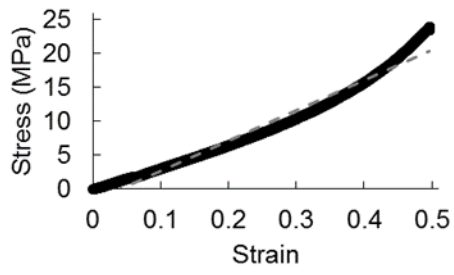
Appendix Figure 2.3: Stress vs. strain relationship for the hard heel material. Black dots are the raw data and dashed grey line is the best-fit least-squares regression line.

Appendix 3 – Supplementary Data for Chapter 4

The biological age class, sex, trabecular BVF, Tb.Th, Tb.Sp., DA, SMI and ConnD for each

specimen in the calcaneal tuberosity (Appendix Table 3.1), calcaneal PAF (Appendix table 3.2) and C2

vertebra (Appendix Table 3.3) are provided in this appendix.

Appendix Table 3.1: Detailed trabecular structure report for the calcaneal tuberosity VOI

Sample ID Number	Age or Age Class	Sex	BVF	Tb.Th (mm)	Tb.Sp. (mm)	DA	SMI	ConnD $(1/mm^3)$
Gorilla								
MCZ 17684	Adult	F	0.249	0.238	0.696	0.545	1.769	5.272
MCZ 20038	Adult	M	0.173	0.271	1.21	0.532	1.548	1.413
MCZ 20039	Adult	M	0.197	0.397	1.341	0.594	1.798	0.917
MCZ 23160	Adult	M	0.233	0.287	0.932	0.647	1.375	2.181
MCZ 23162	Adult	M	0.145	0.243	1.502	0.732	1.263	0.772
MCZ 29047	Adult	F	0.156	0.185	0.84	0.631	2.259	3.032
MCZ 29048	Adult	M	0.179	0.211	0.999	0.551	1.891	2.198
MCZ 29049	Adult	M	0.277	0.317	0.796	0.599	1.576	3.225
MCZ 37264	Adult	F	0.213	0.231	0.835	0.395	1.815	3.151
MCZ 57482	Adult	M	0.254	0.285	0.971	0.622	1.076	1.725
Chimpanzee								
MCZ 23163	Adult	M	0.299	0.276	0.752	0.642	0.674	2.814
MCZ 20041	Adult	M	0.308	0.289	0.778	0.68	0.56	2.349
MCZ 48686	Adult	M	0.258	0.224	0.777	0.625	0.781	2.985
MCZ 19187	Adult	M	0.275	0.235	0.672	0.626	1.225	4.562
MCZ 26849	Adult	F	0.233	0.184	0.66	0.665	1.398	5.214
MCZ 26847	Adult	F	0.183	0.173	0.687	0.581	2.018	5.478
MCZ 15312	Adult	U	0.258	0.198	0.633	0.683	1.11	5.593
Natufian								
10256	Adult	F	0.295	0.274	0.642	0.714	1.348	4.174
10258	Adult	M	0.186	0.282	1.04	0.633	1.896	1.774
10267	Adult	U	0.25	0.263	0.694	0.609	0.1747	3.637
10282	Adult	U	0.224	0.244	0.79	0.641	1.64	2.915
10290	Adult	F	0.264	0.284	0.762	0.639	1.51	2.991
10292	Adult	F	0.337	0.317	0.603	0.619	1.371	3.988
10322	Adult	U	0.224	0.247	0.773	0.599	1.729	3.298
10323	Adult	U	0.259	0.28	0.798	0.643	1.204	2.338
Point Hope								
200	Adult	F	0.206	0.185	0.594	0.729	2.307	6.486
228	Adult	M	0.177	0.22	0.816	0.743	2.312	3.512
252	Adult	M	0.173	0.187	0.694	0.728	2.485	4.739
315	Adult	U	0.186	0.192	0.694	0.692	2.25	4.676
339	Adult	M	0.216	0.219	0.818	0.82	1.328	2.429
353	Adult	M	0.121	0.18	0.885	0.626	2.958	3.628
373	Adult	M	0.158	0.212	0.903	0.727	2.259	2.954

Appendix Table 3.1 (Continued): Detailed trabecular structure report for the calcaneal tuberosity VOI

380	Adult	M	0.167	0.21	0.969	0.803	1.51	1.833
392	Adult	M	0.207	0.239	0.714	0.708	2.491	4.12
397	Adult	M	0.254	0.236	0.762	0.774	1.124	2.704
431	Adult	M	0.097	0.162	1.014	0.772	2.858	2.959
446	Adult	M	0.207	0.199	0.68	0.584	2.185	6.567
462	Adult	M	0.181	0.245	0.856	0.761	2.342	2.713
464	Adult	F	0.202	0.178	0.64	0.76	2.267	5.998
480	Adult	M	0.174	0.225	0.961	0.55	1.964	2.674
481	Adult	M	0.235	0.21	0.612	0.668	1.937	6.231
504	Adult	M	0.19	0.211	0.745	0.718	2.165	4.122
510	Adult	F	0.238	0.198	0.55	0.674	2.126	8.078
540	Adult	F	0.171	0.167	0.581	0.606	3.044	9.416
Mistihalj								
9115	Adult	M	0.131	0.164	0.78	0.707	2.751	4.327
9121	Adult	M	0.205	0.198	0.675	0.621	2.025	5.237
9122	Adult	F	0.134	0.155	0.654	0.592	3.259	7.186
9123	Adult	F	0.22	0.187	0.554	0.693	2.268	8.191
9127	Adult	M	0.131	0.146	0.714	0.615	3.244	7.708
9130	Adult	F	0.084	0.141	0.816	0.581	3.774	4.755
9146	Adult	F	0.266	0.248	0.664	0.617	1.745	5.582
9148	Adult	M	0.144	0.158	0.657	0.513	3.297	9.04
9152	Adult	M	0.144	0.179	0.846	0.66	2.587	3.894
8983	Adult	M	0.264	0.218	0.592	0.709	1.443	5.71
9055	Adult	F	0.207	0.2	0.616	0.765	2.274	6.336
9094	Adult	U	0.163	0.169	0.636	0.66	2.912	7.834
9040	Adult	F	0.179	0.23	0.83	0.633	2.537	4.211
American								
1311321	63	M	0.134	0.186	0.767	0.715	2.849	3.625
1311423	70	M	0.225	0.235	0.673	0.747	1.97	3.952
1311432	63	M	0.208	0.215	0.722	0.699	1.808	3.782
1308747	71	M	0.187	0.225	0.765	0.641	2.251	4.437
1311042	28	M	0.211	0.243	0.721	0.692	2.161	3.641
1311395	68	M	0.16	0.214	0.834	0.718	2.346	3.053
1311434	56	M	0.113	0.219	1.022	0.756	2.727	1.624
1304731	54	M	0.306	0.237	0.521	0.765	1.41	6.125
1311296	55	M	0.195	0.207	0.605	0.665	2.513	6.012
1311259	45	M	0.196	0.196	0.606	0.698	2.453	6.13
1404187	68	F	0.275	0.195	0.492	0.785	1.586	7.628
1407664	65	F	0.087	0.172	0.985	0.717	3.188	2.424
1405461	60	F	0.186	0.182	0.608	0.762	2.447	6.056
1405433	53	F	0.175	0.213	0.846	0.676	2.058	3.006
1407768	64	F	0.157	0.183	0.684	0.529	3.064	5.991
1406557	41	F	0.191	0.192	0.645	0.671	2.301	5.687
1407672	66	F	0.141	0.174	0.662	0.75	2.987	4.995
1407738	53	F	0.147	0.156	0.543	0.702	3.392	8.424
1209562	44	F	0.113	0.171	0.775	0.628	3.213	3.903
1406633	58	F	0.093	0.163	0.846	0.641	3.496	3.075

Appendix Table 3.2: Detailed trabecular structure report for the calcaneal PAF VOI

Sample ID Number	Age	Sex	BVF	Tb.Th (mm).	Tb.Sp. (mm)	DA	SMI	ConnD
Gorilla								
MCZ 17684	Adult	F	0.452	0.374	0.647	0.528	1.551	1.453
MCZ 20038	Adult	M	0.484	0.493	0.82	0.63	0.664	1.055
MCZ 20039	Adult	M	0.532	0.737	1.081	0.711	0.213	0.393
MCZ 23160	Adult	M	0.535	0.557	0.691	0.795	0.262	0.963
MCZ 23162	Adult	M	0.494	0.517	0.983	0.634	0.46	1.066
MCZ 29047	Adult	F	0.298	0.296	0.879	0.772	2.83	1.44
MCZ 29048	Adult	M	0.595	0.566	0.621	0.708	0.433	0.813
MCZ 29049	Adult	M	0.531	0.513	0.754	0.757	0.272	1.222
MCZ 37264	Adult	F	0.515	0.493	0.68	0.767	0.807	1.108
MCZ 57482	Adult	M	0.479	0.434	0.73	0.65	0.928	2.089
Chimpanzee								
MCZ 38019	Adult	F	0.565	0.477	0.66	0.688	0.229	0.856
MCZ 23163	Adult	M	0.551	0.459	0.705	0.564	0.168	2.307
MCZ 20041	Adult	M	0.556	0.461	0.686	0.572	0.145	1.766
MCZ 48686	Adult	M	0.555	0.436	0.665	0.564	0.328	1.786
MCZ 19187	Adult	M	0.562	0.406	0.504	0.467	0.382	4.135
MCZ 26849	Adult	F	0.547	0.355	0.469	0.405	1.045	5.303
MCZ 26847	Adult	F	0.397	0.304	0.614	0.544	2.101	3.789
MCZ 38018	Adult	M	0.513	0.348	0.6	0.736	0.315	1.891
MCZ 15312	Adult	U	0.434	0.277	0.525	0.609	1.635	6.043
MCZ 38020	Adult	M	0.553	0.396	0.564	0.554	0.19	2.401
Natufian								
10256	Adult	F	0.58	0.49	0.568	0.77	0.31	1.865
10267	Adult	U	0.441	0.373	0.722	0.844	1.573	1.672
10282	Adult	U	0.407	0.435	0.896	0.841	1.723	1.016
10289	Adult	U	0.587	0.595	0.603	0.712	0.001	1.198
10290	Adult	F	0.545	0.608	0.738	0.743	0.637	0.707
10292	Adult	F	0.61	0.619	0.576	0.813	0.034	0.9
10322	Adult	U	0.524	0.496	0.63	0.788	1.61	1.129
10323	Adult	U	0.566	0.557	0.627	0.838	0.436	1.313
10259	Adult	M	0.517	0.532	0.75	0.772	0.861	0.722
10258	Adult	M	0.595	0.601	0.679	0.773	0.183	0.838
Point Hope								
200	Adult	F	0.398	0.321	0.605	0.784	2.414	4.099
228	Adult	M	0.392	0.407	0.718	0.754	0.719	2.527
252	Adult	M	0.425	0.355	0.67	0.825	1.934	2.124
315	Adult	U	0.441	0.358	0.61	0.815	1.833	2.655
339	Adult	M	0.397	0.341	0.682	0.893	2.294	2.006
353	Adult	M	0.408	0.333	0.664	0.785	2.045	2.602
373	Adult	M	0.349	0.314	0.754	0.848	2.729	1.974
380	Adult	M	0.43	0.378	0.709	0.822	1.898	1.508
392	Adult	M	0.489	0.469	0.669	0.798	1.177	2.007
397	Adult	M	0.408	0.371	0.702	0.822	2.198	1.867
431	Adult	M	0.256	0.26	0.823	0.856	3.185	2.984
446	Adult	M	0.408	0.341	0.641	0.782	2.24	2.498
462	Adult	M	0.394	0.381	0.697	0.819	1.916	2.314

Appendix Table 3.2 (Continued): Detailed trabecular structure report for the calcaneal PAF VOI

464	Adult	F	0.4	0.306	0.591	0.815	2.569	3.335
480	Adult	M	0.322	0.309	0.761	0.768	3.018	3.132
481	Adult	M	0.368	0.334	0.751	0.86	2.349	2.301
504	Adult	M	0.403	0.367	0.691	0.836	2.227	1.695
510	Adult	F	0.443	0.381	0.543	0.807	2.095	3.73
540	Adult	F	0.331	0.284	0.651	0.807	3.001	3.896
Mistihalj								
9115	Adult	M	0.368	0.308	0.588	0.791	2.16	3.889
9121	Adult	M	0.407	0.42	0.799	0.737	1.647	2.244
9122	Adult	F	0.402	0.335	0.606	0.61	1.767	4.757
9123	Adult	F	0.456	0.363	0.528	0.578	1.423	5.28
9127	Adult	M	0.426	0.34	0.53	0.77	1.649	4.801
9130	Adult	F	0.305	0.276	0.648	0.727	2.57	5.713
9138	Adult	M	0.411	0.339	0.639	0.41	1.336	4.711
9146	Adult	F	0.445	0.368	0.628	0.692	1.231	3.626
9148	Adult	M	0.52	0.41	0.538	0.752	0.733	3.806
9152	Adult	M	0.453	0.369	0.577	0.64	1.307	4.048
8983	Adult	M	0.548	0.458	0.538	0.783	0.264	2.404
9055	Adult	F	0.535	0.436	0.524	0.713	0.236	3.305
9094	Adult	U	0.365	0.322	0.626	0.692	2.141	4.986
9053	Adult	M	0.528	0.503	0.636	0.709	0.387	2.29
9040	Adult	F	0.513	0.417	0.57	0.78	0.548	2.834
American								
1311321	63	M	0.413	0.339	0.609	0.789	1.914	2.91
1311423	70	M	0.396	0.395	0.775	0.707	1.766	2.499
1311324	63	M	0.379	0.35	0.639	0.804	2.004	2.583
1308747	71	M	0.449	0.381	0.622	0.792	1.348	2.21
1310042	28	M	0.459	0.423	0.608	0.791	1.285	3.091
1311395	68	M	0.461	0.371	0.579	0.763	1.371	2.997
1311434	56	M	0.34	0.357	0.749	0.761	2.509	2.796
1304731	54	M	0.521	0.428	0.569	0.81	0.698	5
1311496	55	M	0.411	0.366	0.619	0.785	1.444	2.801
1311259	45	M	0.448	0.342	0.52	0.793	1.191	3.582
1404187	68	F	0.47	0.346	0.474	0.606	1.652	5.673
1407664	65	F	0.288	0.295	0.805	0.689	2.708	3.104
1405461	60	F	0.424	0.309	0.504	0.755	1.955	4.946
1405433	53	F	0.464	0.426	0.703	0.74	1.332	1.641
1407768	64	F	0.471	0.394	0.58	0.729	1.252	2.646
1406557	41	F	0.43	0.296	0.479	0.759	1.961	4.928
1407672	66	F	0.329	0.286	0.598	0.763	2.555	4.559
1407738	53	F	0.427	0.297	0.494	0.708	1.996	6.644
1209562	44	F	0.444	0.348	0.531	0.636	1.777	4.815
1407633	58	F	0.298	0.261	0.603	0.735	2.854	4.902

Appendix Table 3.3: Detailed trabecular structure report for the C2 body VOI

| Sample ID Number	Age	Sex	BVF	Tb.Th (mm).	Tb.Sp.	DA	SMI	ConnD
Natufian								
10239	Adult	U	0.376	0.318	0.679	0.163	0.821	3.954
10252	Adult	U	0.252	0.281	0.832	0.236	1.894	4.378
10253	Adult	F	0.356	0.381	0.827	0.15	1.144	2.57
10256	Adult	F	0.37	0.395	0.851	0.28	0.923	1.74
10260	Adult	M	0.517	0.521	0.719	0.325	0.031	1.042
10315	Adult	U	0.409	0.436	0.835	0.128	1.128	1.945
10323	Adult	U	0.306	0.293	0.739	0.271	1.53	4.875
10351	Adult	U	0.229	0.266	0.982	0.528	1.517	2.5
10357-2	Adult	U	0.382	0.368	0.741	0.318	0.921	2.537
Point Hope								
200	Adult	F	0.279	0.242	0.744	0.277	1.329	4.644
228	Adult	M	0.32	0.29	0.744	0.219	1.26	4.76
315	Adult	U	0.2	0.21	0.87	0.214	1.702	4.427
339	Adult	M	0.225	0.276	1.11	0.48	1.436	2.339
353	Adult	M	0.155	0.256	1.147	0.293	2.452	2.176
373	Adult	M	0.172	0.218	0.995	0.228	1.939	3
380	Adult	M	0.198	0.217	0.923	0.5	1.959	3.1
392	Adult	M	0.322	0.38	0.914	0.209	1.378	2.904
397	Adult	M	0.307	0.282	0.773	0.292	1.276	4.467
431	Adult	M	0.226	0.289	0.991	0.346	1.513	2.659
446	Adult	M	0.163	0.306	1.516	0.249	2.139	1.644
462	Adult	M	0.213	0.314	1.106	0.465	2.09	2.307
464	Adult	F	0.236	0.205	0.748	0.424	1.708	6.189
480	Adult	M	0.218	0.269	0.991	0.213	1.658	2.948
481	Adult	M	0.229	0.295	0.973	0.337	1.885	3.266
491	Adult	U	0.201	0.274	0.985	0.412	2.282	3.177
504	Adult	M	0.218	0.227	0.863	0.404	1.724	5.106
510	Adult	F	0.287	0.28	0.726	0.302	1.596	4.662
540	Adult	F	0.219	0.227	0.813	0.346	2.076	5.104
Mistihalj								
8983	Adult	M	0.352	0.268	0.598	0.147	1.015	7.039
9040	Adult	F	0.315	0.255	0.547	0.289	1.225	9.009
9063	Adult	F	0.196	0.203	0.801	0.23	2.125	5.365
9064	Adult	F	0.308	0.263	0.662	0.197	1.398	6.731
9079	Adult	M	0.274	0.248	0.672	0.201	1.688	6.456
9094	Adult	M	0.303	0.226	0.571	0.187	1.598	9.936
9122	Adult	F	0.27	0.207	0.674	0.12	1.401	6.701
9123	Adult	F	0.344	0.255	0.591	0.305	1.283	9.788
9127	Adult	M	0.266	0.217	0.667	0.297	1.663	6.946
9138	Adult	M	0.214	0.235	0.795	0.096	2.096	4.984
9146	Adult	F	0.371	0.296	0.633	0.23	0.863	5.646
9152	Adult	M	0.192	0.189	0.813	0.243	1.917	4.766

Appendix 4 – Supplementary data for Chapter 5

Appendix 4A: Conditioning cycles

A potential limitation of the conditioning cycles is that they were performed in position control mode rather than the more conventional strain control mode. Pilot data performed in strain control mode indicated that measured strains frequently overshot the prescribed strains, thus making strain control mode unreliable. Given that specimens had slightly different lengths, performing the conditioning cycles in position control mode means that each specimen likely underwent different strains and strain rates which may affect elastic modulus (E) calculations. The purpose of this section is to address any limitations and/or biases in the data caused by using position control mode during the conditioning cycles.

Specimen lengths and strain measurement

During the conditioning cycles, each specimen was loaded in cyclic compression in position control to 0.05 mm at 0.5 Hz. Varying effective lengths amongst the specimens may result in slightly different strains and strain rates. The average (SD) effective length (in mm) of the specimens was 23.4 (+/- 0.69). The average (SD) maximum strain (in percent) reached during the 10th conditioning cycle was 0.22 (+/- 0.04%). The prediction would be that specimens with longer effective lengths would undergo less strain because a length change of 0.022 mm (the prescribed value of actuator displacement) is a smaller fraction of the total length of longer specimens. However, there was no relationship between effective specimen length and maximum strain reached on the 10th loading cycle (appendix figure 4.1; p=0.2).
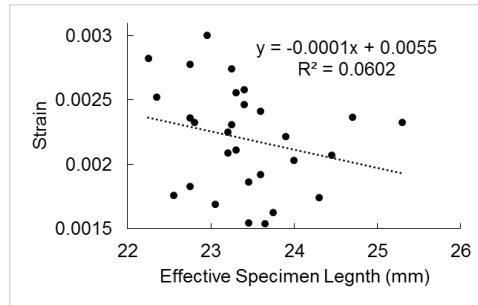
Appendix Figure 4.1: Maximum strain reached during the 10th conditioning cycle versus effective specimen length

Specimen structure and strain measurement

Instead, the data showed an inverse correlation between BVF and the maximum strain reached

on the 10th loading cycle (Appendix Figure 4.2; p<0.0001).
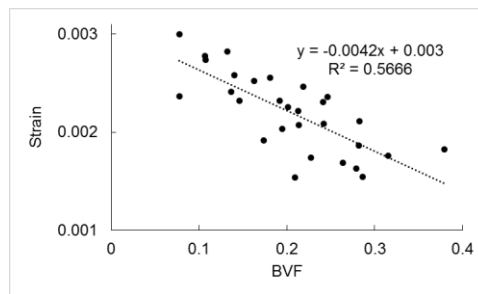
Appendix Figure 4.2: Maximum strain reached during the 10th conditioning cycle versus trabecular BVF

Because BVF is a major predictor of E, this result suggests that specimens with lower E (lower

BVF) underwent greater strains during the conditioning cycles. The data also show an inverse correlation

between strain rate and BVF (Appendix Figure 4.3):
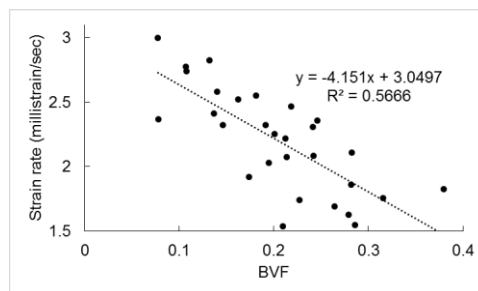
Appendix Figure 4.3: Strain rate during the 10th conditioning cycle versus trabecular BVF

This result indicates that specimens with lower BVF (and therefore lower E) underwent greater strain rates.

Together, these results may have affected E measurement. On the one hand, lower BVF specimens undergoing greater strains would likely lead to a relative underestimate of E if the E was measured between 0 and the maximum strain reached (see section below). This issue was mitigated by measuring E from 0 to 0.154% strain for all specimens, which was the lowest strain reached by all specimens (see section below for further explanation and comparisons between methodologies for measuring E).

On the other hand, increased strain rates on lower BVF specimens might lead to a relative over-estimate of E because E measurements increase as strain rate increases (Carter and Hayes 1976; Linde et al. 1991). A relative over-estimate of E for low BVF specimens would bias against finding a significant relationship between BVF and E. Despite this limitation, we found that BVF was a strong predictor of E.

It is unclear why lower BVF specimens underwent relatively greater strains and strain rates during the conditioning cycles. One hypothesis is that the BVF (and thus E) of the specimen influenced the feedback response of the testing system, causing the actuator to overshoot the prescribed displacement on lower BVF specimens.

Methods for measuring E

The average (SD) maximum strain (in percent) reached during the 10th conditioning cycle was 0.22 (+/- 0.04%). The lowest maximum strain reached by any given specimen during the 10th conditioning cycle was 0.154%. Because every specimen reached at least 0.154% strain, I measured E between 0 and 0.154% strain for each specimen. A plot of BVF vs. E is reproduced below (Appendix Figure 4.4).
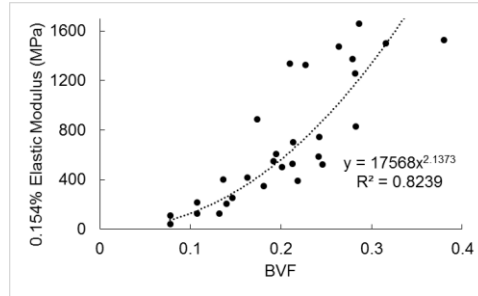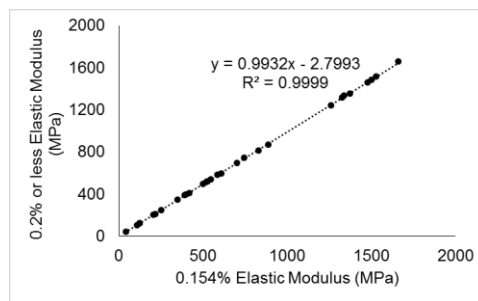
Appendix Figure 4.4: Elastic modulus (via the 0.154% strain method) versus trabecular BVF

The 0.154% E calculations were compared to two other methodologies for calculating E. In the second method, E was calculated between 0 and 0.2% strain (for specimens that reached .2% strain) and between 0 and the maximum strain for specimens that did not reach .2% strain. In the third method, E was calculated between 0 and the maximum strain reached by each specimen during the 10th loading cycle. A paired t-test was used to evaluate the differences in E between the 0.154% method and the other methods, and the 0.154% modulus was regressed against each of the other E calculations to examine the goodness-of-fit between the methods. Below is a table with the specimen ID numbers, the maximum strain reached on the 10th loading cycle, and modulus calculations for each of the three methods.

A paired t-test between the 0.154% method and the 0.2% or less method showed that E using the 0.154% method was significantly greater than the 0.2% or less method (p<0.001). A best-fit linear regression between the 0.154% E values and the 0.2% or less E indicates that the 0.154% values correspond nearly perfectly to the 0.2% or less values (Appendix Figure 4.5).

Appendix Table 4.1: Specimen ID, maximum strain and 3 different measurements of elastic modulus during the 10th conditioning cycle

Specimen ID	Max strain on 10th cycle	0.154% elastic modulus	0.2% or less elastic modulus	Max strain elastic modulus
1407664_3	0.003001892	40.451	39.603	37.764
1407664_2	0.002366434	108.6	106.42	104.49
1406633_2	0.002776906	215.56	212.24	206.1
1311423_3	0.002741311	124.63	122.56	119.39
1311434_3	0.002825649	123.12	120.19	114.65
1311423_2	0.002413831	400.27	395.58	389.9
1311432_3	0.00257978	204.62	201.67	198.03
1209562_2	0.002323263	251.87	247.62	242.66
1311434_2	0.002522617	416.8	409.71	401.95
1407664_1	0.001917656	888.79	871.53	871.53
1304731-3	0.002554338	347.97	346.06	344.2
1407768_3	0.002323154	547.34	537.78	528.79
1311259_2	0.00203024	609.11	596.32	593.2
1304731-2	0.002252829	501.3	495.93	491.25
1406633-1	0.001539323	1337.8	1337.8	1337.8
1407768_2	0.002218074	526.53	519.07	512.71
1404187_2	0.002073246	699.69	693.42	690.11
1311296_2	0.002465855	390.16	387.56	384.68
1311423_1	0.001741538	1327.2	1319.3	1319.3
1405461-3	0.002307121	586.72	582.09	577.04
1405461-2	0.002086265	744.93	741.51	740.36
1406557_2	0.002358043	520.44	513.22	507.2
1311434_1	0.001690034	1475.7	1461.1	1461.1
1407768_1	0.001627302	1373.1	1353.8	1353.8
1304731-1	0.001861803	1258.7	1240.1	1240.1
1406557_1	0.002109469	829.64	809.98	800.93
1311259_1	0.001544725	1659.8	1659.8	1659.8
1404187_1	0.001758099	1502.2	1483.1	1483.1
1209562_1	0.001826453	1528.9	1515.7	1515.7

Appendix Figure 4.5: 0.2% or less elastic modulus versus 0.154% elastic modulus

A paired t-test between the 0.154% method and the max strain method shows that the 0.154% E values are significantly greater than the max strain values (p<0.0001). A best-fit linear regression between the 0.154% E values and the max strain values shows a near perfect relationship between the variables (Appendix 4.6).

y = 0.9966x - 8.4638
R² = 0.9998
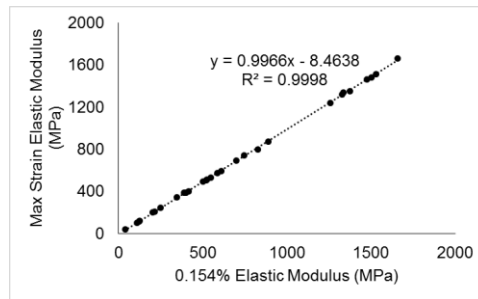
Appendix Figure 4.6: Max strain elastic modulus versus 0.154% elastic modulus

The conclusion for this analysis is that the method of measuring E significantly changes the value of the E measurement (specifically, increasing the strain at which the E is measured decreases the value of the E), but the values between the methods are tightly correlated.

Appendix 4B: Load cell and stress control testing

A 2kN load cell (Honeywell 060-1507-04) and an Instron 8800 controller were used for mechanical testing. The specifications of the controller indicate that the accuracy of the force measurements is 0.002% of load cell capacity, which equates to 0.04 Newtons of a 2kN load cell. In addition, the controller has a 19-bit resolution, making the resolution of the measurements equal to 2 kN divided by 2^19, or 0.004 Newtons. In other words, the accuracy and the resolution of the load measurements should be much lower than 1 N.

However, a common rule of thumb is to avoid measuring loads less than 10% of load cell capacity. In this study, the load used in the stress controlled testing was 30 N, which is less than 10% of

the 2 kN load cell capacity. Therefore, we evaluated how the force measurements varied between

specimens in order to understand any potential errors or sources of bias.

The average (SD) maximum load (in Newtons) reached during the stress-controlled tests was

32.25 (+/- 1.86). In a similar manner to the conditioning cycles, the BVF of the specimen influenced the

maximum load level reached during the load control test. Specifically, the maximum load increased as

BVF increased (Appendix Figure 4.7; p=0.0004):
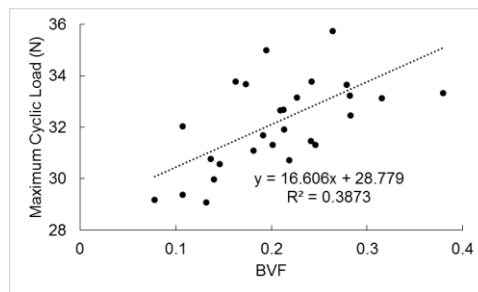
Appendix Figure 4.7: Maximum cyclic load during the stress controlled experiment versus trabecular BVF

The relatively larger maximum cyclic loads on specimens with high BVF likely affected the energy

dissipation (W_d) values of these specimens because W_d was measured between 0 N and the maximum

stress for each specimen. There was a strong inverse relationship between BVF and energy absorbed

during the loading cycle (Appendix Figure 4.8):
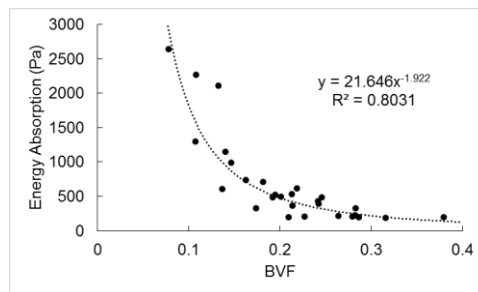
Appendix Figure 4.8: Energy absorbed during the loading cycle versus trabecular BVF during the stress controlled
experiment

And there was a strong relationship between energy absorbed during the loading cycle and energy dissipated (Appendix Figure 4.9; p<0.0001; I've included a second plot (Appendix Figure 4.10) with log-base-10 values of energy absorption and dissipation to remove potential heteroscedasticity):
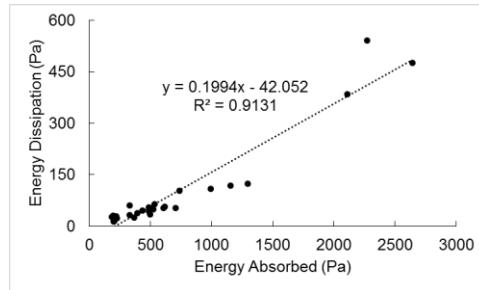
Appendix Figure 4.9: Energy dissipated versus energy absorbed in the stress controlled test
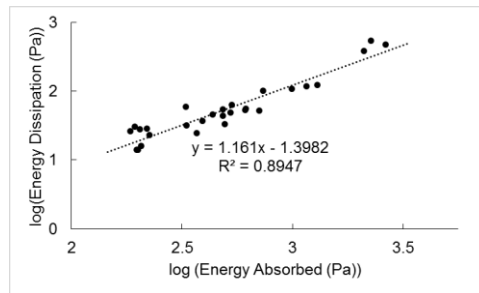
Appendix Figure 4.10: log-log (base 10) plot of energy dissipation versus energy absorbed in the stress controlled test

Therefore, the relatively larger loads applied to high BVF specimens indicates that these specimens likely had larger energy absorbed and energy dissipated values than they would have had if the maximum cyclic load was exactly constant across all specimens.

This finding has implications for the regression relationship between W_d and BVF. W_d is predicted to scale with the inverse of BVF squared; in other words, larger BVF specimens should have smaller amounts of W_d than specimens with smaller BVF. If, however, W_d values for high BVF/elastic modulus specimens are artificially large, then there is a bias against the predicted inverse relationship between BVF and W_d because the W_d values of the high BVF specimens are greater than they would have been had maximum cyclic load been exactly constant across all specimens.

Despite the experimental bias against this prediction, there was a significant inverse relationship between BVF and W_d such that W_d scaled with BVF to the -2.11 power. This suggests that the effect of BVF on W_d is quite strong under stress-controlled conditions. However, the experimental bias may obscure a more-accurate estimation of the power-law relationship between W_d and BVF. Further tests where load is more tightly controlled will be necessary to determine whether the experimental bias in this study affected the relationship between BVF and W_d.

As with the conditioning cycles, it is unclear why specimen structure affected the maximum load level reached during the load control cycles.

Appendix 4C: BVF versus W_d for specimens loaded to 0.2% strain or less

Physiologic loading results in relatively low strains, often 0.2% or less (Burr et al. 1996). A subsample of our specimens (21 of the possible 28) that were loaded to strains of 0.2% and less were used to assess the relationship between BVF and W_d under 'physiologic' strains. The average (SD) BVF of these specimens was 0.234 +/- 0.056. Trabecular BVF weakly but significantly predicted W_d (($R^2 = 0.19$ p=0.04). BVF also predicted W_a ($R^2 = 0.53$, p = 0.0001). Log(W_d) and log(ε) were significantly correlated ($R^2 = 0.66$, p <0.0001), as were log(W_d) and log(W_a) ($R^2 = 0.69$, p < 0.0001). These results are similar to what was found for the entire sample, although the strength of the regression relationships are weaker than what was found for the entire sample.

Appendix Table 4.2: Regression relationships for a subset of specimens loaded to 0.2% strain or less

Independent variable	Dependent variable	Equation	R^2	p-value
BVF	W_d	$y = 8.83x^{-0.945}$	0.19	0.04
BVF	W_a	$y = 40.5x^{-1.47}$	0.53	<0.0001
ε	W_d	$y = 0.82x + 2.39$	0.66	<0.0001
W_a	W_d	$y = 0.89x - 0.73$	0.69	<0.0001

Appendix 4D: Bootstrap analysis of the BVF vs. σ_y and BVF vs. W_f relationships

Raw values

Due to data collection errors, only 7 of the possible 29 specimens were loaded part their yield strength (σ_y) and failure points. Despite the relatively low number of samples for these measurements, there is a wide variation in BVF amongst them (0.07 to 0.28), and strong relationships between BVF and σ_y (σ_y = 159.6*BVF^2.43, R^2=0.90, p=0.001) and between BVF and work-to-failure (W_f = 866597*BVF^2.14, R^2=0.84, p=0.0035).

Because of the low sample size for these measurements, a bootstrapping analysis was used to establish the confidence intervals of the coefficient and power-law relationship between BVF and σ_y and between BVF and W_f. Bootstrapping analysis works by randomly selecting and randomly replacing each value of the original dataset to create a new 'bootstrap' dataset, and then calculating the best-fit regression line for the 'bootstrap' dataset. This process was performed 10,000 times in JMP PRO v11 (thus creating 10,000 'bootstrap' samples and 10,000 regression equations) for both the BVF and σ_y and the BVF and W_f relationships. The distributions of the power law and the coefficient from the 10,000 regression relationships were then analyzed to establish 95% confidence intervals for each.

The results of the bootstrapping analysis are as follows. For the BVF vs. σ_y relationship, the 95% CI for the power law is 1.77 – 2.75 and the 95% CI for the coefficient is 62.2 – 332.7. For the BVF vs. W_f relationship, the 95% CI for the power law is 1.67 – 2.59, and the 95% CI for the coefficient is 456342 – 2006458.

These results indicate two things. First, we can be reasonably assured that both σ_y and W_f increase as BVF increases because the 95% CI for the power law relationships are greater than 0. Second, the 95% CI for both power-law relationships include the value of 2, which is the predicted

power-law relationship for both BVF vs. σ_y and BVF vs. W_f. Thus the results, despite the limited sample size, support the predicted power-law relationships.

Bootstrapping analysis was also performed on the BVF vs. E data in order to gain a relative comparison for how the small sample size in the σ_y and W_f measurements affect the bootstrapping results. The results of the bootstrapping of BVF vs. E show that the 95% CI of the power law is 1.80 – 2.50, and that the 95% CI of the coefficient is 10027 – 32013. Appendix Table 4.3 provides a summary of the above bootstrapping results. Included in the table are calculations of the absolute range of the 95% CI (defined as 95% CI upper bound – 95% CI lower bound) and the relative range of the 95% CI (defined as the difference between the 95% CI upper and lower bounds divided by the 95% CI lower bound).

Appendix Table 4.3: Comparison of bootstrapping results of the power law and coefficient for BVF vs. each of the bone strength variables

|	Power Law			Coefficient		
	BVF vs. E	BVF vs. σ_y	BVF vs. W_f	BVF vs. E	BVF vs. σ_y	BVF vs. W_f
Original estimate	2.14	2.43	2.14	17568	159.6	866597
95% CI lower bound	1.80	1.77	1.67	10027	62.2	456342
95% CI upper bound	2.50	2.75	2.59	32013	332.7	2006458
95% CI Range	0.7	0.98	0.92	21986	270.5	1550116
95% CI relative range	0.39	0.55	0.55	2.19	4.35	3.39

The overall conclusion from this analysis is that the small number of data points in the σ_y and W_f analyses led to relatively larger 95% CI ranges for the power law and coefficient in both the BVF vs. σ_y and BVF vs. W_f relationships.

Scaled values and tradeoff models

Further, it is important to assess the scaled values of σ_y and W_f because these are the values used in the tradeoff models. Using a bootstrapping analysis similar to the one described above, the 95% CI of the power law and of the coefficient was calculated for both BVF vs. scaled σ_y and for BVF vs. scaled W_f. For BVF vs. scaledσ_y, the 95% CI of the power law was 1.79-2.73 and the 95% CI of the coefficient was 891.6 – 4502.2. For BVF vs. scaled W_f, the 95% CI of the power law was 1.64 – 2.62 and the 95% CI of the coefficient was 633.8 – 3016.3.

Using the tradeoff models presented in the main text, the conclusion was that human Pleistocene calcanei resisted impacts by being stiff, strong and avoiding fracture. There may be hesitation to come to this conclusion because of the small sample size of the σ_y and W_f measurements. The 95% CI's from the BVF vs. scaled W_f relationship can be used to investigate the scenarios under which the conclusions and interpretations of the data would change.

Let's say that the interpretation of the data would need to be reconsidered if the optimum BVF that maximized energy dissipation (W_d) and W_f simultaneously (the intersection point of the best fit regression lines) fell within 1SD of the mean BVF value of the Pleistocene calcaneal tuberosity. In this case we might change our interpretation to say that Pleistocene human calcaneal trabecular tissue may be optimized to resist failure and dissipate energy. The average BVF of the Pleistocene population was 0.255 and the standard deviation was 0.046 making the 1 SD lower bound equal to 0.209. The original tradeoff model is reproduced below with the average and minus 1SD of the mean of the Pleistocene calcanei indicated on the graph (Appendix Figure 4.11):
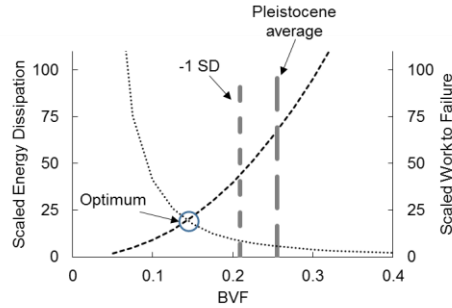
Appendix Figure 4.11: Original tradeoff model of scaled W_f and scaled W_d, with the Pleistocene BVF average and -1 SD shown as dashed vertical lines.

If a new regression of scaled W_f is plotted using the upper bound of the 95% CI power law (2.61) and the lower bound of the 95% CI coefficient (633.8), the intersection of the W_f and W_d graphs approaches the lower 1 SD boundary of the Pleistocene BVF (0.209) (Appendix Figure 4.12):
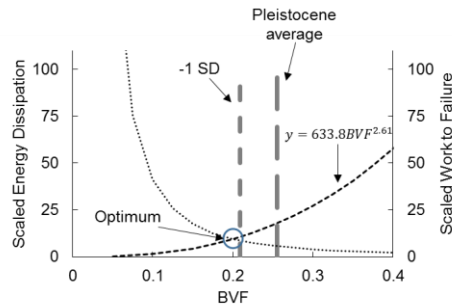

Appendix Figure 4.12: Scaled W_f and scaled W_d tradeoff model with the W_f regression line altered to represent the upper 95% CI value of the power law and the lower 95% CI of the coefficient. The BVF value to optimizes both W_d and W_f approaches -1 SD from the Pleistocene average BVF.

The odds of this event occurring can be calculated. Using the 95% CI values, there is a 2.5% chance that the W_f power law is 2.61 or higher, and a 2.5% chance that the W_f coefficient is 633.8 or lower. Thus the odds of the intersection point of the W_d and W_f graphs approaching 0.209 (and thus the odds of our interpretation changing) is (2.5/100)*(2.5/100) = 0.000625, or 0.06%. This result suggests that the odds of the interpretation changing are minimal despite a limited sample size for W_f and σ_y.

*Scaled elastic modulus values as model for scaled W_f values*

Another way to investigate the effects of a limited sample size of σ_y and W_f is to use the elastic modulus (E) data as a placeholder for W_f values. Using E data as a placeholder for W_f data can provide insight into how an increased sample size may influence our results and interpretations.

The best fit line between scaled E and scaled W_f is extremely strong and statistically significant (Appendix Figure 4.13; p<0.0001):
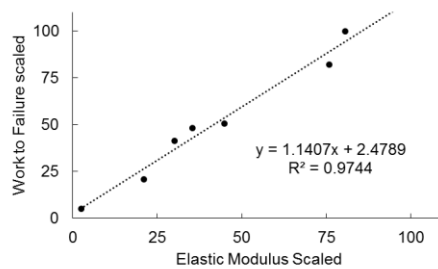
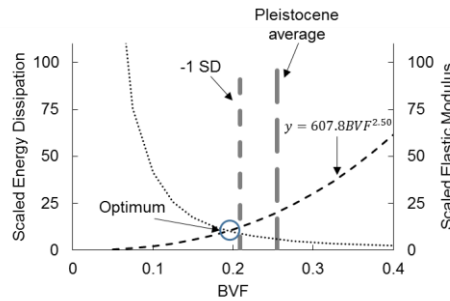**Appendix Figure 4.13:** Scaled E values vs. scaled W_f values.

Further, the 95% CI of the regression line is $0.93 - 1.35$, and thus contains the value 1. Having the value 1 within the 95% CI means that we can reasonably assume that the scaled E values are identical to the scaled W_f values. Thus, scaled E values can be used as a model for scaled W_f values. The original tradeoff model between scaled W_d and scaled E is shown below with the Pleistocene average and -1 SD plotted as dashed vertical lines (Appendix Figure 4.14):
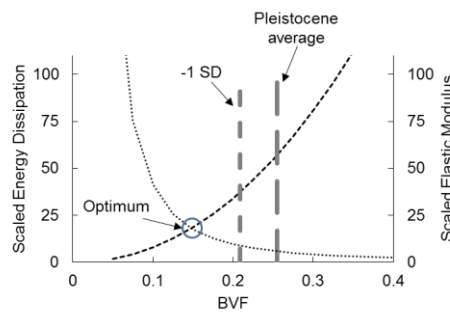
Appendix Figure 4.14: Original tradeoff model of scaled E and scaled energy dissipation, with the Pleistocene BVF average and -1 SD shown as dashed vertical lines.

The confidence intervals of the scaled E power law and coefficient can be used to obtain an estimate of how additional W_f data points might change the results and interpretations of the tradeoff model. Using a bootstrap method similar to the one described above, the 95% CI of the scaled E power law is (1.80 – 2.50) and the 95% CI of the coefficient is (607.8 – 1936.4).

Now, a new regression line of scaled E versus BVF is plotted using the upper bound of the 95% CI power law (2.50) and the upper bound of the 95% CI coefficient (607.8), the intersection of the scaled E and scaled W_d graphs approaches the lower 1SD boundary of the Pleistocene BVF (0.209) (Appendix Figure 4.15):

Appendix Figure 4.15: Scaled E and scaled W_d tradeoff model with the E regression line altered to represent the upper 95% CI value of the power law and the lower 95% CI of the coefficient. The BVF value to optimizes both E and W_f approaches -1 SD from the Pleistocene average BVF. Notice that Appendix Figure 4.12 and Appendix Figure 4.15 are nearly identical because the 95% CI bounds of scaled E and scaled W_f are similar.

Similar to above, the odds of the intersection point of the scaled W_d and scaled E graphs approaching 0.209 (and, again, the odds of our interpretation changing) is (2.5/100)*(2.5/100) = 0.000625, or 0.06%. This outcome is identical to what we found using the 95% CI of the scaled W_f values despite the limited W_f sample size. This exercise indicates that a larger W_f and σ_y sample size will have a limited effect on the 95% CI and thus will be extremely unlikely to change the results or the interpretation of the tradeoff model.

References

Burr, D. B., C. Milgrom, et al. (1996). "In vivo measurement of human tibial strains during vigorous activity." Bone **18**(5): 405-410.

Carter, D. R. and W. C. Hayes (1976). "Bone compressive strength - influence of density and strain rate." Science **194**(4270): 1174-1176.

Linde, F., P. Norgaard, et al. (1991). "Mechanical-properties of trabecular bone - dependency on strain rate." Journal of Biomechanics **24**(9): 803-809.